International Pyrheliometer Comparison

wrc pmod

IPC-IX

25.9. – 13.10.2000

Davos, Switzerland

International Pyrheliometer Comparison IPC-IX
25 September - 13 October 2000
Davos, Switzerland

Results and Symposium

Isabelle Rüedi

PMOD/WRC Internal Report
MeteoSwiss Working Report No. 197
Davos and Zürich, May 2001

Contents

Part I

RESULTS

Chapter 1 Organization and Procedures

1.1 Introduction

The Ninth International Pyrheliometer Comparison (IPC-IX) was held, for the first time together with Regional Pyrheliometer Comparisons (RPCs) of all WMO Regional Associations (RA I to RA IV), from 25 September to 13 October 2000 at the Physikalisch-Meteorologisches Observatorium Davos/World Radiation Center (PMOD/WRC) in Davos/Switzerland. This combination slightly extended the practice already introduced at previous IPCs and was considered highly effective in coping best with the urgent needs for carrying out RPCs of most Regions and most efficiently using the limited financial resources available in WMO for supporting these events. This led to the largest number of experts' and instruments' participation compared with all previous IPCs.

The results presented in this report are based on the measurements carried out during the 3 weeks assigned to the IPC-IX. However, due to unfavorable weather conditions prevailing for the whole period, measurements could be carried out on 6 days only, while suitable sky conditions were available on 2 days only. The measurements obtained during these 2 days were the main basis for the evaluation and calculation of the calibration factors for the participating pyrheliometers. Time on other days was used for technical preparations and training of participants as well as for a course on meteorological radiometry and the traditionally organized Scientific Symposium. Additional measurements recorded on 2 other days were also used for the analysis of some instruments which stayed at the WRC after the official end of the comparison. Finally, the evaluation of the World Standard Group (WSG) was done using data recorded on 6 days (2 of them during the official IPC and 4 after) in order to ensure a good transfer of the World Radiometric Reference (WRR) into the future.

1.2 Participation

65 participants took part in the comparison and operated a total number of 82 pyrheliometers (including the WSG instruments). They originated from 18 out of the 21 Regional Radiation Centers (RRCs) and from 22 National Radiation Centers (NRCs) as well as from 11 institutions, manufacturers, etc. which are not linked to WMO. From these instruments 47 had already participated in IPC-VIII.

Tables 1.1 and 1.2 list the participants and their instruments according to the WMO regions and other participating institutions respectively. A complete list of participants with addresses can be found in Chapter 4. The second column of Table 1.1 indicates the type of radiation center: World Radiation Center (WRC), World Radiation Data Center (WRDC), Regional Radiation Center (RRC) or National Radiation Center (NRC).[1] The WSG instruments are printed bold in the table.

[1]Note, this classification corresponds to the nomination given by the Regional Associations but does unfortunately not imply that all of these centers fully comply with the specifications for World, Regional and National Radiation Centers as specified in the WMO Guide to Meteorological Instruments and Methods of Observation (WMO-No. 8, 1996).

Table 1.1: IPC-IX Participation: *World, Regional and National Radiation Centers*

Country	*Type*	*Institution*	*Participant(s)*	*Instrument(s)*
World Radiation Center				
Switzerland	WRC	Physikalisch-Meteorologisches Observatorium Davos/ World Radiation Center, Davos	I. Rüedi HJ. Roth M. Roveretto R. Venturi S. Degli Esposti C. Fröhlich K. Kruse R. Philipona W. Schmutz Ch. Wehrli J. Wyss	**PMO2** **PMO5** **CROM2L** **CROM3R** **PAC3** **HF 18748** **TMI 67814** EPAC 11402 PMO609 PMO611 PMO6-0101 PMO6-SOVIM
RA I				
Algeria	RRC	Office National de Météorologie, Alger	B. Ouchene	HF 29225
Egypt	RRC	Egyptian Meteorol. Authority, Cairo	T. N. El-Hosary	HF 31103
Ethiopia	NRC	National Meteorol. Services Agency, Addis Ababa	H. K. Gedamu	N-18653
Nigeria	RRC	Dep. of Meteor. Services, Lagos	I. D. Nnodu	Å 576
Uganda	NRC	Ministry of Lands, Water and Environment, Dept. of meteorology, Kampala	E. Bagarukayo	Å 6549
RA II				
China	NRC	Academy of Meteorological Sciences, Beijing	W. Lu Y. Yang	HF 19743 PMO6-850406
India	RRC	Meteorological Dept., Pune	Ch. Rahalkar	EPAC-13219
Japan	RRC	Meteorol. Agency, Regional Radiation Center, Tokyo	K. Honda	PMO6-811107 HF 32446
Philippines	NRC	Philippine Atmospheric, Geophys. and Astron. Services PAGASA, Quezon City	V. S. Esquivel	Å 12578
Thailand	NRC	Meteorological Department, Bangkok	N. Suppjaroen A. Ying-Ariyakul	HF 27796

Table 1.1: (continued)

Country	*Type*	*Institution*	*Participant(s)*	*Instrument(s)*
RA III				
Argentina	RRC	Servicio Meterológico Nacional, Buenos Aires	F. Giménez	HF 30112
Chile	RRC	Direction Meteorol., Santiago	G. Lara Azocar	PMO6-850410
Colombia	NRC	IDEAM, Bogota	O. Simbaqueva	PMO6-79-123
Peru	NRC	National Meteorological & Hydrological Service, SENAMHI, Lima	I. Trebejo Verillas	Å 18020
RA IV				
Canada	RRC	National Atmosph. Radiation Centre, Downsview	B. McArthur	HF 18747 HF 20406
Cuba	NRC	Inst. de Meteorol., Habana	F. A. Vigón del Busto	Å 18587
Mexico	RRC	Inst. de Geofisica, México	A. Muhlia Velázquez	HF 29223
Mexico	NRC	Universidad de Colima, Colima	J. Fonseca I. Galindo G. Rios	HF 28965
USA	RRC	NOAA, Boulder	D. W. Nelson	HF 28553 HF 32448 TMI 67502
RA V				
Australia	RRC	Bureau of Meteorology, Melbourne	B. Forgan P. Novotny	Å 578 HF 27160 TMI 69137
RA VI				
Austria	NRC	Zentralanstalt für Meteorologie und Geodynamik, Wien	E. Wessely	Å 15192 TMI 68025
Belgium	RRC	Inst. Royal de Météorologie, Bruxelles	A. Chevalier Ch. Conscience S. Dewitte S. Ginion P. Malcorps	CROM05R CROM06R CROM09L
Czech Republic	NRC	Czech. Hydrometeor. Institute, Solar and Ozone Observatory, Hradec Kralove	J. Pokorny	HF 30497

Table 1.1: (continued)

Country	*Type*	*Institution*	*Participant(s)*	*Instrument(s)*
Estonia	NRC	Meteorological & Hydrological Inst., Toravere	A. Kallis	PMO6-850405
France	RRC	Centre Radiométrique, Carpentras-Serres	J. Oliviéri	TMI 68016
Germany	RRC	Deutscher Wetterdienst, Potsdam	K. Behrens	HF 27157 PMO6-5 PMO6-811103
Hungary	RRC	Hungarian Meteorological Service, Div. f. Methodology/Quality Control, Budapest	Z. Nagy	HF 19746
Israel	NRC	Meteorological Service, Bet-Dagan	A. Baskis	HF 27162
Lithuania	NRC	Lithuanian Hydrometeor. Service, Vilnius	D. Mikalajunas	Å 567
Norway	NRC	Norwegian University of Science and Technology, Dept. of Physics, Trondheim	M. Dhavraj	HF 31117
Poland	NRC	Institute of Meteorology and Water Management, Warsaw	B. Bogdanska	HF 30716
Portugal	NRC	Instituto de Meteorologia, Lisboa	F. Carvalho	HF 23737
Romania	NRC	National Institute of Meteor. Atmosph. Physic Laboratory, Bucaresti	C. Oprea	Å 702
Russian Federation	WRDC	Main Geophysical Observatory, World Radiation Data Center, St. Petersburg	A. Pavlov	Å212
Slovakia	NRC	Slovak Hydrometeorol. Institute, Bratislava	V. Horecká	Å 13439
Sweden	RRC	Meteorol. and Hydrol. Institute, Norrköping	Th. Persson	Å 171 HF 15744
Switzerland	NRC	MeteoSwiss, Payerne	–	PMO6-79-121
Ukraine	NRC	Central Geophysical Observatory, Kyiv	O. Pakhaljuk	Å 538
United Kingdom	NRC	Meteorological Office, Berkshire	P. Fishwick S. Goldstraw D. Shearn	TMI 67604 HF 31110

Table 1.2: IPC-IX Participation: *Various Institutions, Manufacturers, ...*

Country	*Institution*	*Participant(s)*	*Instrument(s)*
China	Institute of Optics, Fine Mechanics and Physics, Changchun	W. Fang G. Wang H. Yao B. Yu	SIAR-1
Israel	National Physical Laboratory of Israel	–	HF 30492
Italy	European Commission DG-JRC, Environment Institute, Ispra	T. Sample W. J. Zaaiman	PMO6-81109 PMO6-911204
Japan	EKO Instruments Trading CO., Ltd.	–	PMO6-850408
Russia	VNIIO, All-Russian Research Inst., Moscow	S. Morozova M. Pavlovitch	MAR-1-1
Sweden	Swedish National Testing and Research Institute, Boras	L. Liedquist	PMO6-811108
USA	AS & M, NASA Langley, Hampton	F. Denn B. Fabbri K. Larman	HF 31041
USA	DSET Lab., Phoenix	–	HF 17142
USA	Eppley Lab., Newport	J. R. Hickey	HF 14915 HF 27798 HF 32449
USA	Nat. Renewable Energy Lab., Golden	T. Stoffel I. Reda	HF 28968 HF 29220 HF 30713 HF 68018
USA	SUNY Albany Battelle, Richland	J. Michalsky	TMI 68023

1.3 Data Acquisition and Evaluation

The WSG instruments and additional radiometers of the WRC as well as auxiliary parameters were measured by an analog data acquisition system based on eight HP3478A voltmeters with relay scanners that are controlled by a Dell computer.

All the participating instruments were operated with their standard equipment in order to avoid electrical interface problems and mutual interferences. The data from the participating instruments were acquired via a number of micro-terminals operated by the participants and controlled by the Dell

computer. Each terminal could accept at the most 3 different values from two instruments. After each series, a summary of the values entered by micro-terminal was printed and distributed to be checked by the participants. If necessary, the raw data could be edited to correct typing errors.

The participants having their own computer controlled systems (synchronized to the timing of the IPC's measurement series) had the possibility to deliver their data on diskettes at the end of each day. These were converted and incorporated into the data files residing on the Dell computer for further processing.

Data from 82 pyrheliometers were acquired: 14 by the analog data acquisition system of PMOD/WRC, 28 through micro-terminals and 40 via diskettes.

1.3.1 Timing of the Measurements

The measurements were taken in runs (series) lasting 21 minutes with a basic cadence of 90 seconds. Voice announcements ending in a buzzer signal were used to inform the participants about the sequence of operations. The timing for the different instrument types was as follows:

- Ångström pyrheliometers: Before the start and after the end of the run the zero of the instrument was established. Alternating right and left strip readings were performed, starting with the right hand strip exposed to the sun. The following readings were paired as L-R, R-L, etc., yielding a total of 12 irradiance values per run.
- PACRAD: the run started with the shutter closed, after 60 s the heater was turned on for 40 s (this was introduced after IPC-III in order to have a well defined thermal state of the instrument independent of the operation sequence before the run). At 270 s the zero of the thermopile was read and the heater switched on again. At 450 s the heater voltage, current and thermopile was read, the heater turned off and the shutter opened. From 540 s on readings were taken every 90 s yielding 8 irradiance values per run. After the last reading the shutter was closed.
- HF type pyrheliometers: the run started with the shutter closed, after 90 s the zero was read and the heater turned on until at 180 s the voltage, current and thermopile were read. The heater was then turned off and the shutter opened. From 270 s onward the instrument was read every 90 s yielding 11 irradiance values per run. Some instruments which were providing their data with diskettes performed the calibration between the series and consequently measured 13 irradiance values per run.
- TMI type pyrheliometers: the run started with the shutter closed and the calibration procedure was performed until the end of the first 90 s. Starting at 180 s readings were taken every 90 s yielding 12 irradiance values per run.
- Active cavity type pyrheliometers: the run started with a reference phase (shutter closed) of 90 s, followed by a measurement phase (shutter open) of 90 s. This was repeated for the next 18 minutes. A total of 6 open and 7 closed readings were taken yielding a total of 6 irradiance values during a run. PMO2 was read at twice that pace, with a reference phase of 32 s and a measurement phase of 58 s, producing 13 irradiance values per run so that for all readings of the basic sequence a PMO2 irradiance was available.
- Normal Incidence Pyrheliometers (NIP): it took 12 irradiance values every 90 s after an initial zero reading at 90 seconds.

1.3.2 Data Evaluation

For each instrument the irradiance was obtained with the appropriate evaluation procedure as listed below. After each day a summary of the computed irradiances was printed and distributed to be

checked by the participants. As indication the mean and standard deviation of the ratios to PMO2 were also given for each series. PMO2 was used as the local reference during the time of the comparison since it delivers an irrdiance value every 90 seconds. If necessary, the raw data could be edited for gross errors. A general daily summary with the means and standard deviations of the ratios to PMO2 for each series and each instrument was put up for comparison purposes.

The procedure used to calculate the irradiance S of each instrument type is described below. The notations are:

V_{th}	output of the thermopile
U_h, U_i	voltage across the heater (h) or across the standard resistor (i)
R_n	standard resistor
C	calibration factor
C_2	correction factor for lead heating
P	electrical power in the active cavities

- Å-pyrheliometers: the current through the right or left strip was measured as voltage drop across a standard resistor and the irradiance was obtained as:

$$S = C\frac{U_i(\text{left})U_i(\text{right})}{R_n^2}$$

  This corresponds to the geometric mean of the irradiances at the time of right and left readings. Thus, the ratio to WRR was calculated using the geometric mean of the WSG irradiances at the corresponding instances.

- PACRAD and HF type pyrheliometers: the irradiance was calculated from the thermopile output V_{th}(irrad) when the receiver was irradiated. The sensitivity was determined by the calibration during which the cavity was shaded and electrically heated and U_h and U_i were measured together with the corresponding thermopile output V_{th}(cal). Furthermore, the zero of the thermopile V_{th}(zero) was measured and subtracted.

$$S = C\frac{V_{th}(\text{irrad}) - V_{th}(\text{zero})}{V_{th}(\text{cal}) - V_{th}(\text{zero})}\frac{U_i}{R_n}\left(U_h - \frac{U_i}{R_n}C_2\right)$$

- TMI type pyrheliometers: most were operated in the "normal" way, that is by calibrating the readout directly in units of $mW\,cm^{-2}$. The values were entered in Wm^{-2} and no irradiance calculation was needed. Others were operated and evaluated like HF pyrheliometers.

- Active cavity pyrheliometers: the irradiance was obtained from P(closed) averaged from the closed values before and after the open reading P(open).

$$S = C(P(\text{closed}) - P(\text{open}))$$

  The power calculation was done according to the prescription of the instrument type with

$$P = U_h^2 \qquad \text{or} \qquad P = U_hU_i \qquad \text{or} \qquad P = U_h\frac{U_i}{R_n}$$

- Normal Incidence Pyrheliometer (NIP): the thermopile reading was divided by the calibration factor after subtraction of the zero point reading.

- PMO2: As during preceding IPCs, PMO2 was used as the local reference instrument because it can be operated fast enough to provide an irradiance value every 90 seconds. The values of PMO2 were obtained with the algorithm for active cavity radiometers. At the end of the open phase, 8 readings were taken in rapid succession. For the on-line calculations the first value was used as reference for the values entered by the terminals. The standard deviation of the 8 readings was used during the final evaluation as a quality control parameter to judge the stability of the radiation during each acquisition sequence (see Sect. 2.1).

1.3.3 Auxiliary Data

The meteorological parameters (air temperature, relative humidity and atmospheric pressure) were obtained from the automatic weather station ASTA of MeteoSwiss located at PMOD/WRC. The ASTA values are 10-minute averages. The direct solar radiation was taken from PMO2 and the diffuse radiation from the PMOD/WRC shaded pyranometer. The global radiation was computed from the 2 previous values. The values allocated to each measurement run are averages over the period and the results are plotted in Figures 3.2.1 and 3.2.2.
Sunphotometer measurements were used to determine the vertical aerosol optical depth at 368, 500 and 778 nm. Daily total Ozone values measured at Arosa (about 15 km south-west of Davos) were used for the evaluation of the 500 nm channel. The total amount was: 269.8, 287.2, 268.3, 267.9, 319.8 and 265.1 mcm (Dobson units) on 27 September, 2, 22 and 23 October, 1 November and 5 December 2000, respectively. The optical depth results are plotted in Figure 3.2.3.

1.4 Approvement and Dissemination of the Results

According to Resolution 1 of CIMO-XI an Ad-hoc Group was established to discuss the preliminary results of the IPC-IX, based upon criteria defined by the WRC, evaluate the above reference and recommend the updating of the calibration factors of the participating instruments. It was chaired by the CIMO-Rapporteur on Meteorological Radiation Measurements Mr Klaus Behrens, Germany, and composed as follows: T.N. El-Hosary (Egypt, RA I), K. Honda (Japan, RA II), O. Simbaqueva and F. Giménez (Columbia and Argentina, both RA III), B. McArthur and A. Muhlia Velázquez (Canada and Mexico, both RA IV), B. Forgan (Australia, RA V) and J. Olivieri (France, RA VI). The WRC was represented by I. Rüedi and W. Schmutz.

The procedures used to compute the new WRR factors of the WSG and participating instruments have been approved by the Ad-hoc Group and the final results of IPC-IX were calculated accordingly.

Besides its official duties, the Ad-hoc Group also discussed the future of the IPCs and the most efficient way of transferring the WRR worldwide. The results of these discussions are summarized in the Appendix.

Chapter 2 Measurements and Results

Since the weather conditions were unfortunate throughout the IPC-IX. Measurements were taken on 6 days only. Two days (September 27 and October 9) had acceptable sky conditions that satisfied the minimal conditions as stated in Sect. 2.1. and have been selected for the final evaluation.

The Ad-hoc Group found that it would be desirable to use more data for the determination of the WRR-factors of the WSG instruments in order to transfer the WRR with more reliability into the future. Consequently, more data were used for the evaluation of the WSG (September 27, October 9, 22, 23, November 1 and December 5).

One participant and some instruments stayed after the end of the comparison until two clear-sky days took place. Those 2 days (October 22 and 23) were also used for the evaluation of the instruments which were present at that time. These instruments can be recognized on the graphics of Sect. 3.

2.1 Data Selection Criteria for the Final Evaluation

At the beginning of the IPC, the Ad-hoc Group responsible for the approval of the final evaluation procedure (c.f. Sect. 1.4) met and set the following criteria for the acceptance of IPC data:

1. Only observations falling within the appropriate measurement periods be accepted and that the last series for any group of instruments stop before the end of the period is reached (based on calculations associated with the instrument field-of-view).

2. That no measurements be used for the comparison of Ångstrom pyrheliometers if a cloud is within $\pm 15^\circ$ of the sun. No measurements will be used for the absolute cavity radiometers (field-of-view $= 5^\circ$) if a cloud is within $\pm 8^\circ$ of the sun.

3. That no measurements be used if the measured wind speed is greater than $2.5\,\mathrm{ms}^{-1}$.

4. That no data be used if the 500 nm AOD is greater than 0.12.

5. That an individual point be excluded from a series if the variation of the 8 fast PMO2 measurements is greater than $0.5\,\mathrm{Wm}^{-2}$.

6. That an entire series be removed from consideration if more than two (out of 13) individual observations do not meet criterion (5).

7. That the minimum number of acceptable data points be 150 for the PMO2 taken over a minimum of three days during the comparison period.

Unfortunately criterion (7) could not be fulfilled due to the adverse weather conditions. Criterion (2) could only be applied quantitatively on October 9 when a cloud detector was installed on the WSG tracker. On the other days, it was estimated using the WSG observer's notes. The same is true for criterion (3) since wind speed values at the measurement site were not available for that period. Otherwise, the runs and measurements which have been selected for the final evaluation are in conformity with the above criteria.

The start times of the runs from the IPC period which were finally used for the evaluation are: 09:30, 10:00, 10:30, 11:00, 11:30, 12:30, 13:00, 13:30, 14:30, 15:00 on September 27 for all instruments and 14:15 on October 9 for the absolute cavities. Note that all the times given in this report are given in Mean European Times (MET = UTC+1).

For the instruments which were still present after the end of the IPC, the following series are also taken into account: 09:00, 09:30, 10:00, 11:00, 11:30, 12:00, 12:30, 13:00, 13:30, 14:00, 14:30, 15:00, 15:30 on October 22 and 09:30, 10:00, 10:30, 11:00, 11:30, 13:00, 13:30, 14:00, 14:30, 15:00 on October 23.

Finally, the additional series which were used for the evaluation of the WSG instruments started at: 09:31, 09:55, 10:20, 10:43 on November 1 and 10:31, 11:41, 12:18, 12:44, 13:09 on December 5.

From the chosen series, individual points were rejected when the standard deviation of the 8 fast PMO2 readings was larger than 0.5 Wm^{-2}, indicating a radiation instability (criterion 5).

2.2 Status of the WSG

The main objective of the periodic International Pyrheliometer Comparisons is the dissemination of the World Radiometric Reference (WRR) in order to ensure worldwide homogeneity of meteorological radiation measurements. The WRR is realized by the World Standard Group (WSG) which is frequently inter-compared at PMOD/WRC to detect possible deviations of individual members of the group and to ensure the stability of the WRR. Independently, the stability of the WRR can be checked by instruments that have participated in previous IPC's.

Since the last comparison (IPC-VIII which was held in 1995), some instruments of the World Standard Group exhibited problems. CROM3R was very unstable during the whole period due to malfunctioning of the instrument's electronics. PMO5 presented a drift which was also due to an electronic problem caused by the drift of the heater's current amplifier, as was found just after IPC-IX. PAC3 measurements were off and unstable over a long time period which happened to be due to the presence of an insect in its cavity. It was found in summer 2000 prior to the IPC-IX. Since the insect was removed and the cavity cleaned, the instrument has gone back to its past (IPC-VII) performances. Finally, a new electronic was built for TMI67814 and was fully operational only in summer 2000, shortly before IPC-IX.

2.3 Transfer of the WRR

Taking the problems mentioned in Sect. 2.2 into account, only PMO2, CROM2L, HF18748 and TMI67814 could be used for the transfer of the WRR from IPC-VIII to IPC-IX. Though the electronic of TMI67814 was replaced this instrument may be used for the transfer of the WRR since it was shown that the change did not affect it.

In a first step the irradiances of all WSG radiometers were scaled to WRR using their WRR factors from IPC-VIII. These factors are listed in the 2nd column of Table 2.1. For the sequences where PMO2, CROM2L, HF18748 and TMI67814 had valid irradiance values their median value was determined. The sequences for which one (or more) of the four instruments did not lie within 0.3% of the median were discarded. For the remaining sequences, the mean of the 4 instruments' irradiances were used as the WRR for that time. Those values were then used to determine the ratios to WRR of all the WSG instruments. First the ratios and their median value are determined. The ratios lying more than 0.3% away from the median of the instrument's ratios are discarded and finally the mean of the remaining ratios is the new "ratio to WRR" for the instrument under consideration. The WRR-factors are 1/"ratio to WRR". Their means, standard deviations and the numbers of points used are listed in column 3 to 5 of Table 2.1 for the WSG pyrheliometers.

Table 2.1: New WRR-factors for the WSG instruments computed using PMO2, CROM2L, HF18748 and TMI67814 and the IPC-VIII WRR-factors.

Instrument	*WRR factors IPC-VIII*	*WRR factors IPC-IX*	*Standard. Deviation*	*N*	*Change [ppm] IPC-IX - IPC-VIII*
PMO2	0.99936	0.999548	0.00050	160	188
CROM2L	1.00290	1.00301	0.00093	160	107
TMI67814	1.00068	1.00066	0.00043	160	-18
HF18748	0.99595	0.995675	0.00047	160	-275
PAC3	1.00186	1.00065	0.00056	132	-1214
PMO5	1.00091	0.998974	0.00071	44	-1936
CROM3R	0.99897	0.997669	0.00167	52	-1301

The changes exhibited by the radiometers used to transfer the WRR are similar to those observed at other IPCs and thus, demonstrates its stability. Note that PMO5 has only few data points because its electronics suddenly became very unstable and there are no measurements after October 9. The small number of points for CROM3R is due to the large continuous scatter of its value so that many points do not satisfy the 0.3% criterion.

2.4 Computation of the New WRR-Factors

For the final evaluation of the instruments participating in IPC-IX the factors of Table 2.1 were used to calculate the WRR for each sequence as the mean of at least 3 instruments from the WSG with the exception of PMO5 and CROM3R.

For each sequence the median of the available irradiances of PMO2, CROM2L, HF18748, TMI67814 and PAC3 was computed (the new WRR-factors determined above were used to compute these irradiances). The median value of those irradiances was computed. If at least 3 instruments' irradiances lie within 0.3% of the median, then the mean of those values is the WRR for that sequence. For the Ångström pyrheliometers, the actual Ångström-WRR is the average of the WRR at the times when they had their left/right slit illuminated.

For each instrument the ratios WRR/instrument irradiance were computed for all the points for which there was a valid WRR value. The median of the ratios was determined. The ratios which do not lie within 0.3% of the median were discarded. Finally the mean of the remaining ratios is the new WRR-factor of the instrument.

Table 2.2 shows the performances of each individual instrument: column 2 gives the final ratios to WRR of the instruments and column 3 their corresponding standard deviations. Column 5, 6 and 7 give the minimum, maximum ratios and number of points used to determine the mean while column 7 gives the total number of points available for the evaluation (i.e. before points were removed by using the 0.3% criterion).

A graphical representation of the results of each instrument is also provided in Section 3.

Table 2.2: General performances of the instruments

Instrument	*Ratio to WRR*	*Standard Deviation*	*Min Ratio*	*Max Ratio*	*N used*	*N tot*	*Country/ Owner*
Å 171	0.99701	0.00140	0.99427	1.00002	81	93	Sweden
Å 212	0.99935	0.00101	0.99721	1.00147	48	49	Russia
Å 538	1.00093	0.00132	0.99847	1.00359	38	39	Ukraine
Å 567	1.00086	0.00155	0.99823	1.00402	83	94	Lithuania
Å 576	1.00264	0.00169	0.99935	1.00529	56	94	Nigeria
Å 578	0.99432	0.00111	0.99180	0.99691	83	89	Australia
Å 702	0.99607	0.00157	0.99309	0.99872	60	81	Romania
Å 6549	0.95987	0.00125	0.95877	0.96145	6	82	Uganda
Å 12578	0.99405	0.00195	0.99148	0.99735	44	93	Philippines
Å 13439	0.99763	0.00122	0.99541	1.00018	92	92	Slovakia
Å 15192	0.99843	0.00142	0.99573	1.00162	83	94	Austria
Å 18020	0.99081	0.00155	0.98777	0.99362	74	88	Peru
Å 18587	0.99791	0.00116	0.99506	1.00049	93	94	Cuba
CROM5R	1.00181	0.00102	0.99924	1.00307	13	13	Belgium
CROM6R	1.00170	0.00142	0.99999	1.00339	9	12	Belgium
CROM9L	1.00143	0.00051	1.00069	1.00213	10	10	Belgium
EPAC 11402	1.00075	0.00081	0.99827	1.00272	206	228	WRC
EPAC 13219	1.00295	0.00156	0.99985	1.00554	32	71	India
HF 14915	0.99974	0.00077	0.99813	1.00124	102	102	USA/EPLAB
HF 15744	1.00085	0.00064	0.99926	1.00252	113	113	Sweden
HF 17142	1.00107	0.00062	0.99929	1.00263	93	93	USA/DSET
HF 18747	0.99787	0.00067	0.99572	0.99940	73	73	Canada
HF 19743	0.99851	0.00157	0.99535	1.00118	83	113	China
HF 19746	1.00034	0.00058	0.99896	1.00164	113	113	Hungary
HF 20406	0.99630	0.00058	0.99492	0.99803	72	72	Canada
HF 23737	1.00271	0.00087	1.00012	1.00562	91	98	Portugal
HF 27157	1.00099	0.00131	0.99844	1.00370	104	104	Germany
HF 27160	1.00324	0.00051	1.00141	1.00425	113	113	Australia
HF 27162	0.99918	0.00079	0.99746	1.00147	90	101	Israel
HF 27796	1.00310	0.00081	1.00108	1.00555	113	113	Thailand
HF 27798	1.00012	0.00091	0.99789	1.00209	101	102	USA/EPLAB
HF 28553	1.00268	0.00049	1.00045	1.00383	211	212	USA/NOAA
HF 28965	1.00177	0.00043	1.00068	1.00288	78	88	Mexico
HF 28968	1.00135	0.00062	0.99954	1.00337	113	113	USA/NREL
HF 29220	1.00154	0.00063	0.99977	1.00323	113	113	USA/NREL
HF 29223	1.00254	0.00082	1.00074	1.00435	93	113	Mexico
HF 29225	1.00292	0.00064	1.00162	1.00478	77	77	Algeria
HF 30112	1.00313	0.00065	1.00157	1.00477	112	112	Argentina
HF 30492	1.00396	0.00088	1.00179	1.00599	102	102	Israel
HF 30497	1.00226	0.00050	1.00069	1.00349	113	113	Czech Rep.
HF 30713	1.00140	0.00059	0.99989	1.00289	113	113	USA/NREL
HF 30716	1.00256	0.00114	0.99970	1.00526	102	104	Poland
HF 31041	1.00188	0.00070	1.00006	1.00342	94	94	USA/NASA
HF 31103	1.00101	0.00059	0.99928	1.00236	113	113	Egypt

Table 2.2: (continued)

Instrument	*Ratio to WRR*	*Standard Deviation*	*Min Ratio*	*Max Ratio*	*N used*	*N tot*	*Country/ Owner*
HF 31110	1.00212	0.00065	1.00020	1.00464	106	113	United K.
HF 31117	1.00035	0.00058	0.99890	1.00237	81	91	Norway
HF 32446	1.00025	0.00064	0.99864	1.00183	113	113	Japan
HF 32448	0.99962	0.00042	0.99850	1.00069	135	135	USA/NOAA
HF 32449	1.00290	0.00078	1.00049	1.00513	101	101	USA/EPLAB
MAR-1-1	1.00058	0.00075	0.99913	1.00268	47	47	Russia/VNIIO
PMO6-5	0.99947	0.00078	0.99807	1.00130	47	47	Germany
PMO609	0.99568	0.00050	0.99405	0.99700	122	124	WRC
PMO611	0.99450	0.00068	0.99281	0.99735	161	161	WRC
PMO6 79-121	1.00014	0.00053	0.99860	1.00161	161	161	Switzerland
PMO6 79-123	0.99661	0.00133	0.99359	0.99936	98	114	Colombia
PMO6 81109	1.00054	0.00060	0.99923	1.00244	113	113	Italy
PMO6 811103	1.00002	0.00073	0.99850	1.00157	42	47	Germany
PMO6 811107	0.99991	0.00098	0.99737	1.00195	36	37	Japan
PMO6 811108	1.00003	0.00053	0.99862	1.00136	47	47	Sweden
PMO6 850405	1.00071	0.00065	0.99964	1.00244	47	52	Estonia
PMO6 850406	0.99968	0.00060	0.99843	1.00089	52	52	China
PMO6 850408	0.99171	0.00057	0.99031	0.99384	124	124	Japan/EKO
PMO6 850410	0.98495	0.00076	0.98329	0.98662	45	52	Chile
PMO6 911204	0.99919	0.00079	0.99664	1.00206	112	113	Italy
PMO6 0101	0.99987	0.00091	0.99814	1.00237	52	63	WRC
PMO6 SOVIM	0.99480	0.00084	0.99279	0.99711	160	161	WRC
SIAR-1	1.00078	0.00114	0.99960	1.00216	5	5	China
TMI 67502	1.00034	0.00066	0.99847	1.00200	219	221	USA/NOAA
TMI 67604	1.00072	0.00084	0.99833	1.00282	104	104	United K.
TMI 68016	1.00222	0.00148	0.99987	1.00472	102	104	France
TMI 68018	1.00152	0.00053	1.00035	1.00293	113	113	USA/NREL
TMI 68023	1.00134	0.00091	0.99953	1.00341	101	102	USA/SUNY
TMI 68025	0.99994	0.00115	0.99711	1.00229	111	111	Austria
TMI 69137	0.99771	0.00070	0.99540	0.99907	113	113	Australia
N-18653	1.03431	0.00139	1.03067	1.03667	63	113	Ethiopia

2.5 Recommended Calibration- and WRR-Factors

Tables 2.3 to 2.4 list the final results of the comparison, i.e. the recommended calibration- and WRR-factors. Column 2 to 4 give the constants which were used to compute the irradiances at the IPC-IX. Column 5 gives the calibration factors derived at IPC-VIII. The ratios to WRR, new WRR-factors and recommended calibration factors derived from the IPC-IX analysis are listed in columns 6 to 8. Finally, column 9 gives the changes of the recommended calibration factors between IPC-IX and IPC-VIII.

Table 2.3: Recommended WRR- and calibration factors for the WSG instruments

Instrument	*C used at IPC-IX*	C_2	C_3	*C from IPC-VIII*	*Ratio to WRR*	*New WRR*	*New C*	*Change [ppm]*	*Owner*
PMO2	24.1800			24.1645	1.00045	0.99955	24.1691	188	WRC
CROM2L	127.687			128.057	0.99700	1.00301	128.071	107	WRC
HF 18748	19989.0	0.07	75	19908.0	1.00434	0.99568	19902.5	-275	WRC
TMI 67814	10007.0		90	10013.8	0.99934	1.00066	10013.6	-18	WRC
PAC3	9962.60	0.07	75	9981.17	0.99936	1.00065	9969.03	-1214	WRC
PMO5	31.6150			31.6438	1.00103	0.99897	31.5826	-1936	WRC
CROM3R	127.549			127.416	1.00234	0.99767	127.933	-1301	WRC

Table 2.4: Recommended WRR and calibration factors for the participating instruments

Instrument	*C used at IPC-IX*	C_2	C_3	*C from IPC-VIII*	*Ratio to WRR*	*New WRR*	*New C*	*Change [ppm]*	*Country/ Owner*
Å 171	5717.00		1	5715.34	0.99701	1.00300	5734.15	3280	Sweden
Å 212	10535.0		500	10554.6	0.99935	1.00065	10541.8	-1210	Russia
Å 538	2480.00		200		1.00093	0.99907	2477.70		Ukraine
Å 567	5782.00		200		1.00086	0.99914	5777.02		Lithuania
Å 576	5885.13		1000	5885.13	1.00264	0.99737	5869.65	-2637	Nigeria
Å 578	6241.00		1	6251.58	0.99432	1.00571	6276.65	3994	Australia
Å 702	6141.14		200	6141.14	0.99607	1.00394	6165.35	3927	Romania
Å 6549[1]	4418.60		2000		0.95987	1.04181	4603.34		Uganda
Å 12578	4439.33		1000	4439.33	0.99405	1.00599	4465.90	5950	Philippines
Å 13439	4411.80		1000	4411.80	0.99763	1.00237	4422.28	2369	Slovakia
Å 15192	4487.89		1000	4487.89	0.99843	1.00157	4494.93	1566	Austria
Å 18020	4582.00		1000		0.99081	1.00927	4624.49		Peru
Å 18587	4567.19		1000	4567.19	0.99791	1.00210	4576.77	2094	Cuba
CROM5R	19680.4				1.00181	0.99819	19644.9		Belgium
CROM6R	19750.9				1.00170	0.99831	19717.5		Belgium
CROM9L	12780.9				1.00143	0.99857	12762.6		Belgium
EPAC 11402	10024.0	0.07	90		1.00075	0.99925	10016.5		WRC
EPAC 13219	10079.0	0.06		10071.1	1.00295	0.99706	10049.3	-2165	India
HF 14915	20010.0	0.07		20019.2	0.99974	1.00026	20015.2	-199	USA/EPLAB
HF 15744	20020.0	0.07		20009.4	1.00085	0.99916	20003.1	-315	Sweden
HF 17142	19982.0	0.07		19959.2	1.00107	0.99893	19960.6	69	USA/DSET
HF 18747	20014.0	0.07		20033.0	0.99787	1.00214	20056.8	1186	Canada
HF 19743	20012.0	0.07	10000		0.99851	1.00149	20041.8		China
HF 19746	20013.8	0.07	10000	20013.8	1.00034	0.99966	20007.1	-336	Hungary
HF 20406	20038.0	0.07		20065.5	0.99630	1.00371	20112.4	2333	Canada
HF 23737	20030.0	0.07	1000		1.00271	0.99730	19975.9		Portugal
HF 27157	20037.6	0.07	10000	20037.6	1.00099	0.99902	20017.9	-985	Germany
HF 27160	20030.0	0.07	10	19971.7	1.00324	0.99677	19965.3	-321	Australia

[1] All the irradiance values available for this instrument are the same. This shows that Å6549 was not operated properly. Consequently, the derived factor does not represent the instrument's factor and should not be applied to it!

Table 2.4: (continued)

Instrument	*C used at IPC-IX*	C_2	C_3	*C from IPC-VIII*	*Ratio to WRR*	*New WRR*	*New C*	*Change [ppm]*	*Country/ Owner*
HF 27162	20020.0	0.07	1000	20039.2	0.99918	1.00082	20036.4	-142	Israel
HF 27796	19986.1	0.07	1000		1.00310	0.99691	19924.3		Thailand
HF 27798	20020.0	0.07		19999.6	1.00012	0.99988	20017.5	896	USA/EPLAB
HF 28553	19986.0	0.07		19937.2	1.00268	0.99733	19932.6	-230	USA/NOAA
HF 28965	19986.0	0.07		19957.7	1.00177	0.99823	19950.7	-350	Mexico
HF 28968	19980.2	0.07		19945.7	1.00135	0.99866	19953.3	382	USA/NREL
HF 29220	19999.0	0.07		19971.4	1.00154	0.99846	19968.2	-160	USA/NREL
HF 29223	19998.0	0.07		19946.9	1.00254	0.99747	19947.4	26	Mexico
HF 29225	20004.2	0.07			1.00292	0.99709	19946.0		Algeria
HF 30112	19999.0	0.07			1.00313	0.99688	19936.7		Argentina
HF 30492	19989.0	0.07	10		1.00396	0.99605	19910.1		Israel
HF 30497	19989.0	0.07			1.00226	0.99774	19943.8		Czech Rep.
HF 30713	19989.0	0.07			1.00140	0.99861	19961.1		USA/NREL
HF 30716	20009.2	0.07	10000		1.00256	0.99745	19958.1		Poland
HF 31041	19999.2	0.07			1.00188	0.99813	19961.7		USA/NASA
HF 31103	20009.2	0.07	10000		1.00101	0.99899	19989.0		Egypt
HF 31110	19989.0	0.07		19944.4	1.00212	0.99789	19946.8	118	United K.
HF 31117	19989.2	0.07			1.00035	0.99965	19982.3		Norway
HF 32446	19992.0	0.07			1.00025	0.99975	19986.9		Japan
HF 32448	19992.0	0.07			0.99969	1.00031	19998.2		USA/NOAA
HF 32449	20009.0	0.07			1.00290	0.99711	19951.2		USA/EPLAB
MAR-1-1	35568.0			35568.3	1.00058	0.99943	35547.6	-583	Russia/VNIIO
PMO6-5	23.6812			23.6812	0.99947	1.00053	23.6938	533	Germany
PMO609	24.0392			24.1154	0.99568	1.00434	24.1435	1165	WRC
PMO611	23.9442			24.0232	0.99450	1.00553	24.0766	2219	WRC
PMO6 79-121	23.8800				1.00014	0.99986	23.8767		Switzerland
PMO6 79-123	24.0000				0.99661	1.00340	24.0817		Columbia
PMO6 81109	23.9995				1.00054	0.99946	23.9865		Italy
PMO6 811103	23.9400			23.9400	1.00002	0.99998	23.9395	-22	Germany
PMO6 811107	24.0300			24.0315	0.99991	1.00009	24.0323	31	Japan
PMO6 811108	24.0887			24.0907	1.00003	0.99997	24.0880	-112	Sweden
PMO6 850405	24.1940			24.1940	1.00071	0.99929	24.1768	-713	Estonia
PMO6 850406	23.9930				0.99968	1.00032	24.0008		China
PMO6 850408	24.0000				0.99171	1.00836	24.2006		Japan/EKO
PMO6 850410	600.000				0.98495	1.01528	609.171		Chile
PMO6 911204	24.1040				0.99919	1.00081	24.1234		Italy
PMO6 0101	22.9450				0.99987	1.00013	22.9479		WRC
PMO6 SOVIM	127.500				0.99480	1.00522	128.166		WRC
SIAR-1	23.6498				1.00078	0.99922	23.6313		China
TMI 67502	1.00390			1.00256	1.00034	0.99966	1.00355	990	USA/NOAA
TMI 67604	1.00520			1.00519	1.00072	0.99928	1.00448	-709	United K.
TMI 68016[2]	10036.4		90	10050.0	1.00222	0.99779	10014.2	-3572	France
TMI 68018	1.00460			1.00348	1.00152	0.99848	1.00308	-402	USA/NREL

[2]TMI68016 was not functioning properly during the IPC. Consequently, the derived factor should not be applied to this instrument!

Table 2.4: (continued)

Instrument	*C used at IPC-IX*	C_2	C_3	*C from IPC-VIII*	*Ratio to WRR*	*New WRR*	*New C*	*Change [ppm]*	*Country/ Owner*
TMI 68023	1.00000				1.00134	0.99866	0.99865		USA/SUNY
TMI 68025	1.00200			1.00186	0.99994	1.00006	1.00206	195	Austria
TMI 69137	10020.0		10	10047.9	0.99771	1.00230	10043.0	-487	Australia
N-18653	9260.31				1.03431	0.96683	9578.01		Ethiopia

2.6 Stability of the WRR and Recommendations for the WSG

The stability of the WRR could be further checked by calculating the average change of all pyrheliometers that had participated in IPC-VIII. Taking all instruments (43, including the WSG but excluding instruments known to have had problems: PMO5, PAC3, CROM3R (all 3 from the WSG) and TMI68016 (France)) the average change amounts to 494 ppm with a 1-σ standard deviation of 1629 ppm. If instruments with changes larger than 0.3% (0.2%) are excluded the mean changes are 105$\pm$1076 ppm (-4$\pm$622 ppm) with 39 (33) instruments remaining. Doing the same analysis without the Ångstrom pyrheliometers, the results are the following 56$\pm$842 ppm for 34 instruments and excluding the instruments with changes larger than 0.3% (0.2%) the changes are 56$\pm$842 ppm (-15$\pm$531 ppm) with 34 (31) instruments remaining. These results are certainly confirming the stability of the WRR derived by the results of the WSG alone. The observed changes are also very well in agreement with results from previous IPCs. This suggests that in spite of the unfortunate weather conditions, the strict rules used for the analysis enabled a reliable transfer of the WRR.

All the radiometers belonging to the WSG are at least 20 years old. Instruments of that age may of course be subject to failures. In order to be able to coping with such an eventuality potential replacement instruments (and/or additional instruments) should be found. Such instruments should be operated together with the WSG for as long as possible in order to gain some history so that their stability and ratio to WRR be well known.

Finally, the following statement was made by the Ad-hoc Group: "The Ad-hoc Group to requests that the World Radiation Center removes CROM3R from the World Standard Group because of its erratic behavior over the last inter-comparison period. The WRC is instructed to return the instrument to the manufacturer. A replacement instrument from the manufacturer, including a refurbished CROM3R, would be welcomed, but would have to be operational for a minimum of one inter-comparison period before being reintegrated into the WSG."

Chapter 3 Graphics

3.1 Graphical Representation of the Results

The following figures show the performances of the instruments. The deviation from WRR (i.e. "ratio to WRR"-1) is plotted. All the points which may be used for the analysis (i.e. the points fulfilling the selection criterion mentioned in Sect. 2.1) have been plotted with a corresponding histogram on the side. The horizontal solid line represents the derived ratio to WRR and the dashed lines its 1-σ standard deviation. The values of the ratio to WRR and its standard deviation is printed on top of the plot with the number of points used to determine this value. The number in parentheses corresponds to the total number of points available for the analysis. For the instruments of the WSG points are plotted only if the irradiance values of PMO2, CROM2L, HF18748 and TMI67814 all lied within 0.3% of their median value (c.f. Sect. 2.3).

3.1.1 PMO2, PMO5, CROM2L

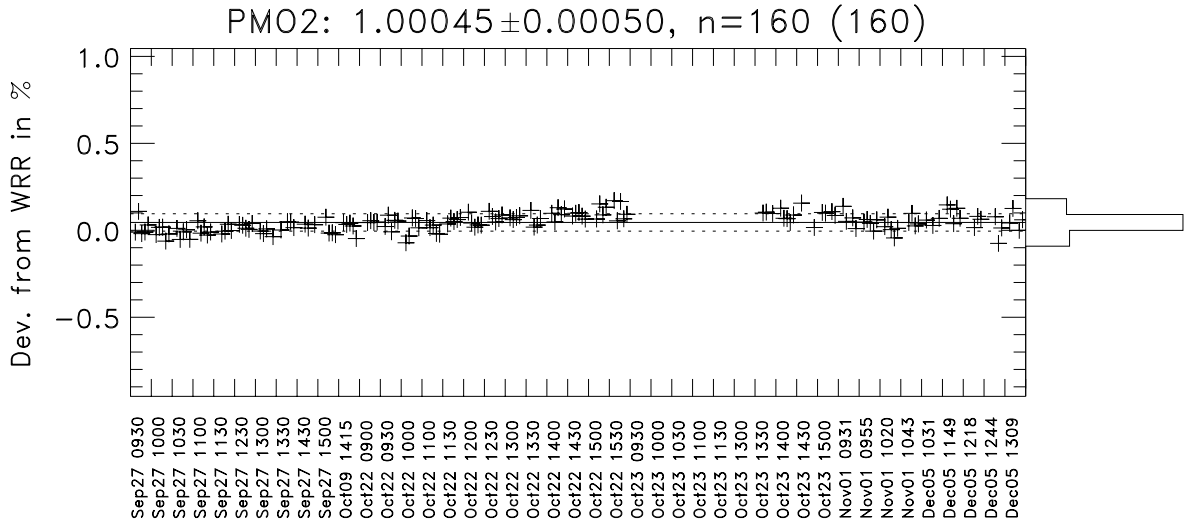

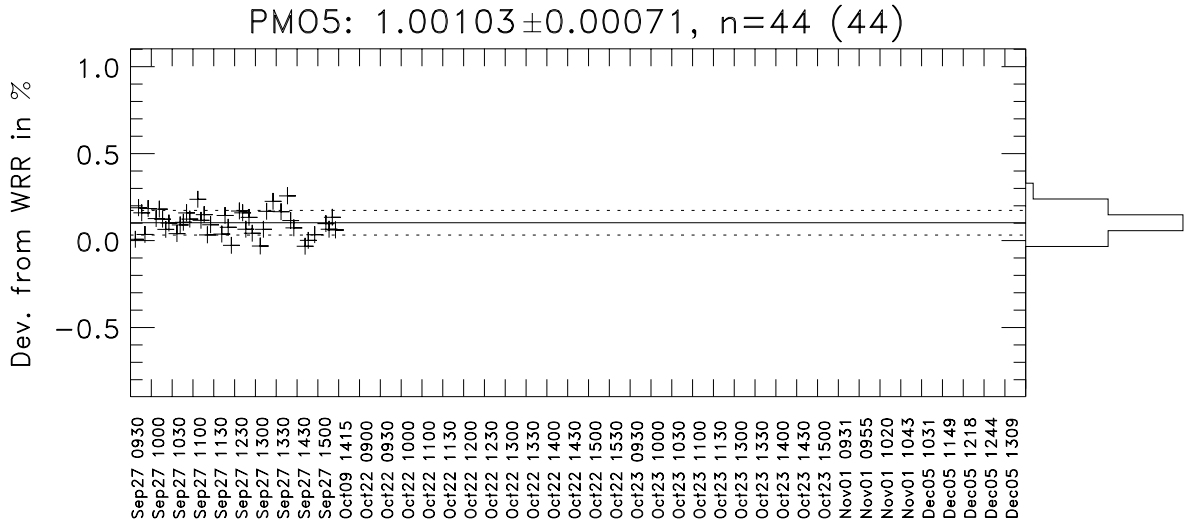

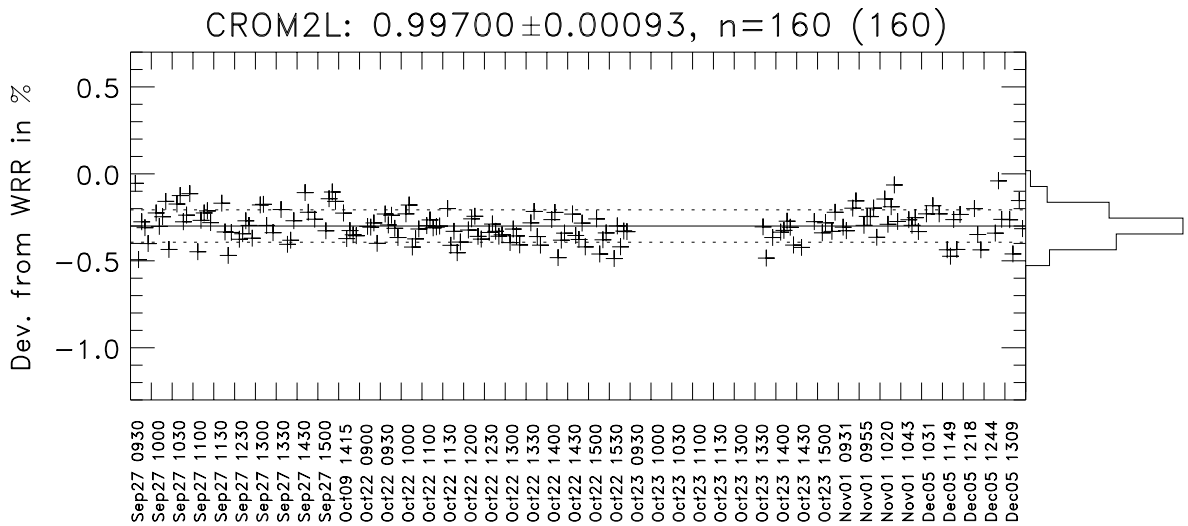

3.1.2 CROM3R, PAC3, HF18748

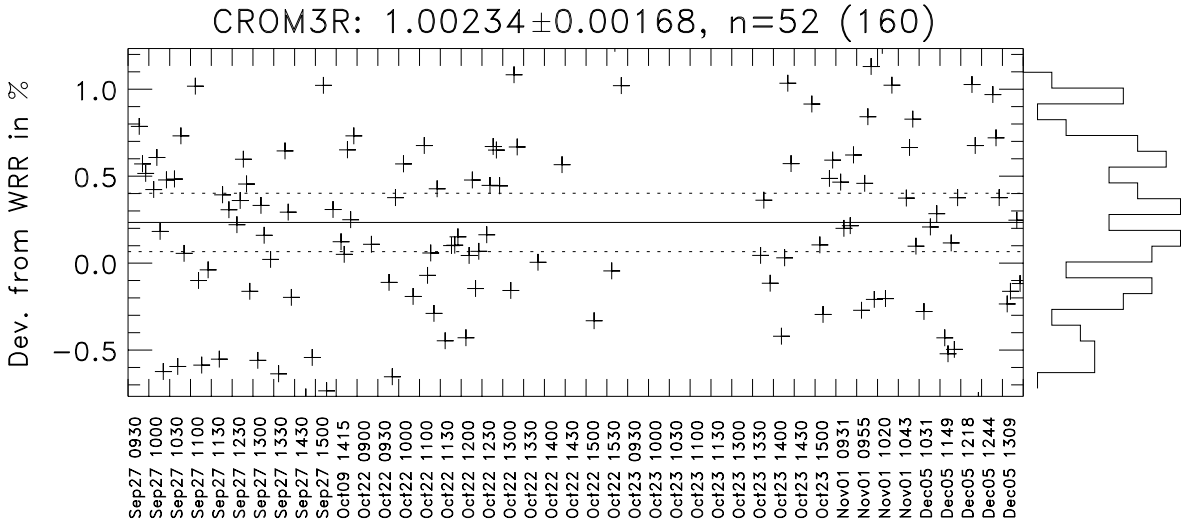

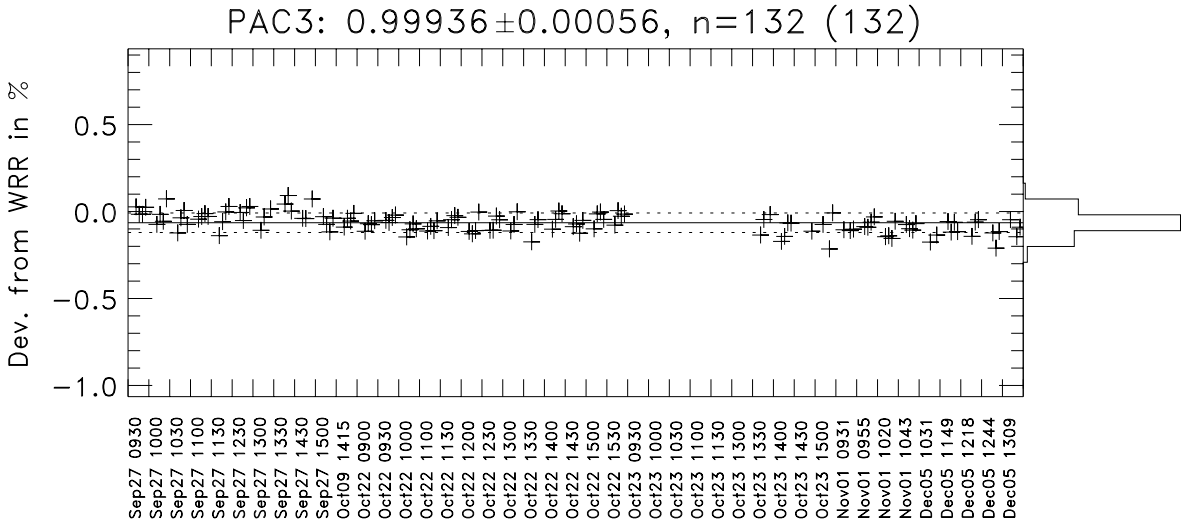

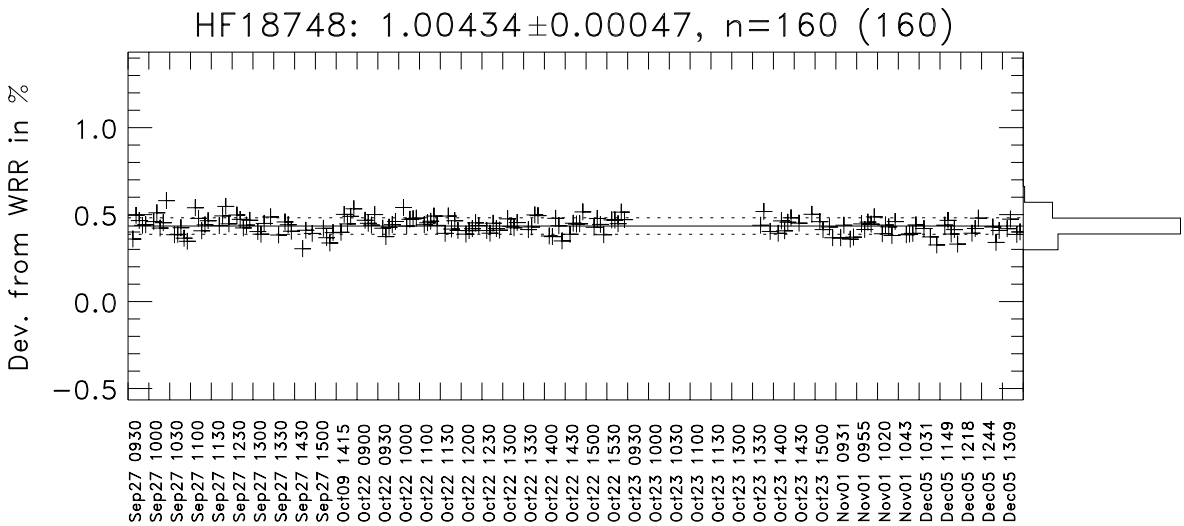

3.1.3 TMI67814

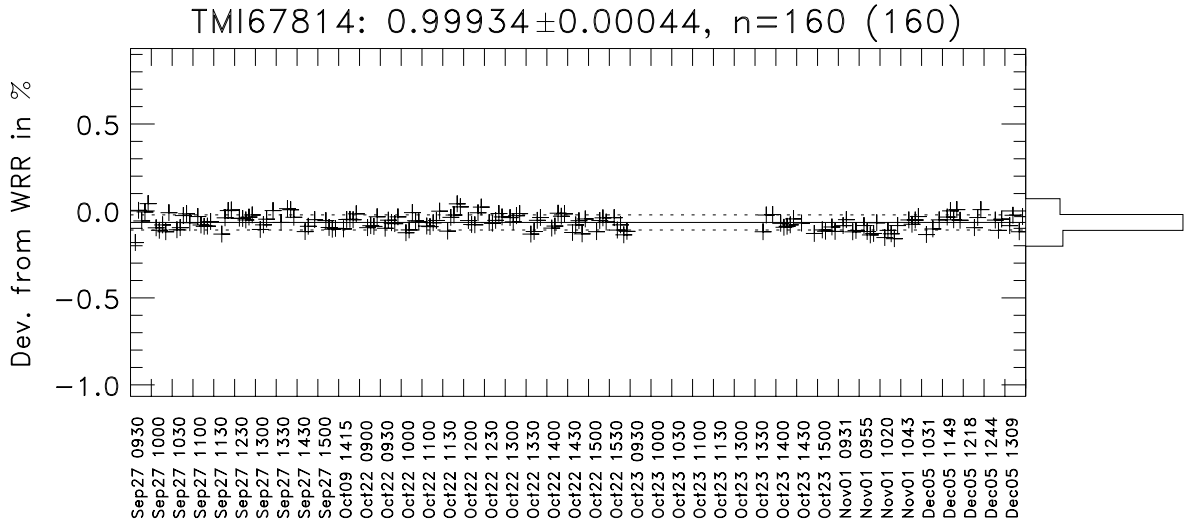

3.1.4 Å171, Å212, Å538

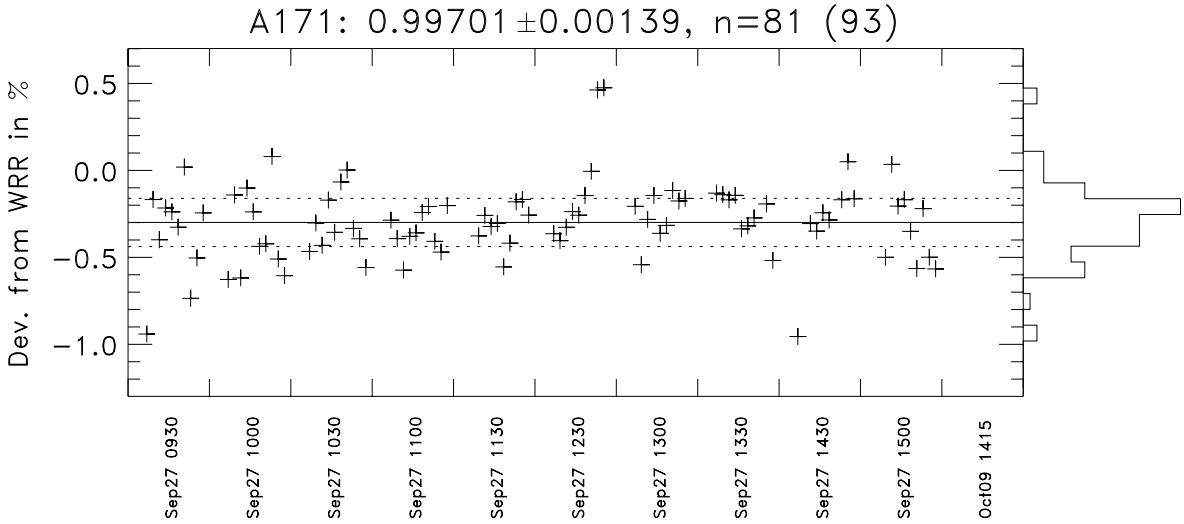

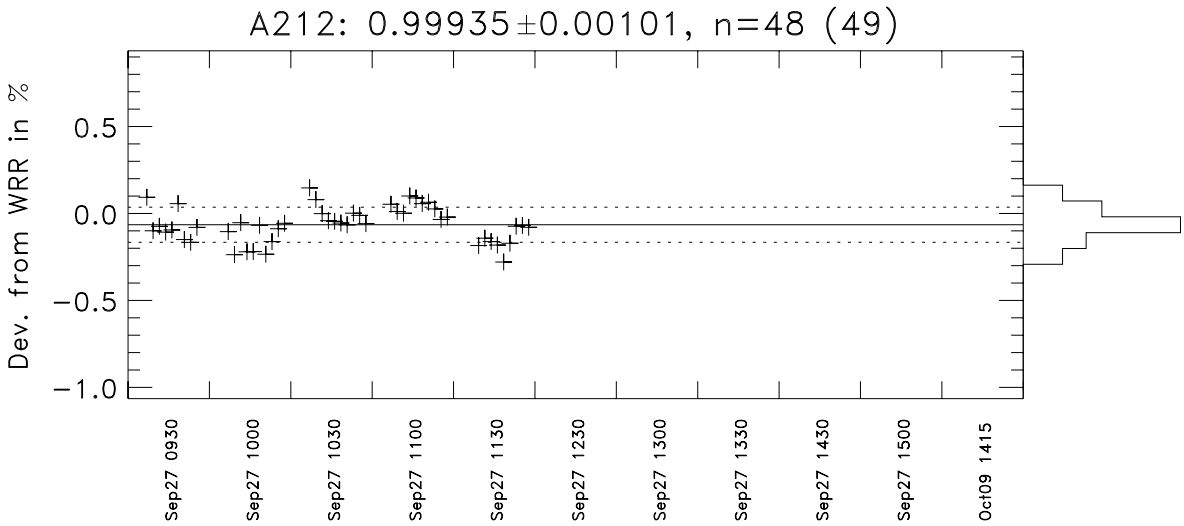

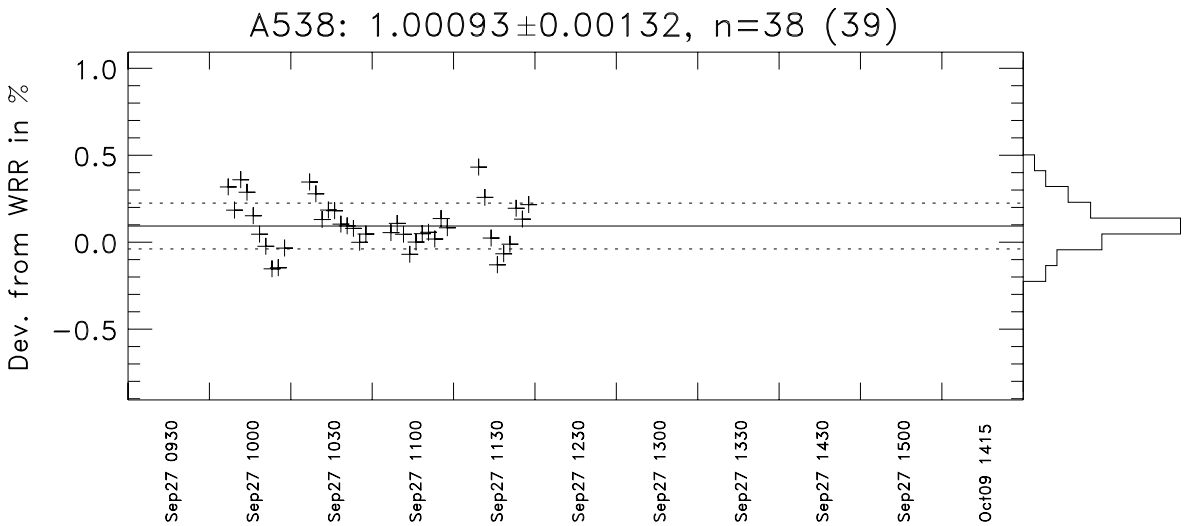

3.1.5 Å567, Å576, Å578

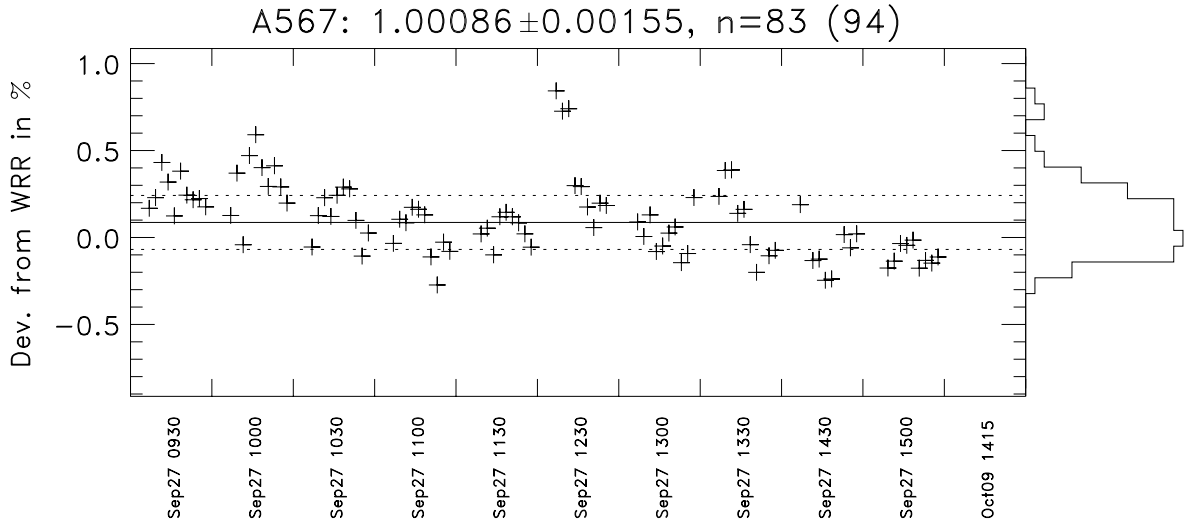

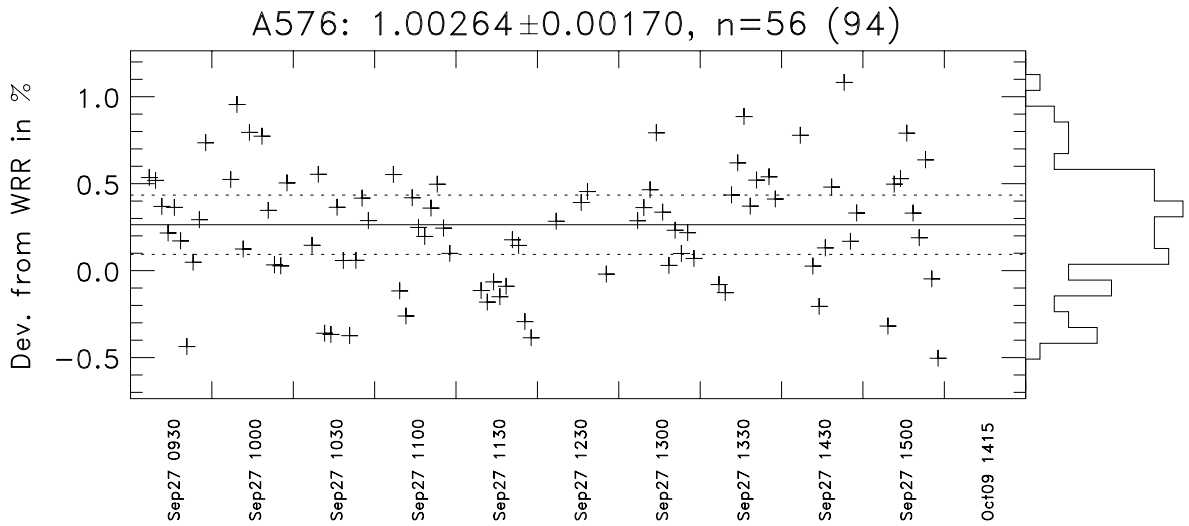

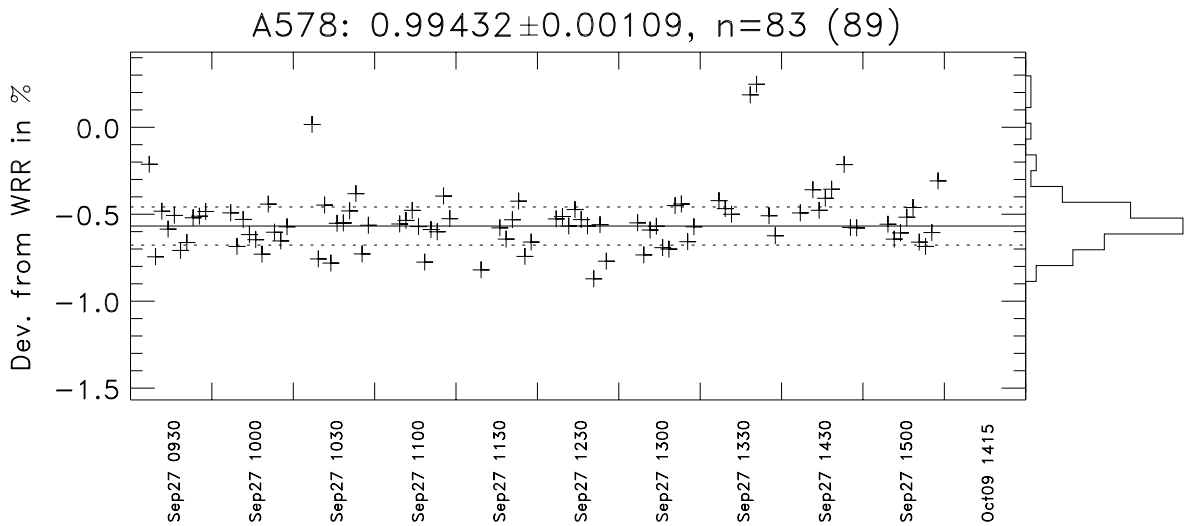

3.1.6 Å702, Å6549, Å12578

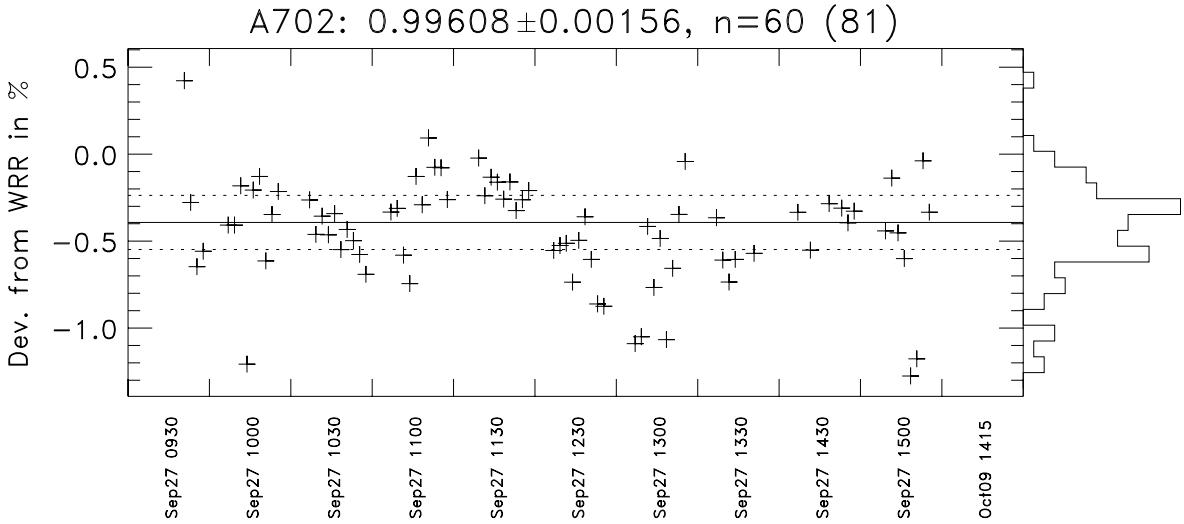

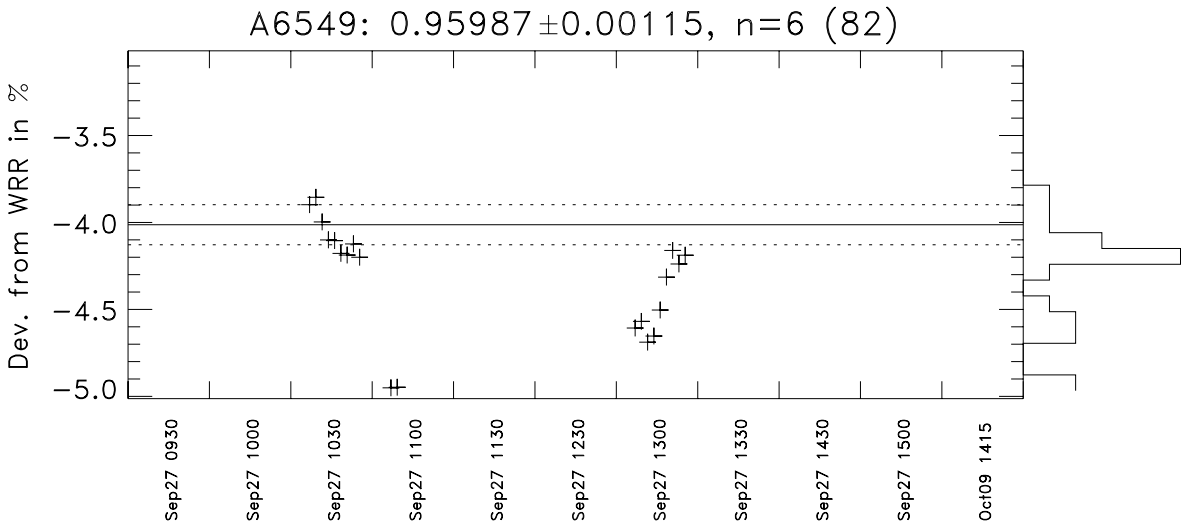

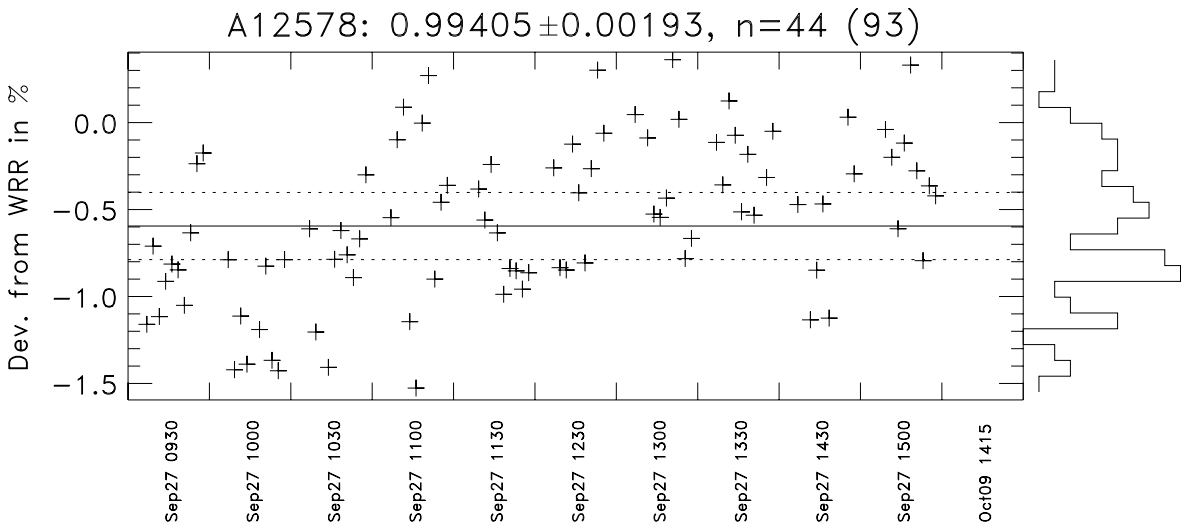

3.1.7 Å13439, Å15192, Å18020

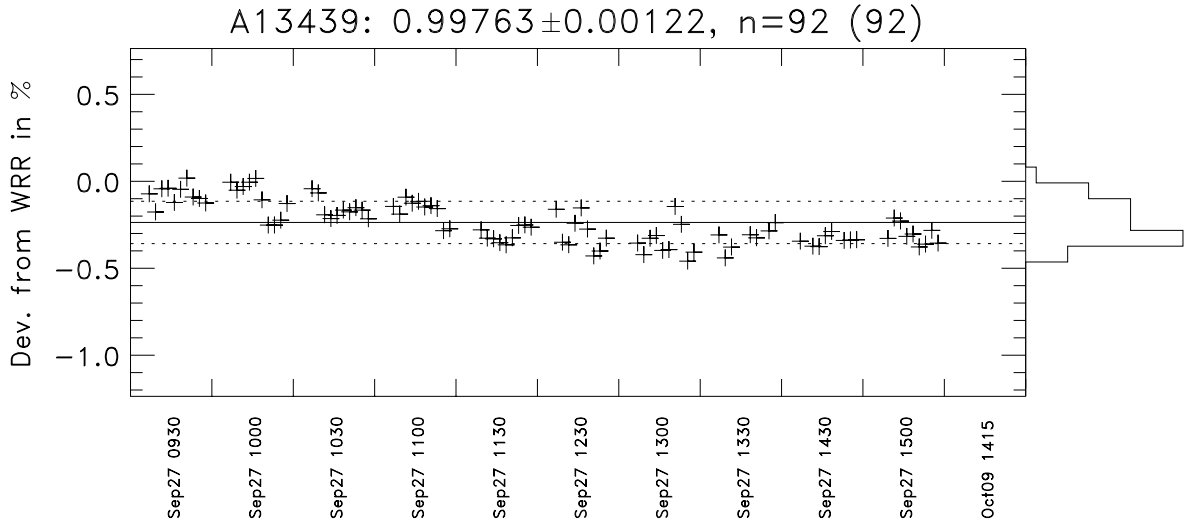

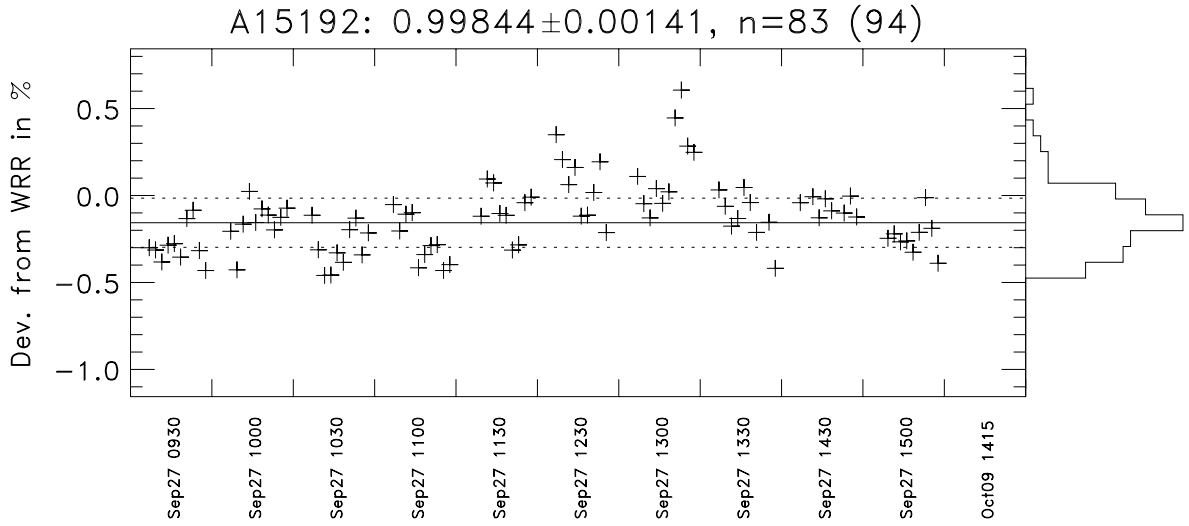

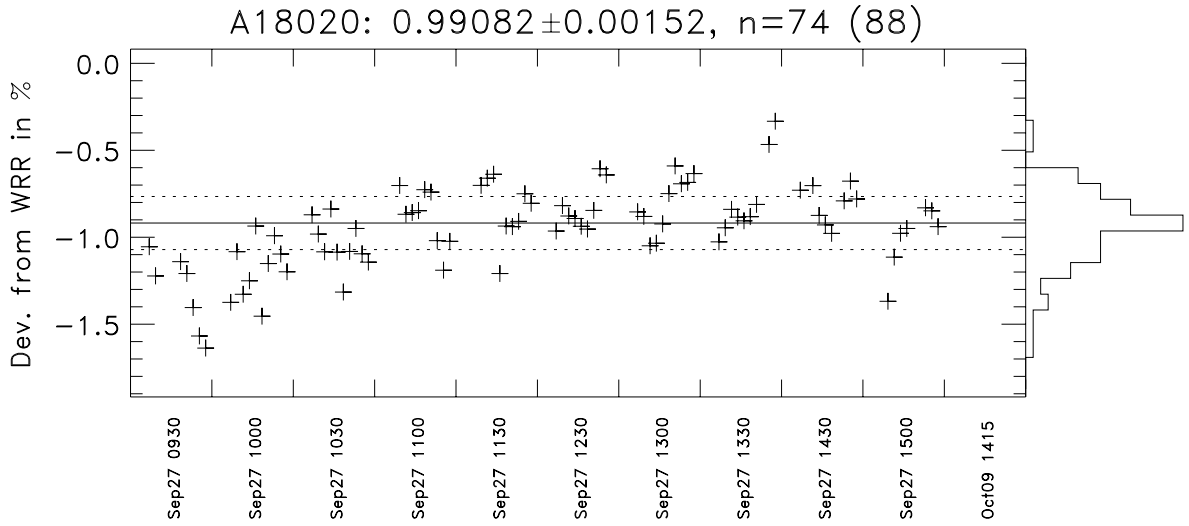

3.1.8 Å18587, CROM5R, CROM6R

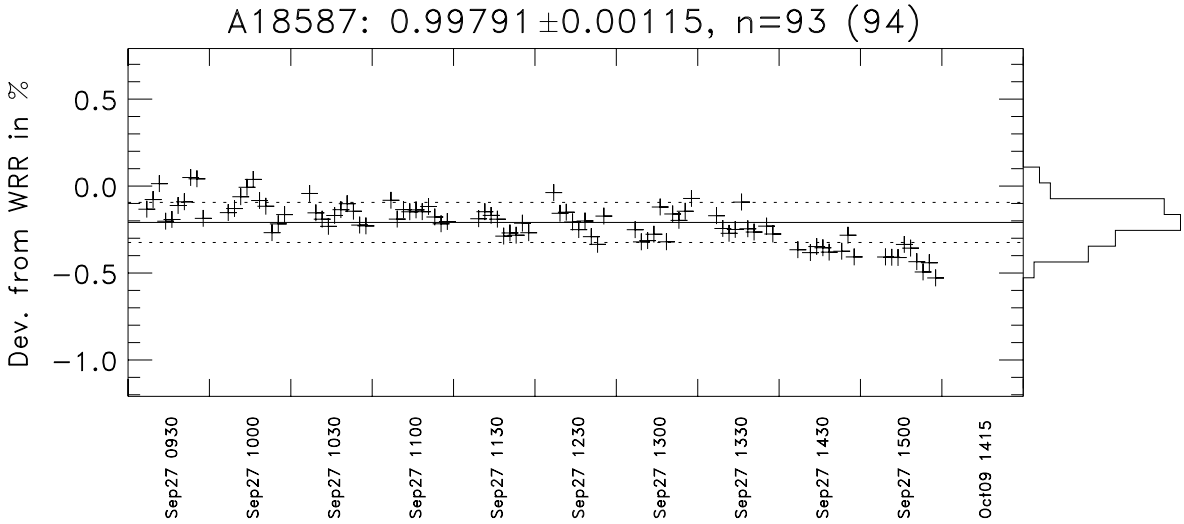

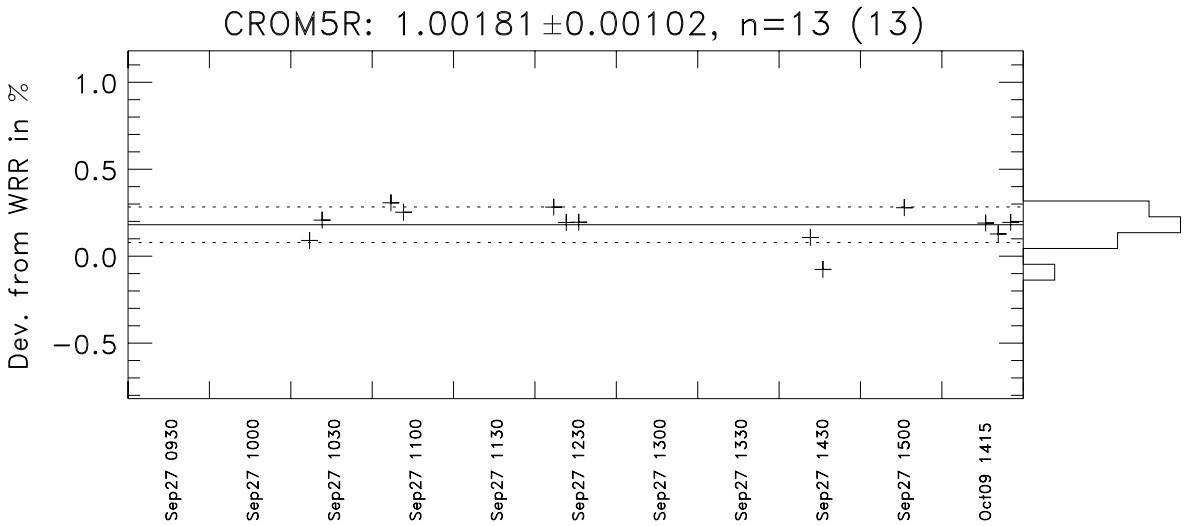

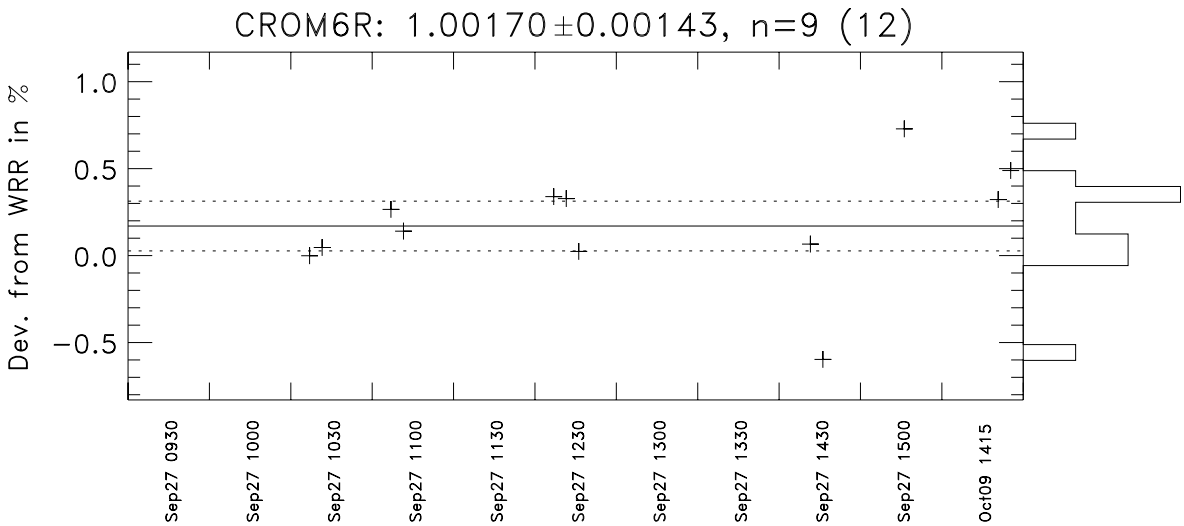

3.1.9 CROM9L, EPAC-11402, EPAC-13219

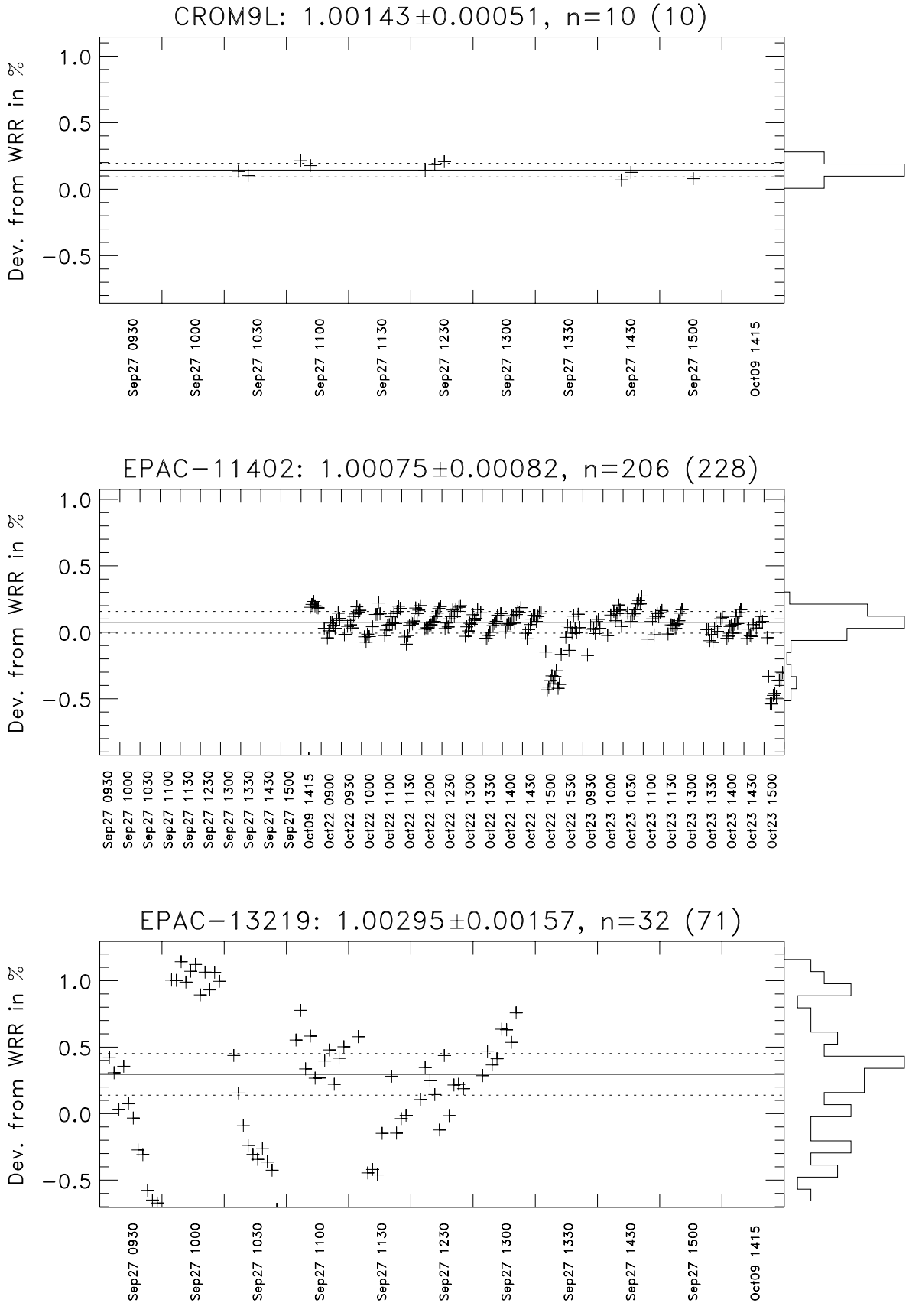

3.1.10 HF14915, HF15744, HF17142

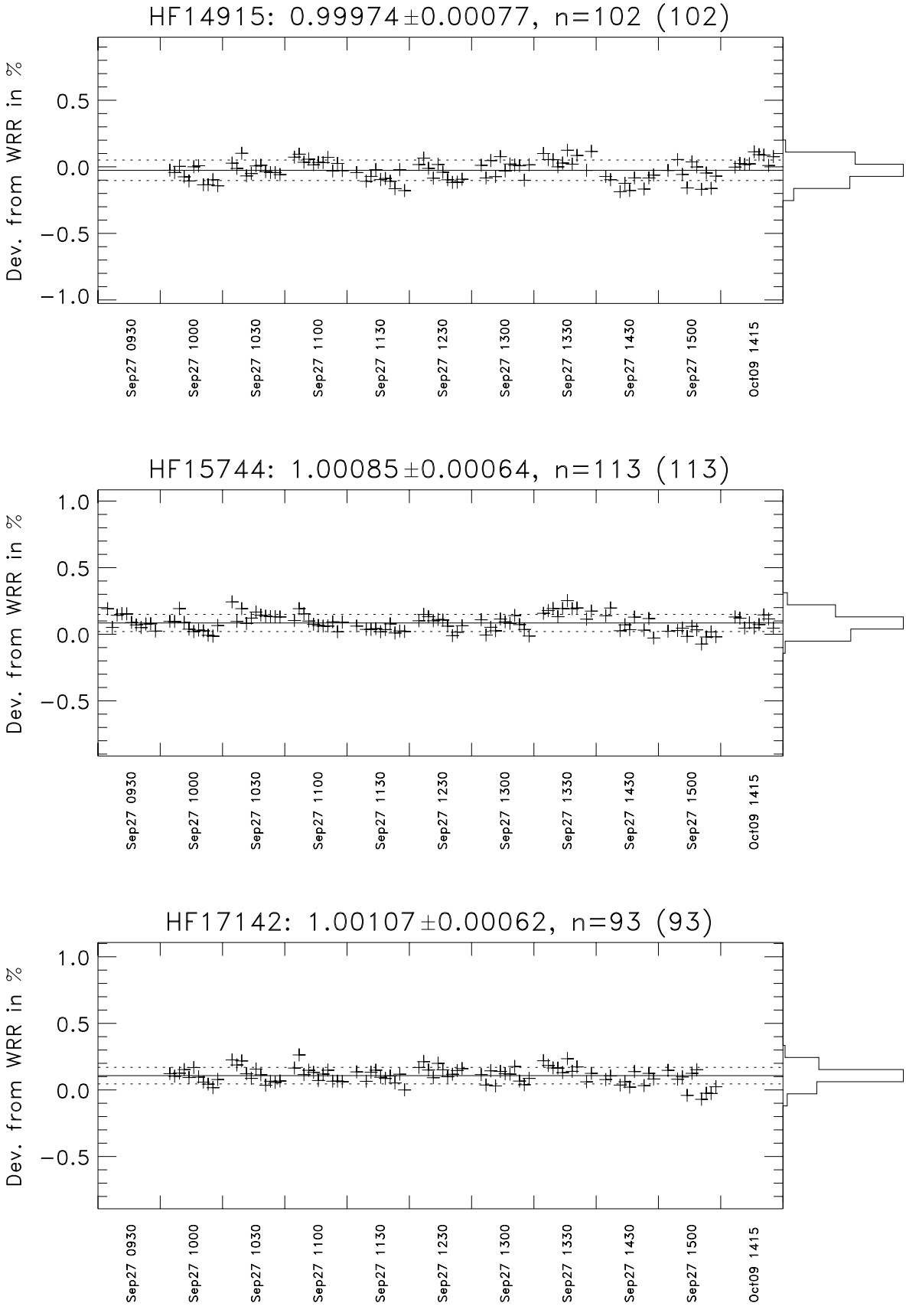

3.1.11 HF18747, HF19743, HF19746

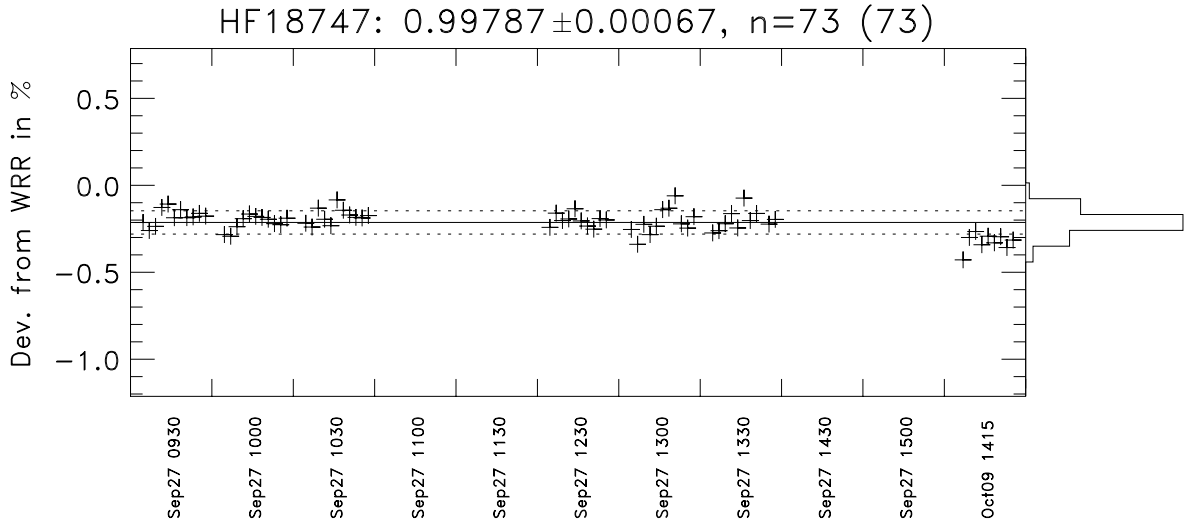

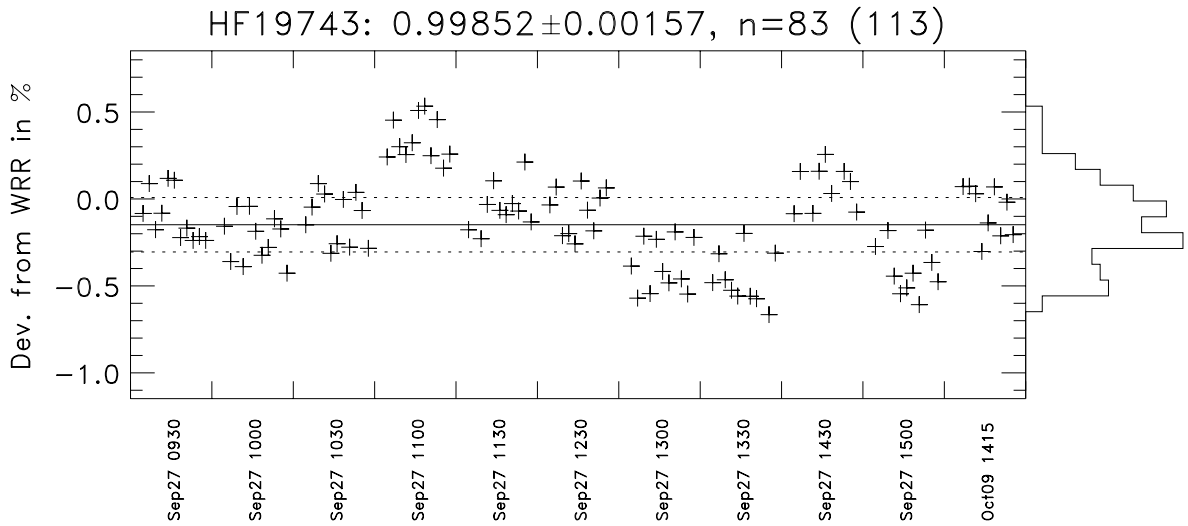

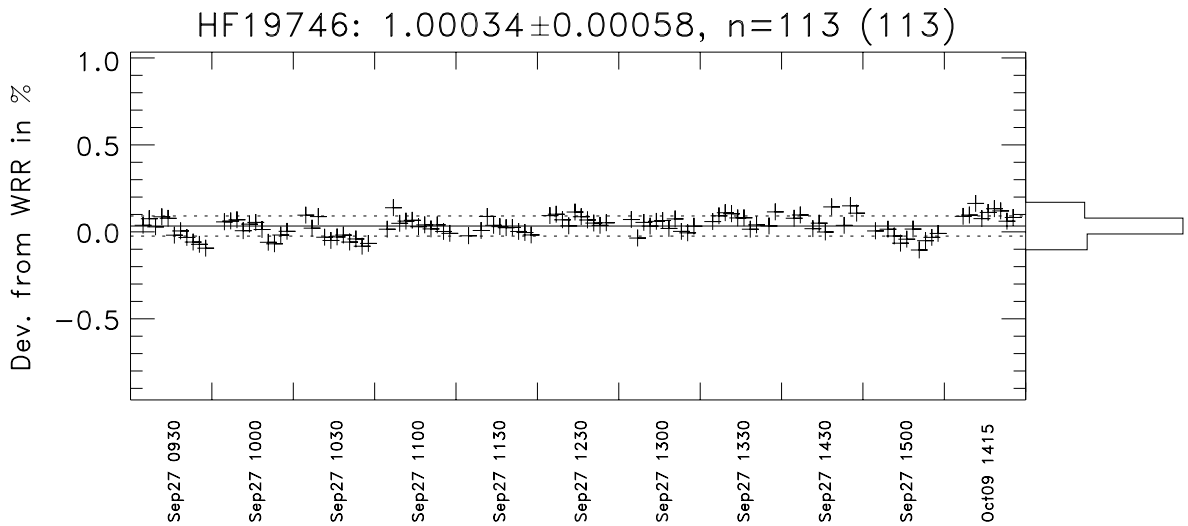

3.1.12 HF20406, HF23737, HF27157

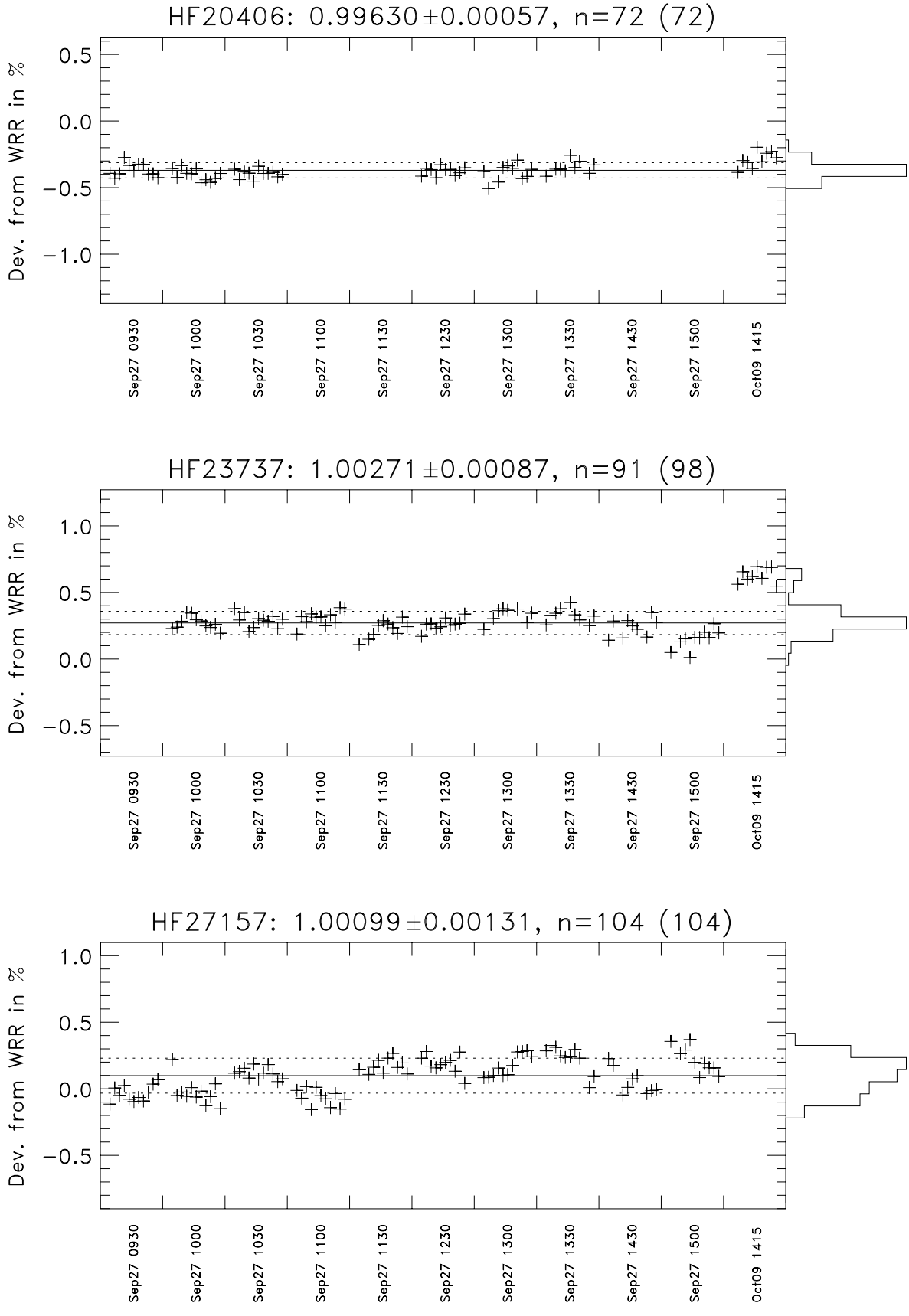

3.1.13 HF27160, HF27162, HF27796

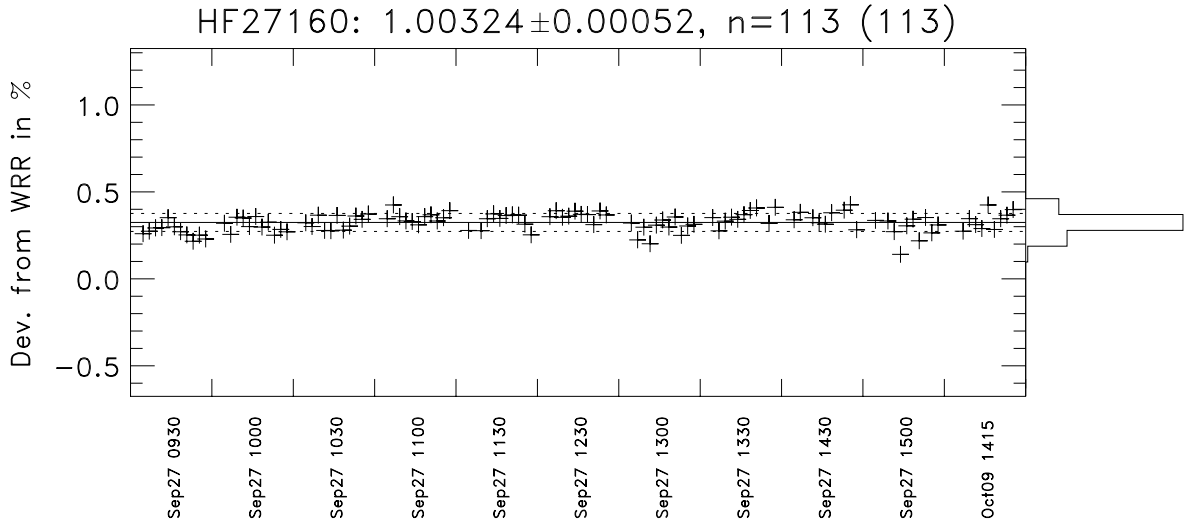

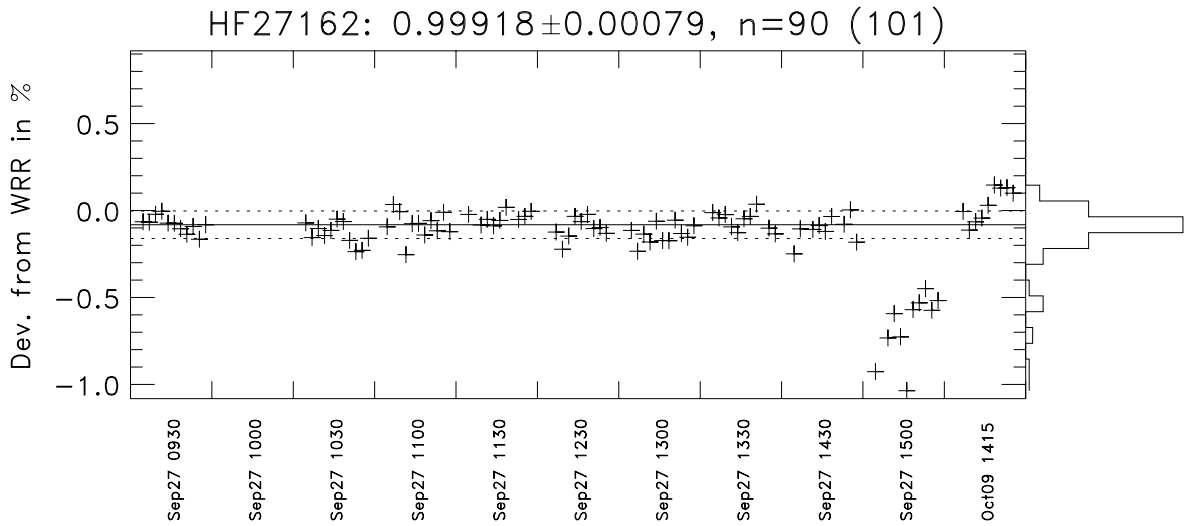

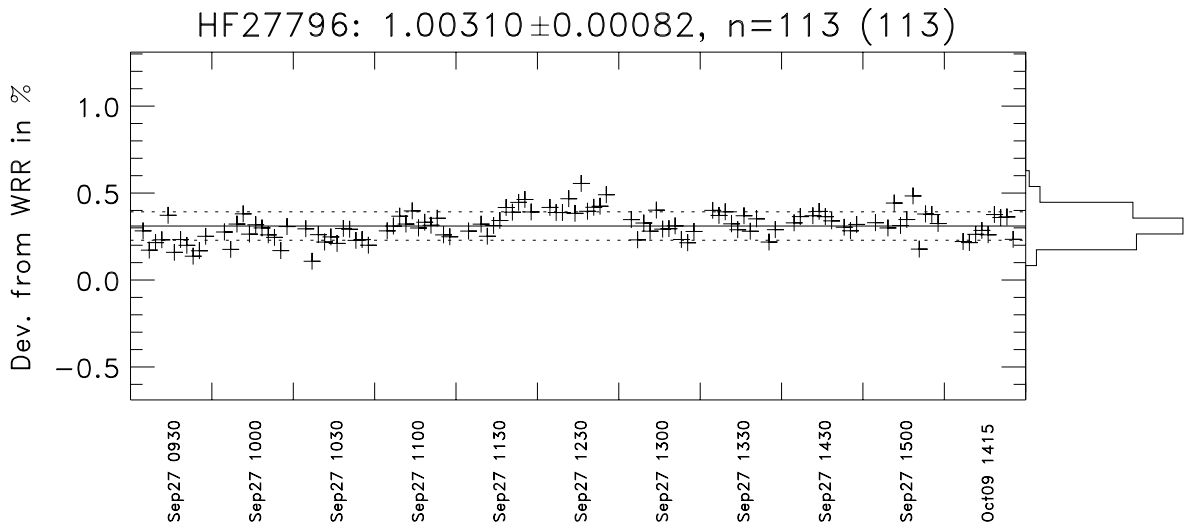

3.1.14 HF27798, HF28553, HF28965

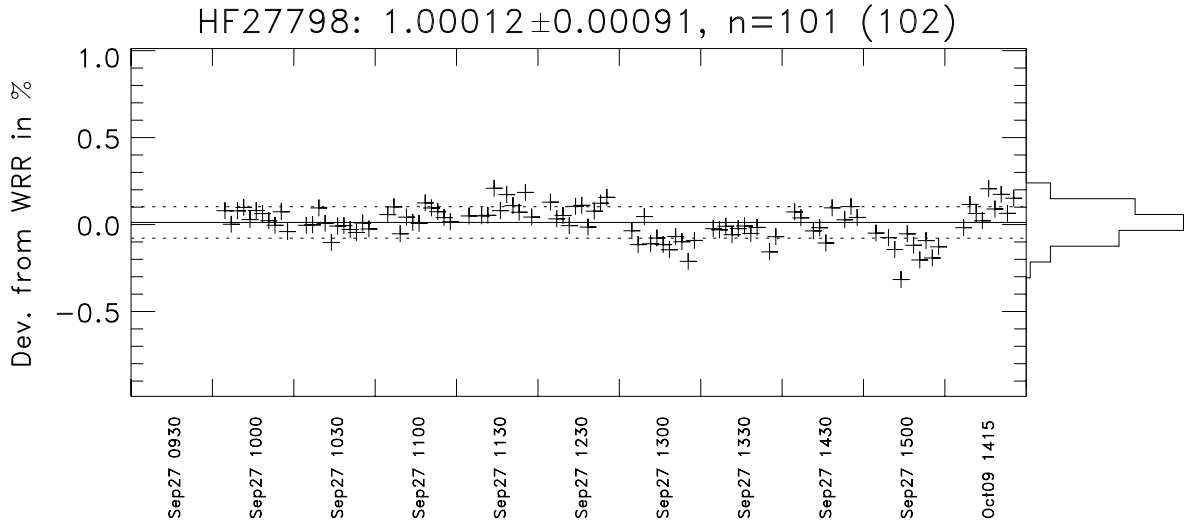

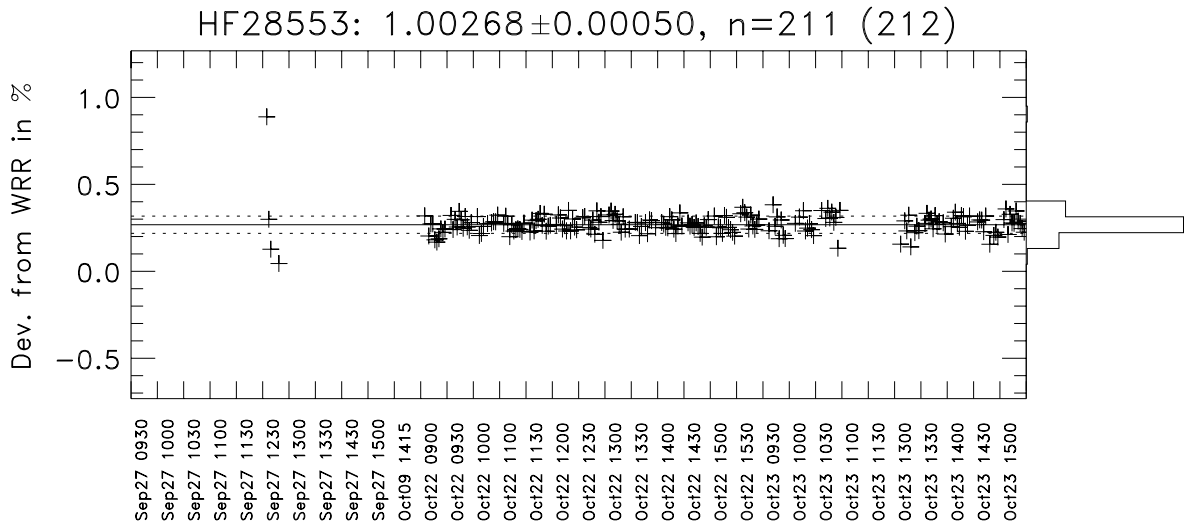

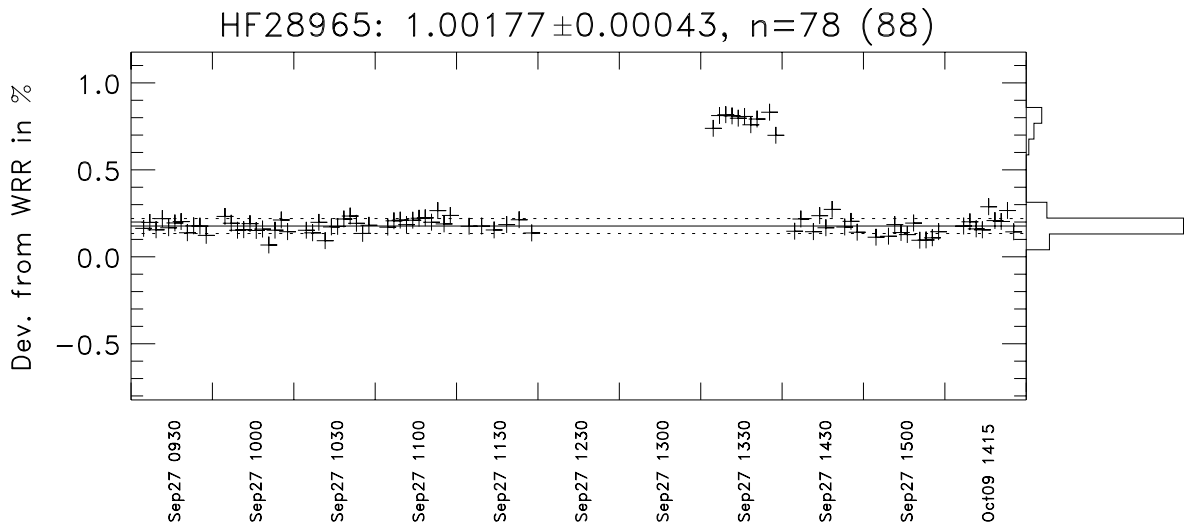

3.1.15 HF28968, HF29220, HF29223

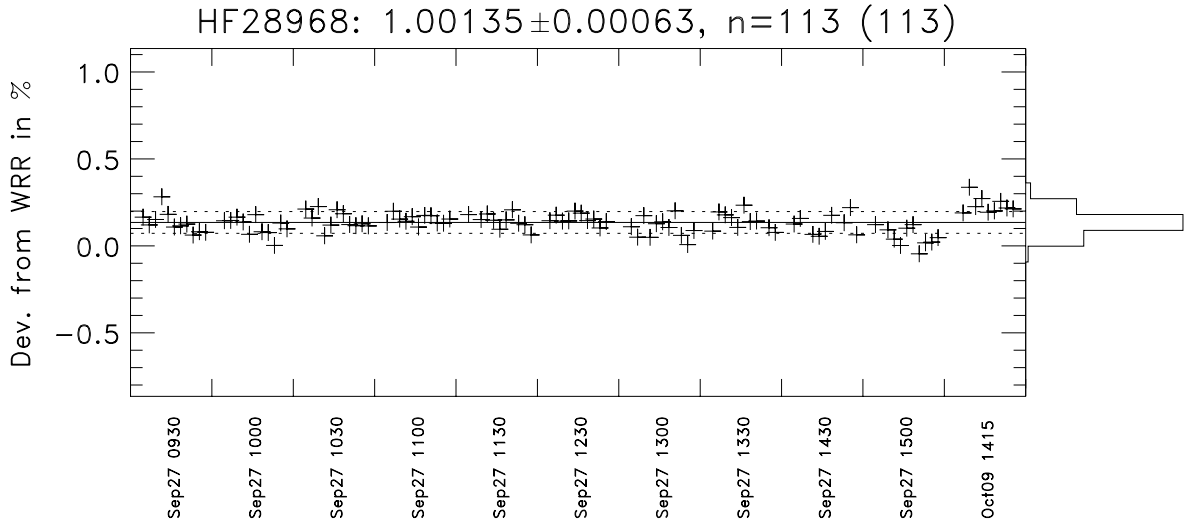

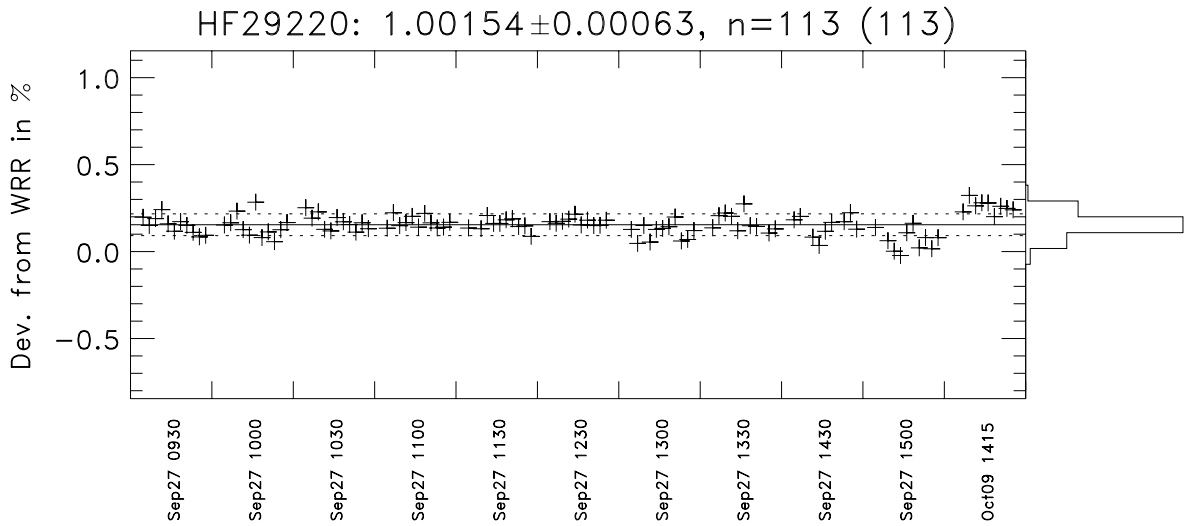

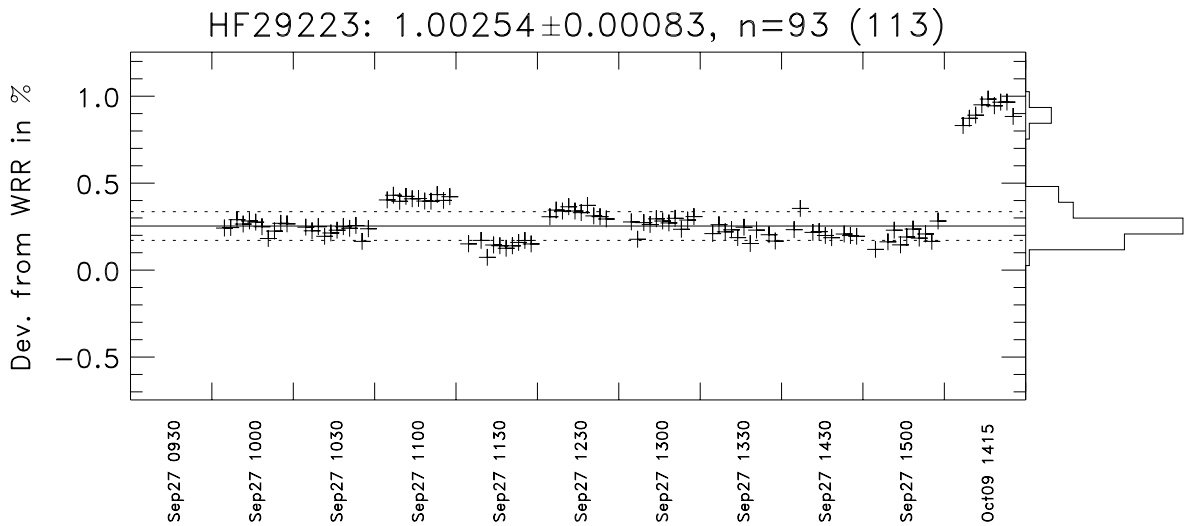

3.1.16 HF29225, HF30112, HF30492

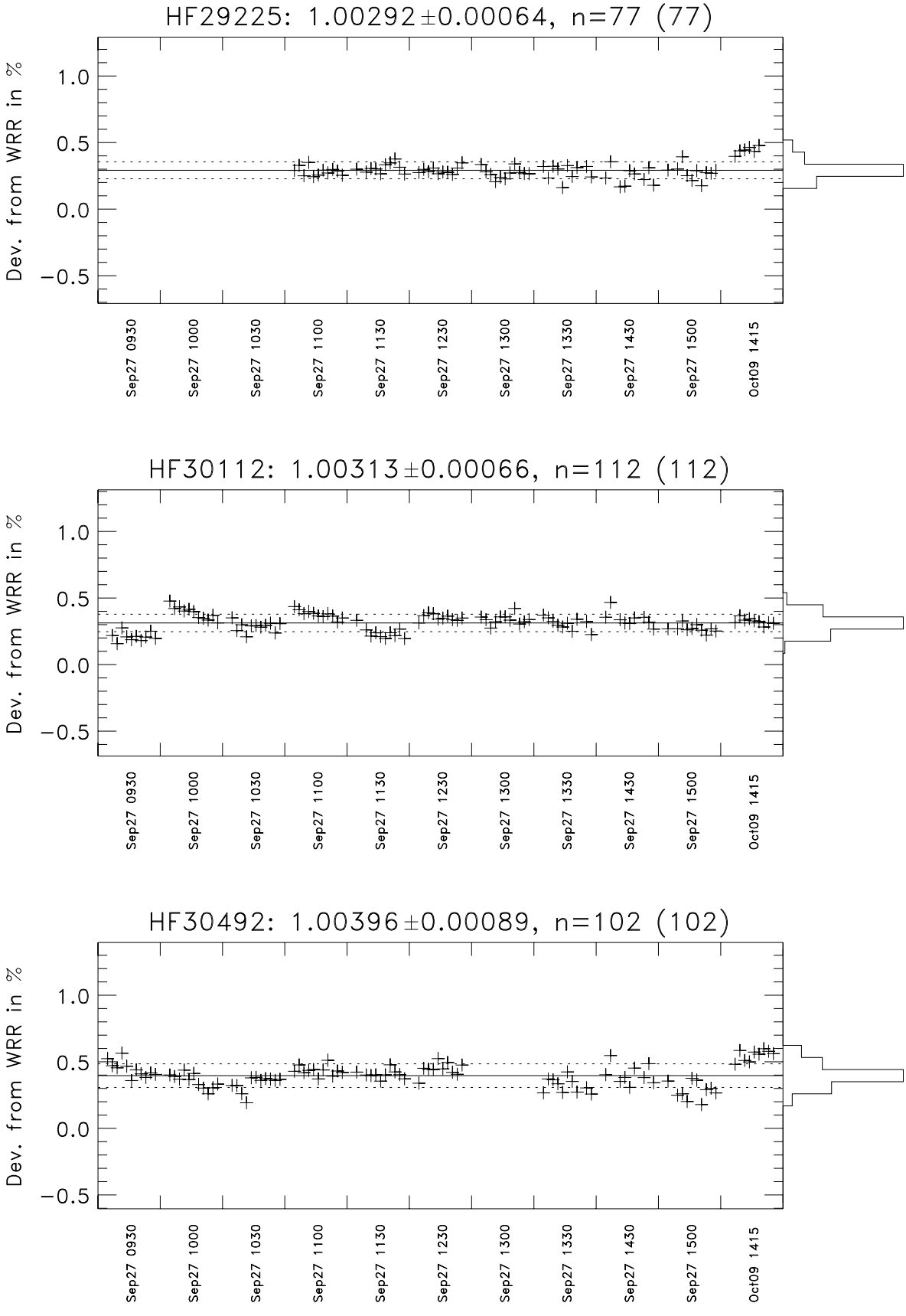

3.1.17 HF30497, HF30713, HF30716

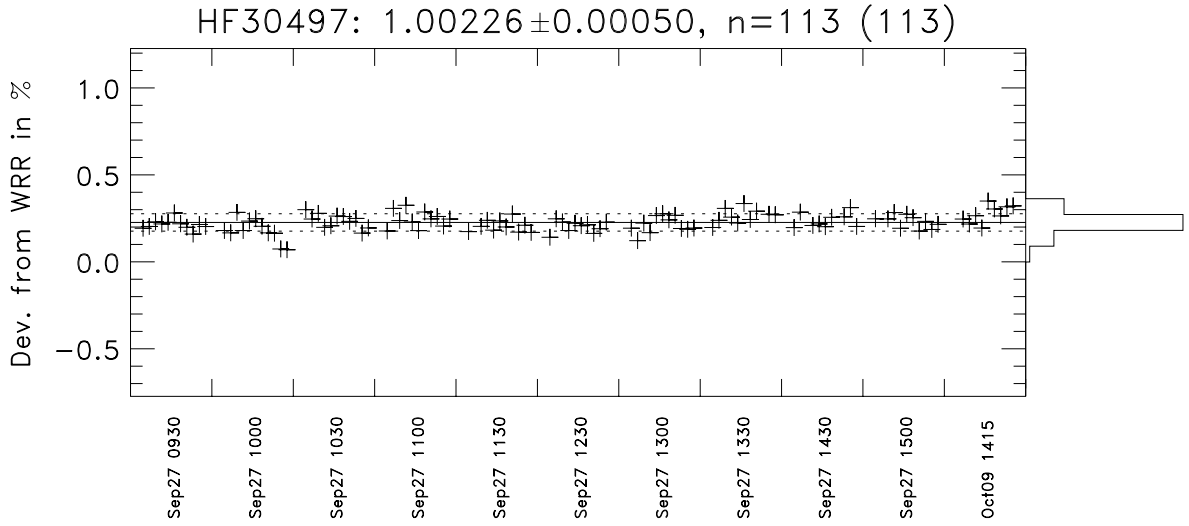

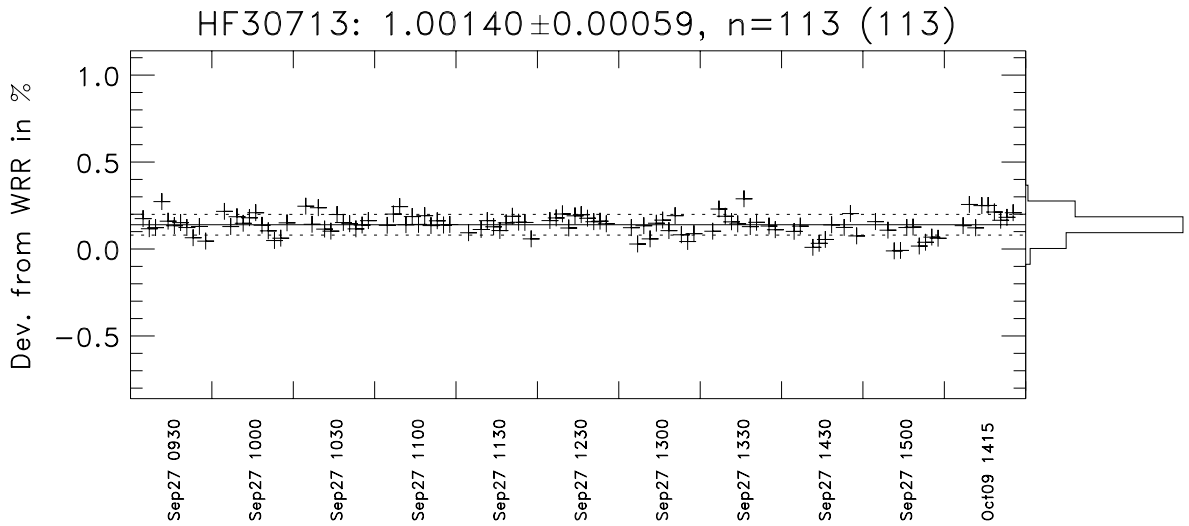

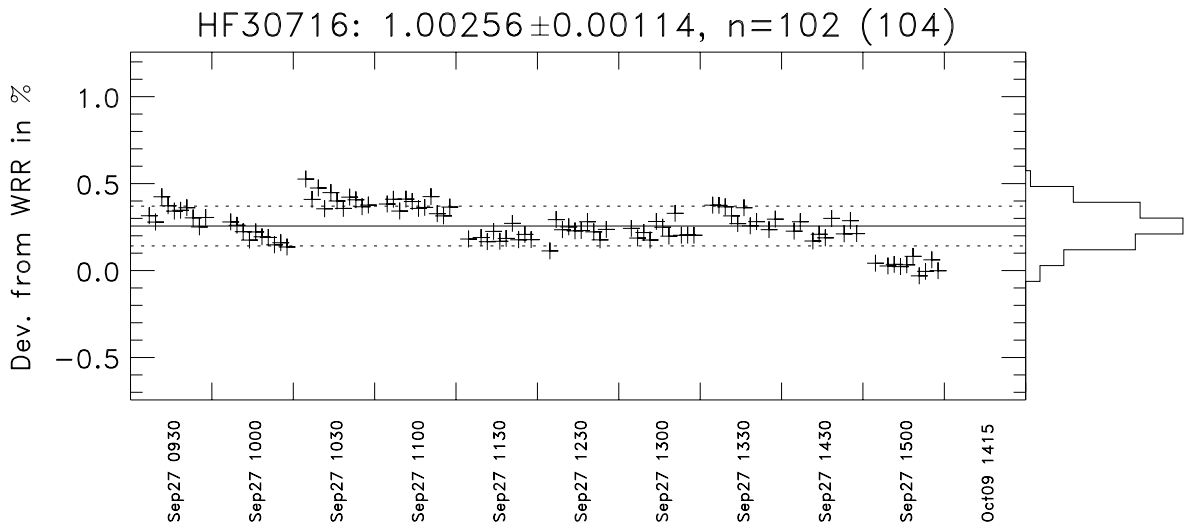

3.1.18 HF31041, HF31103, HF31110

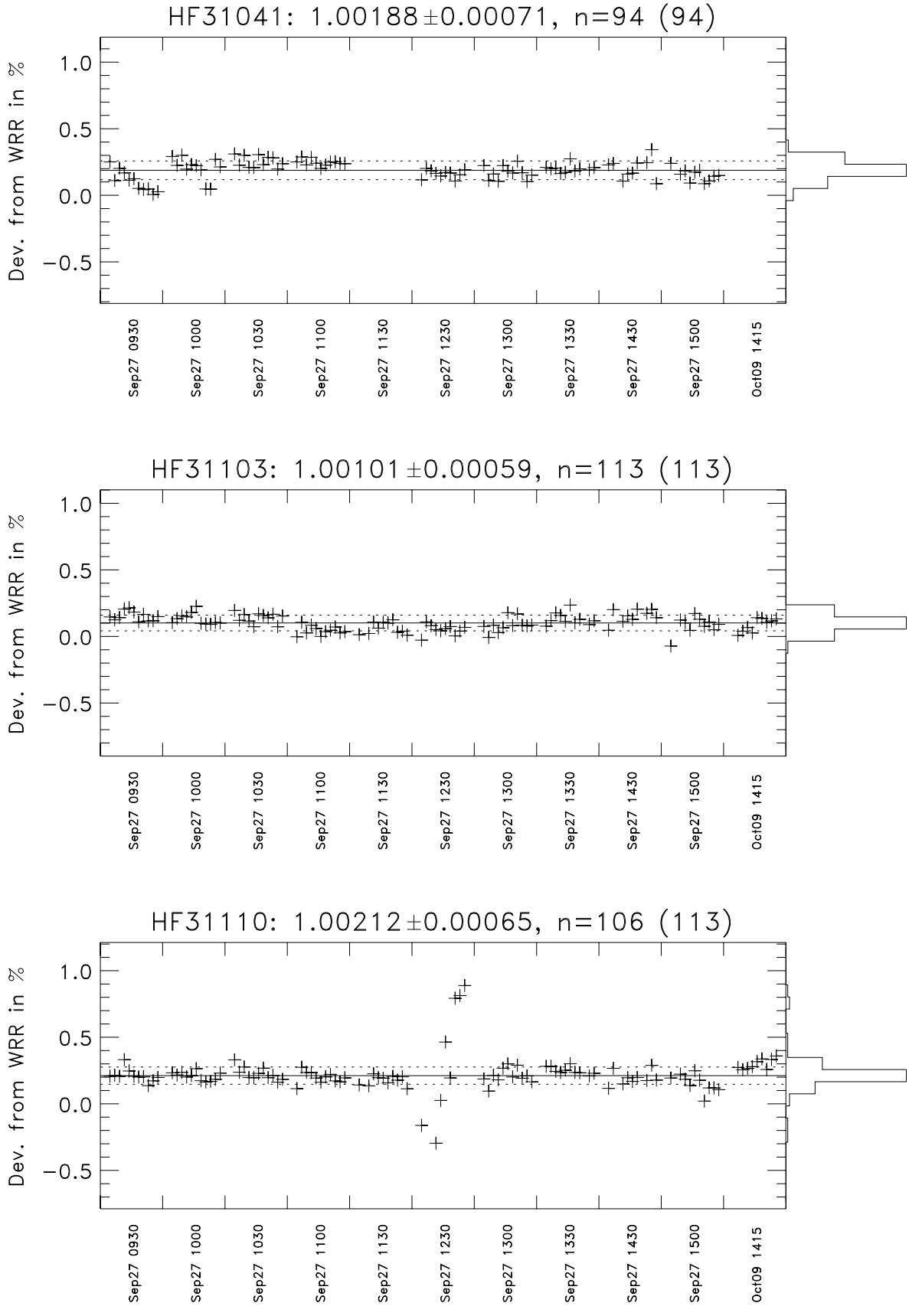

3.1.19 HF31117, HF32446, HF32448

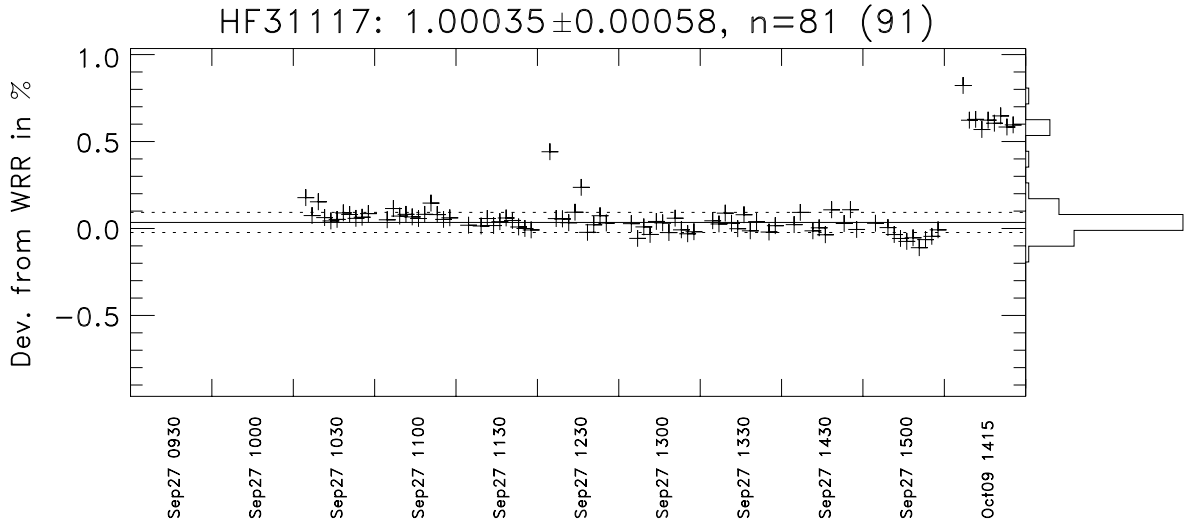

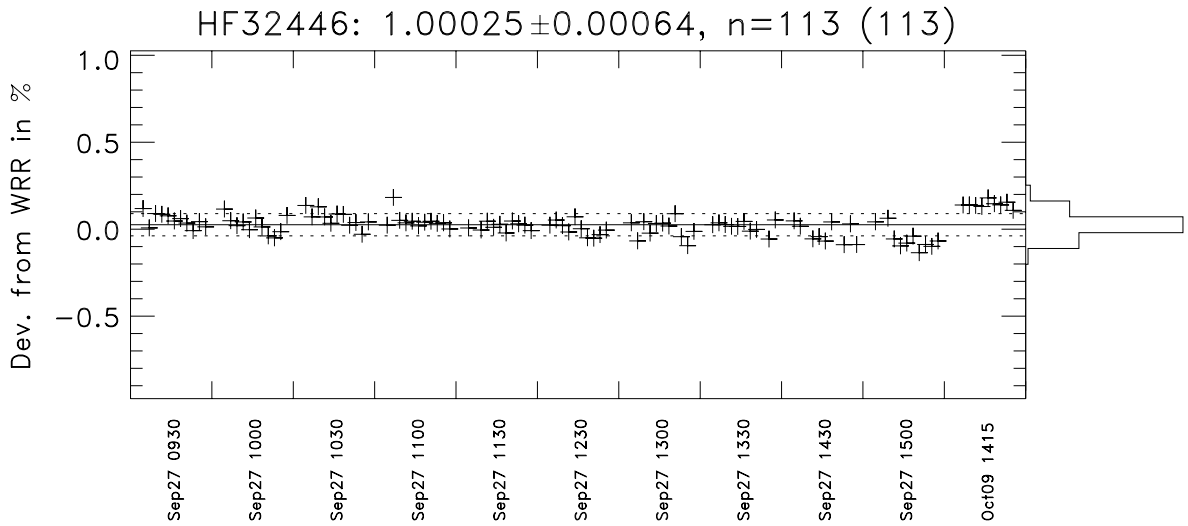

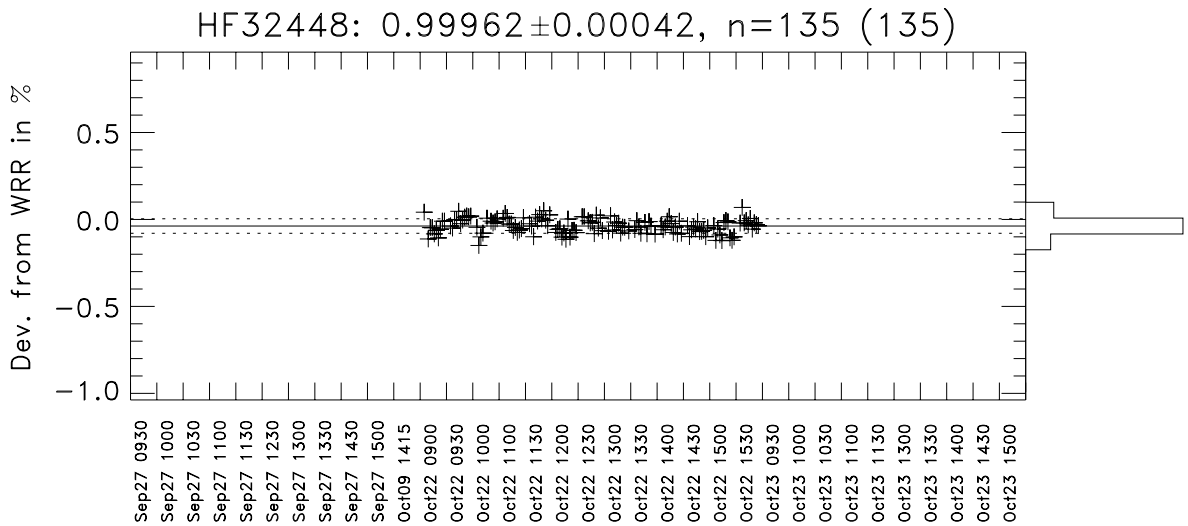

3.1.20 HF32449, MAR-1-1, PMO6-5

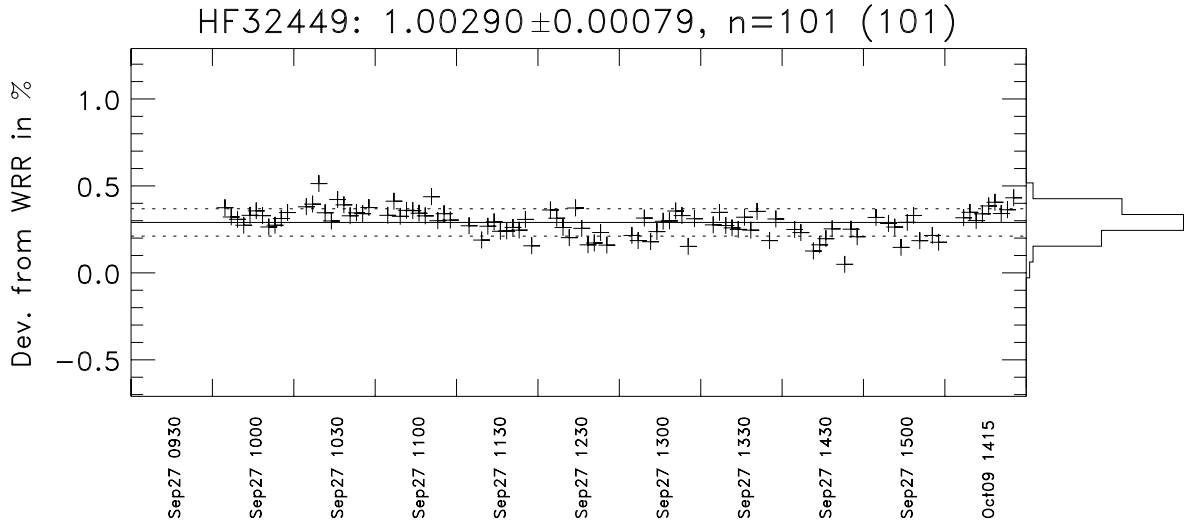

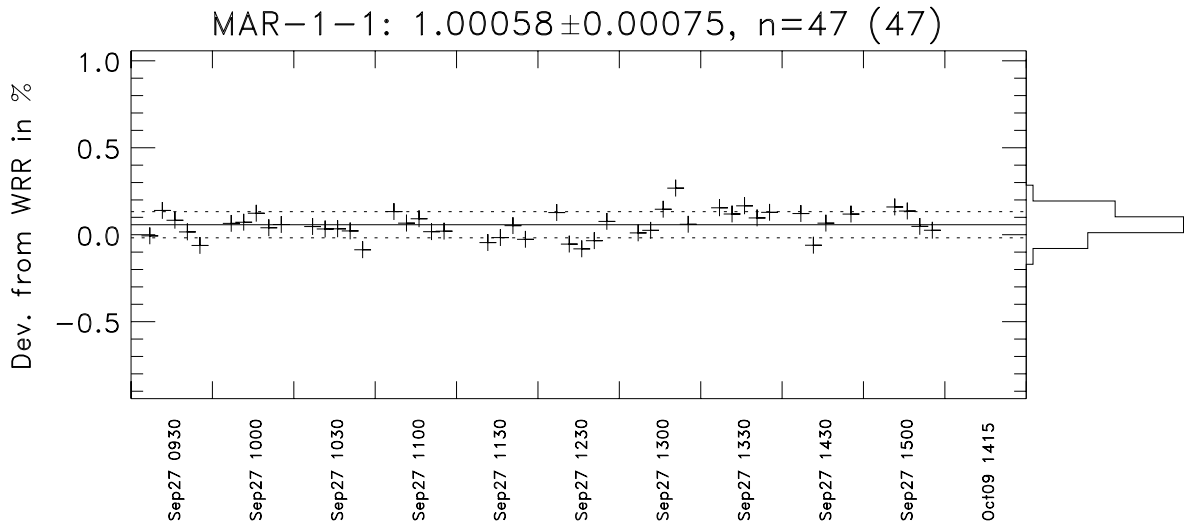

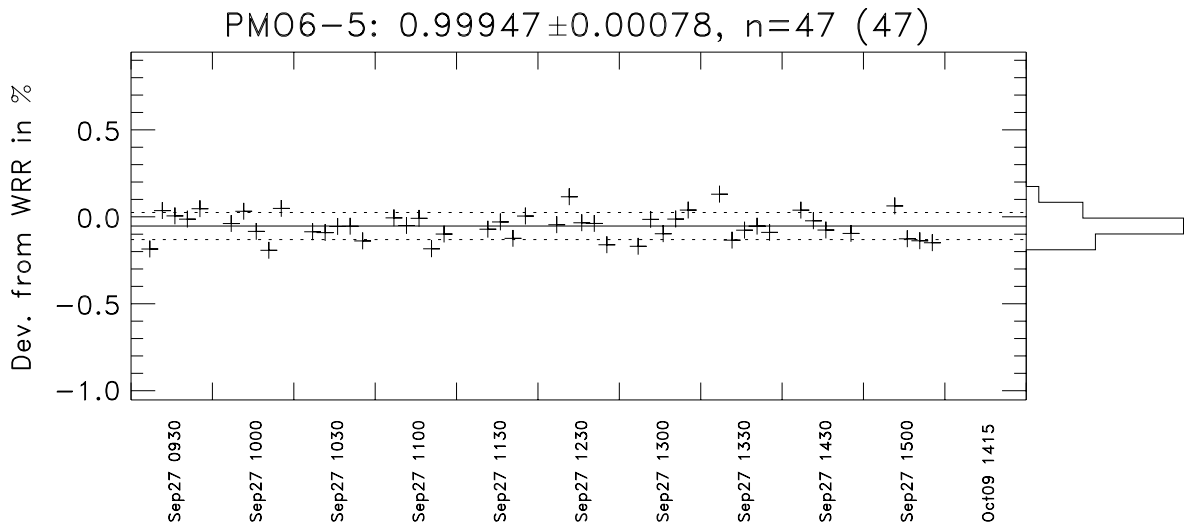

3.1.21 PMO609, PMO611, PMO6-79-121

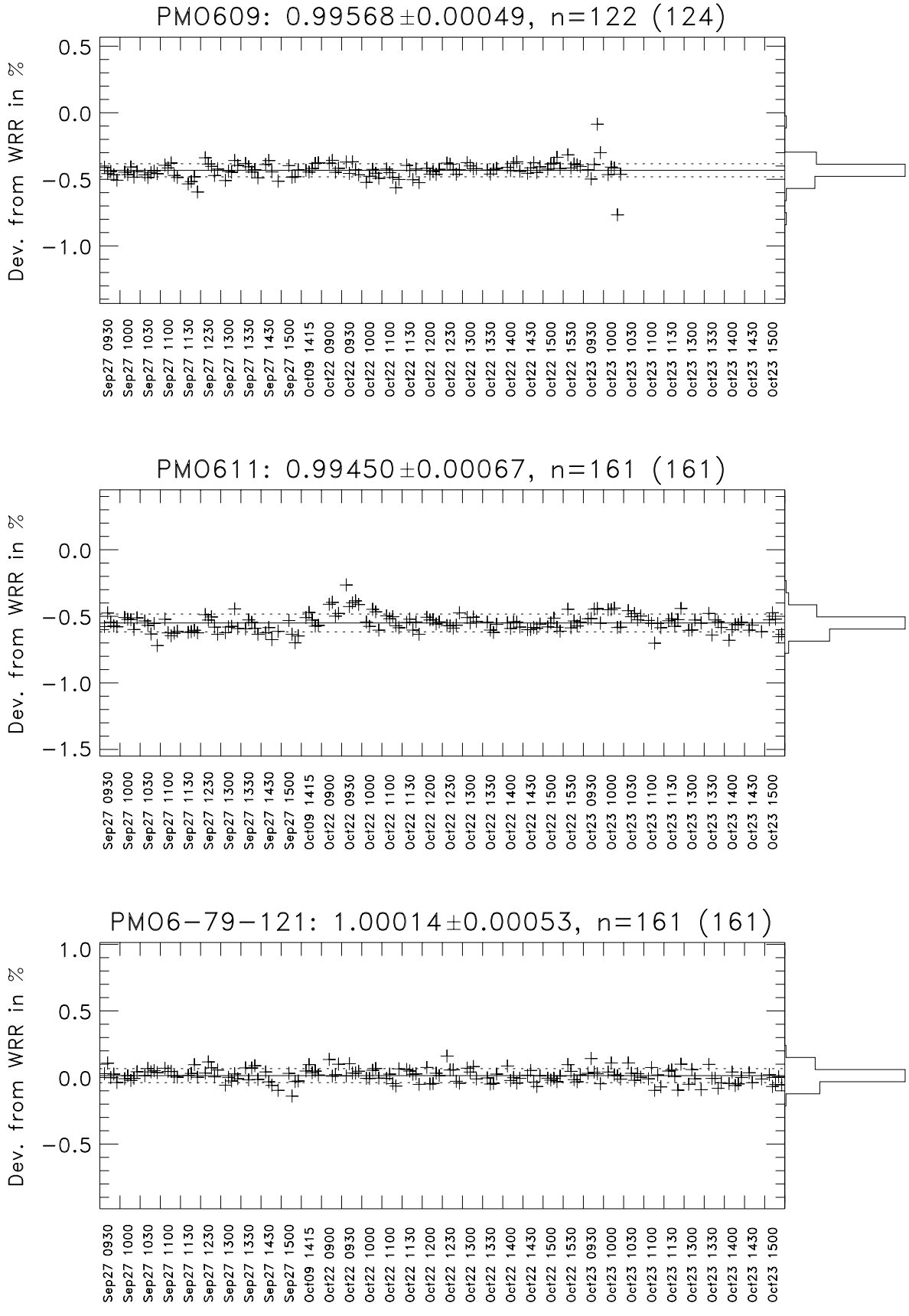

3.1.22 PMO6-79-123, PMO6-81109, PMO6-811103

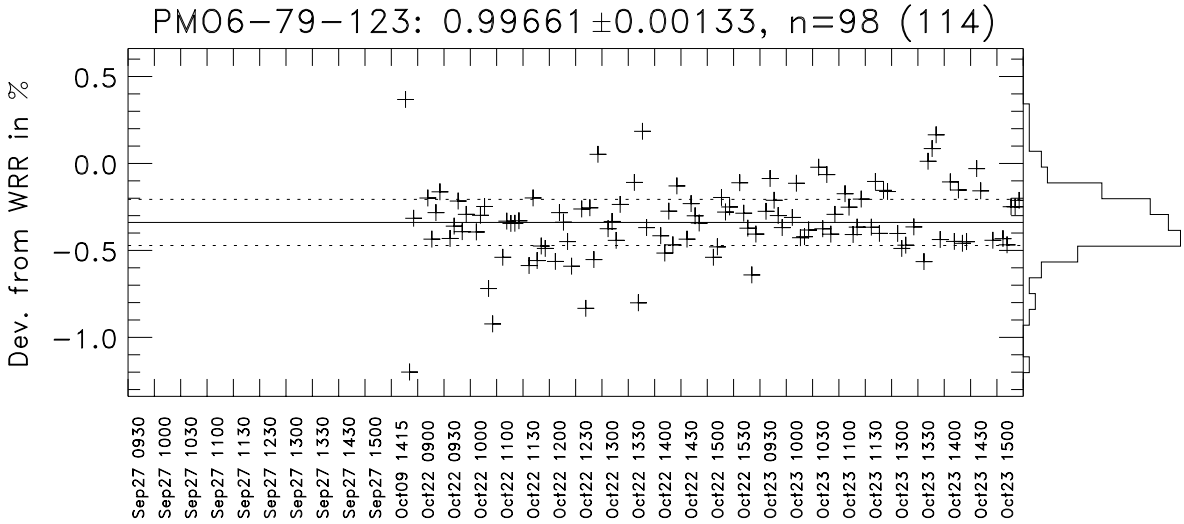

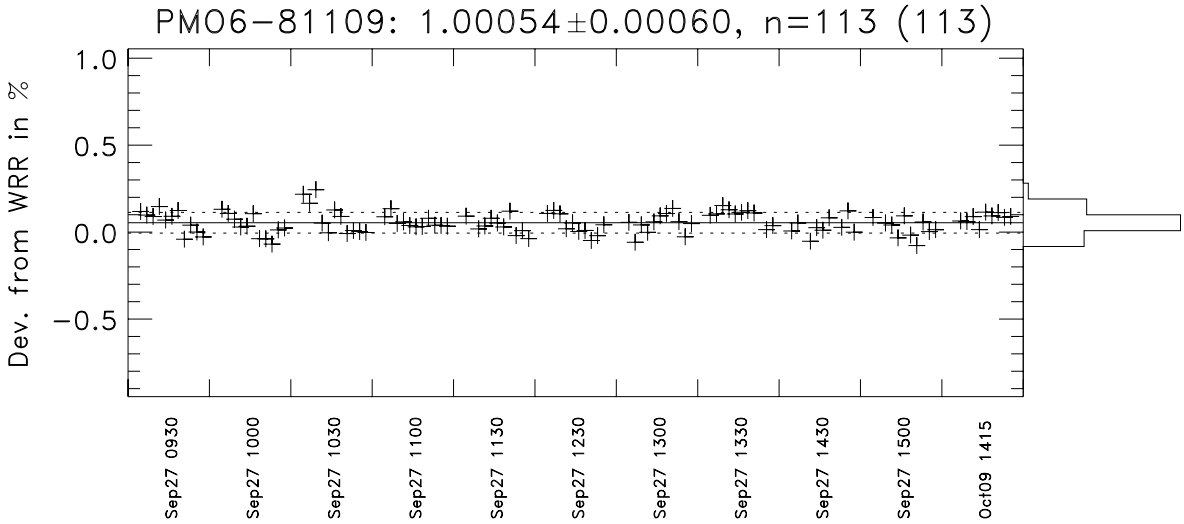

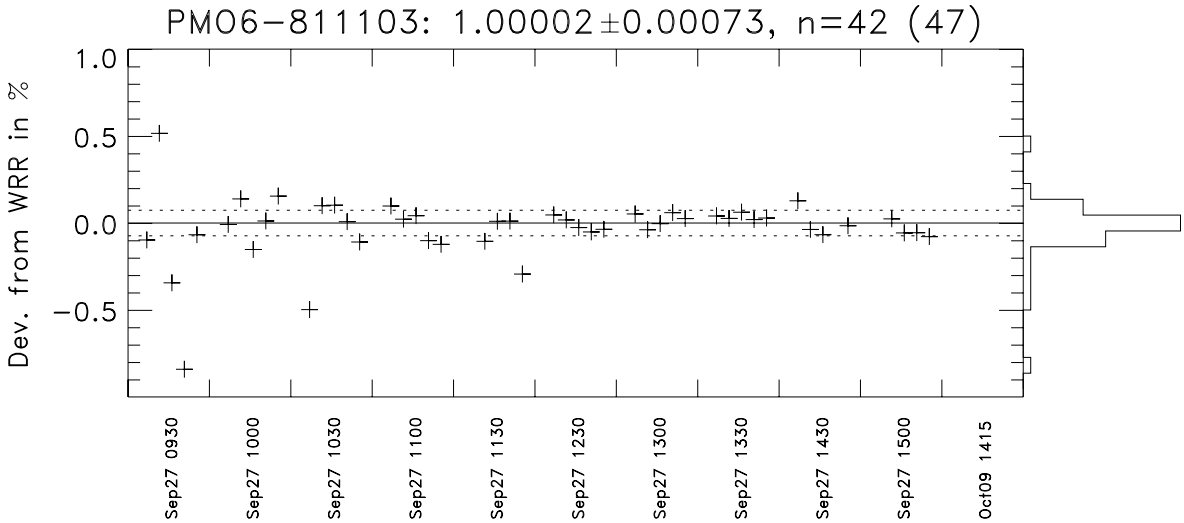

3.1.23 PMO6-811107, PMO6-811108, PMO6-850405

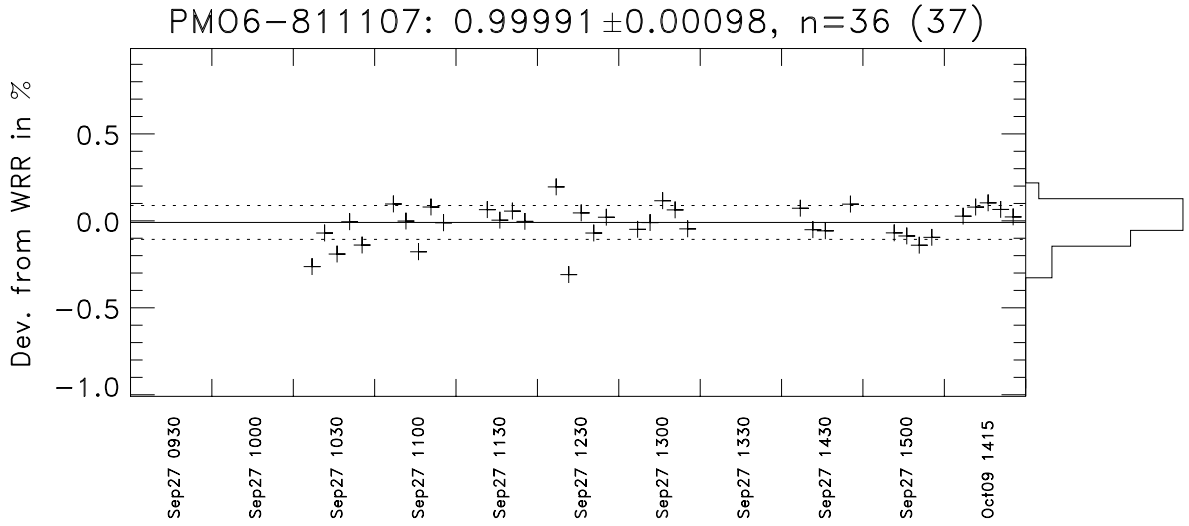

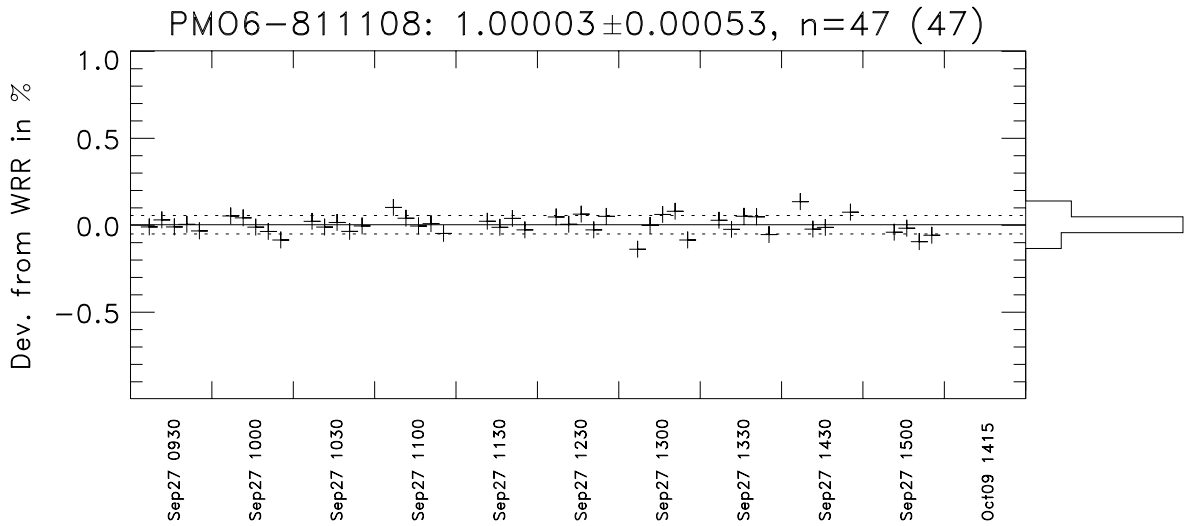

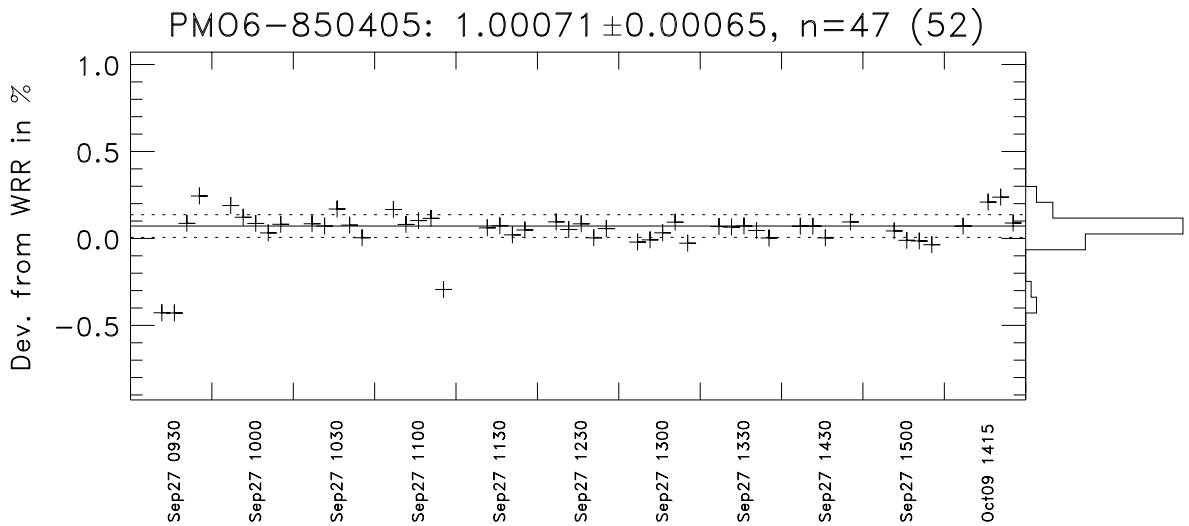

3.1.24 PMO6-850406, PMO6-850408, PMO6-850410

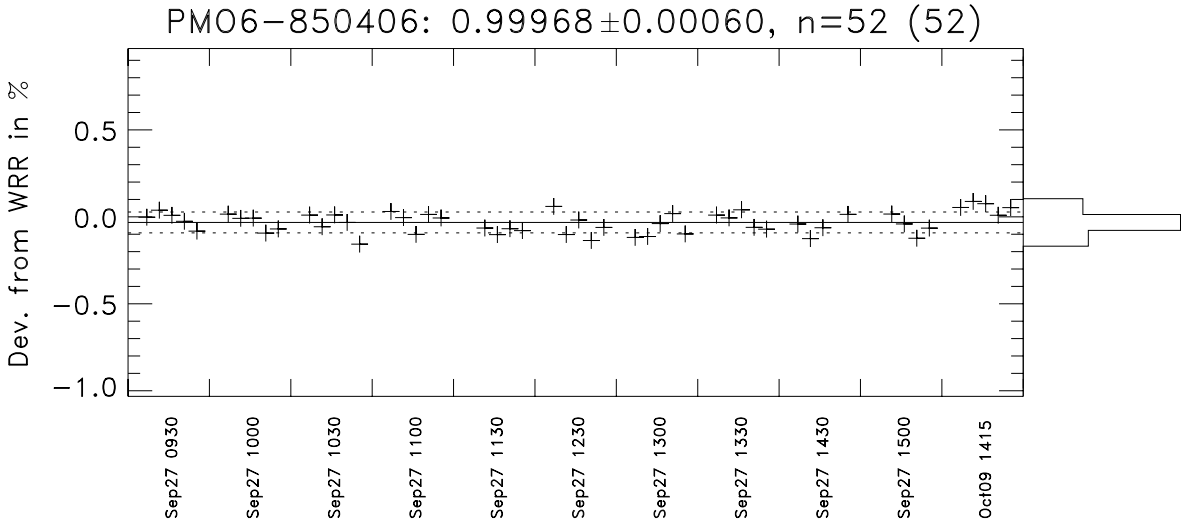

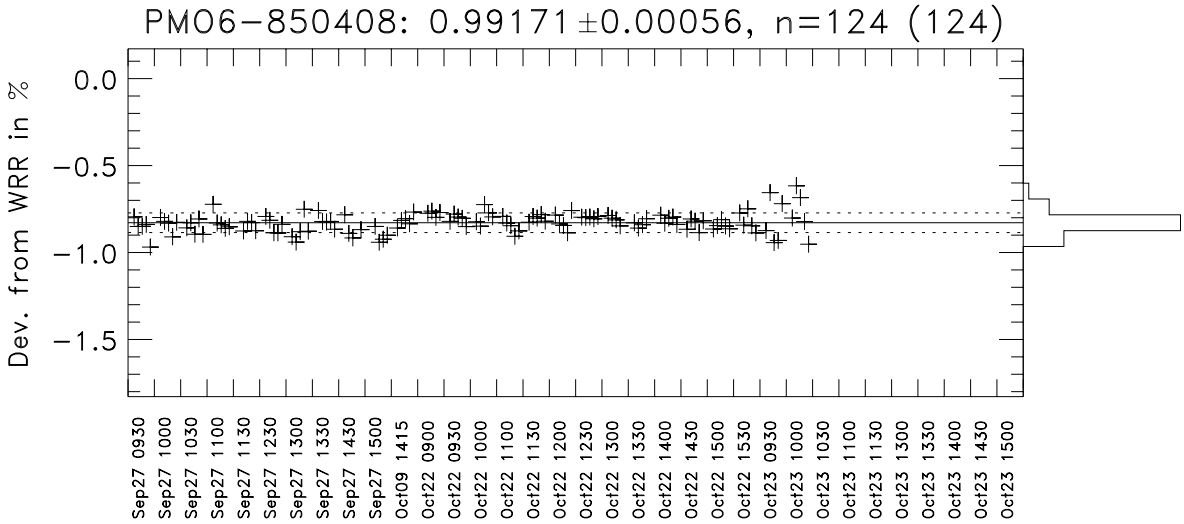

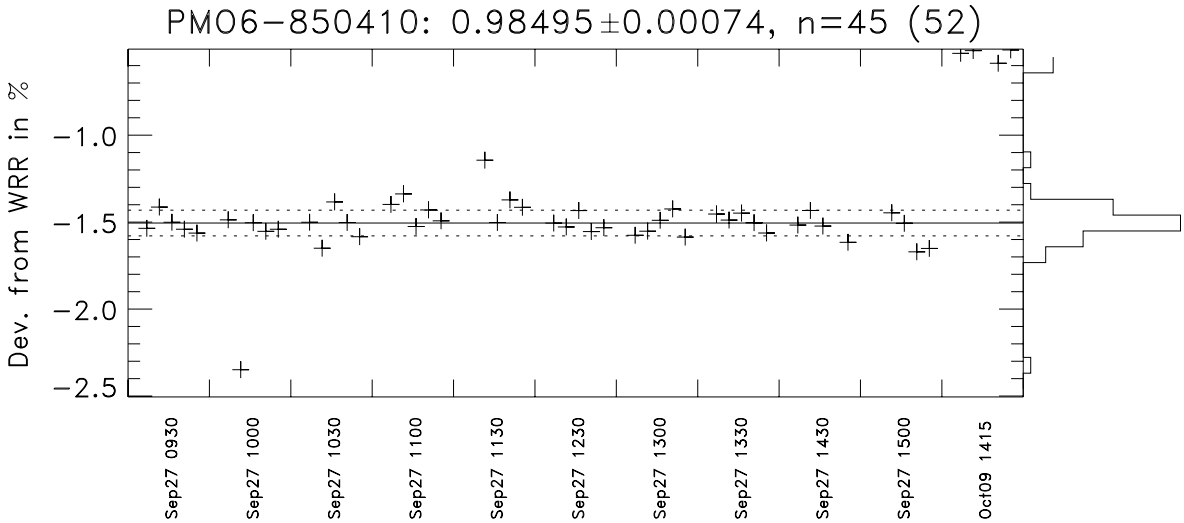

3.1.25 PMO6-911204,PMO6-0101, PMO6-SOVIM

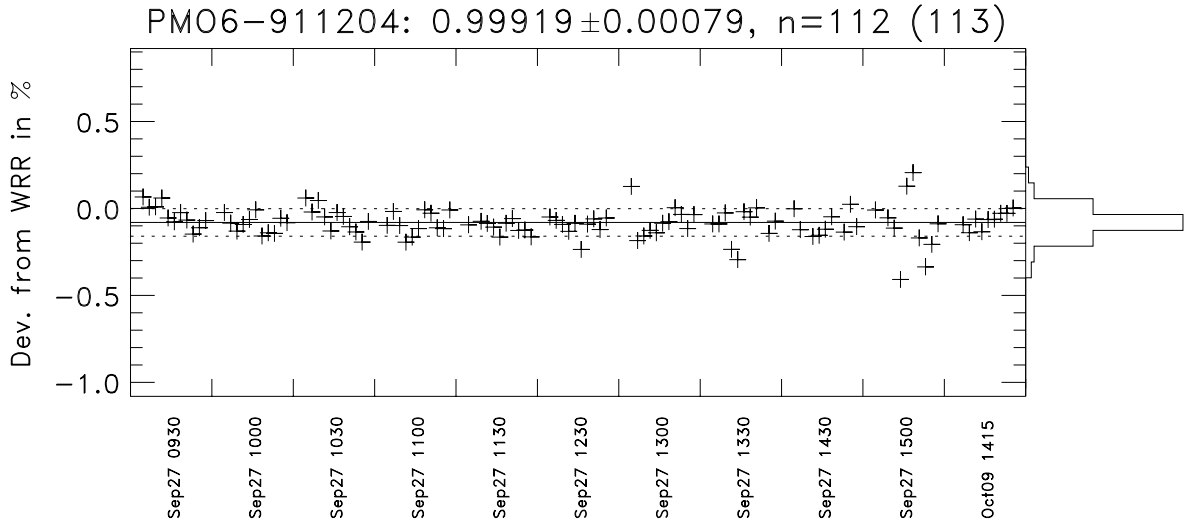

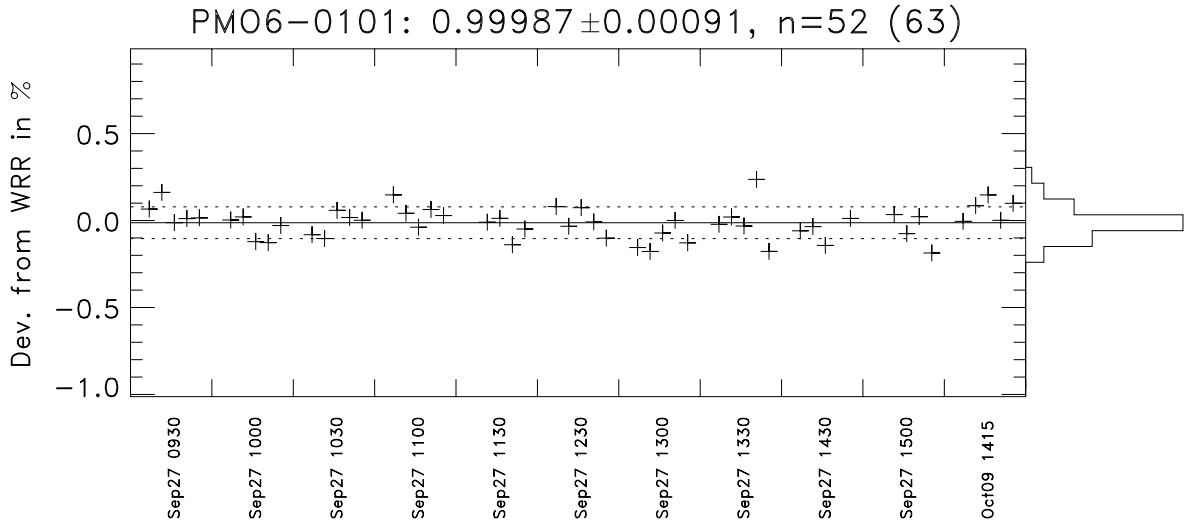

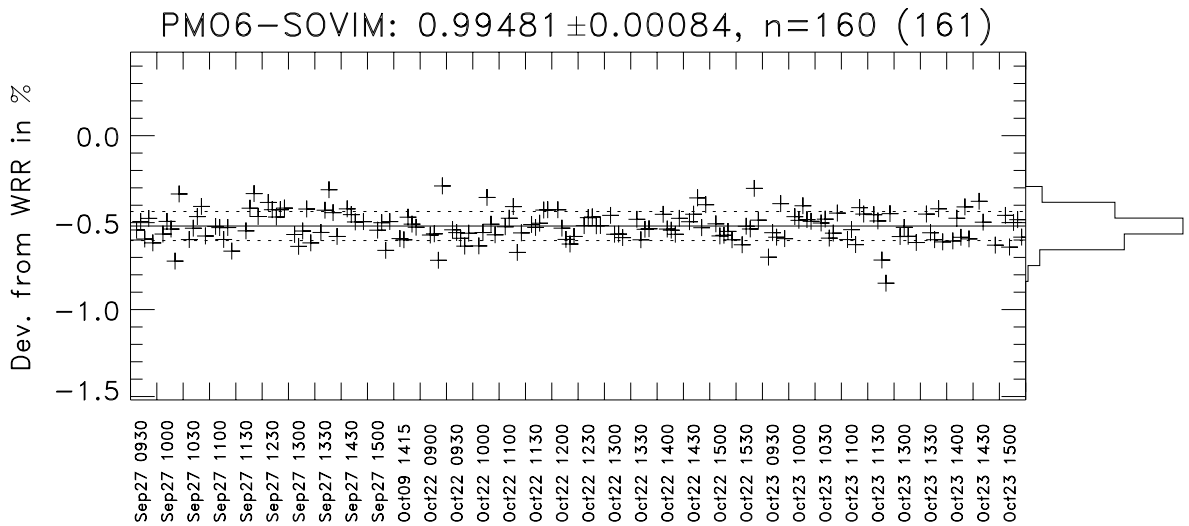

3.1.26 SIAR-1, TMI67502, TMI67604

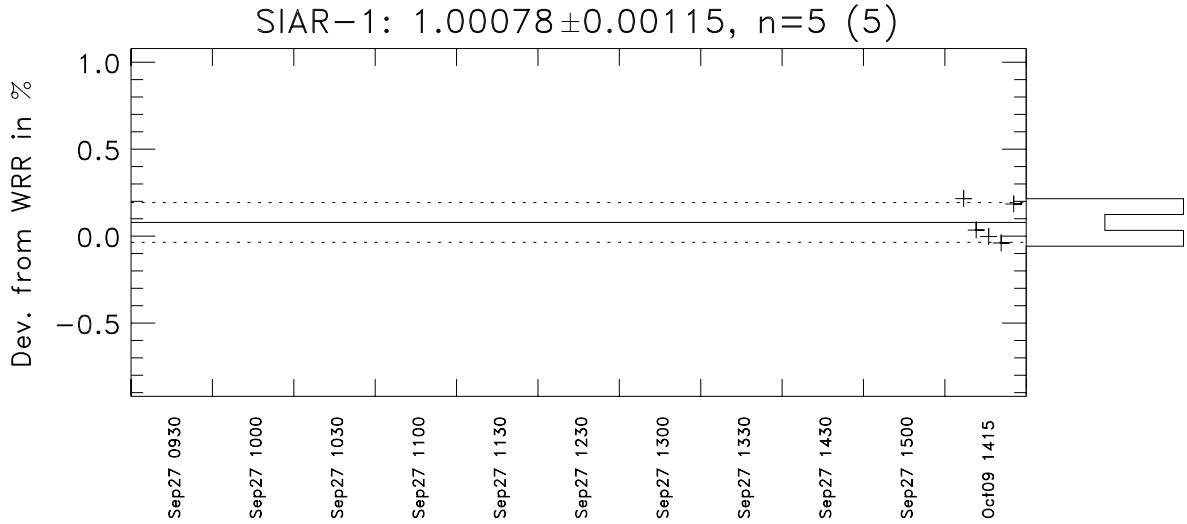

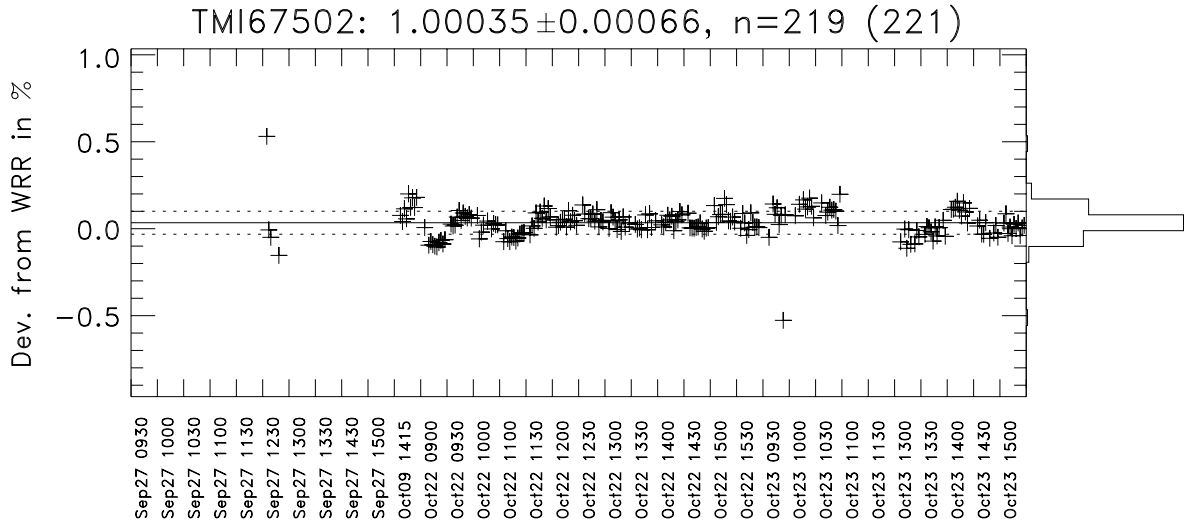

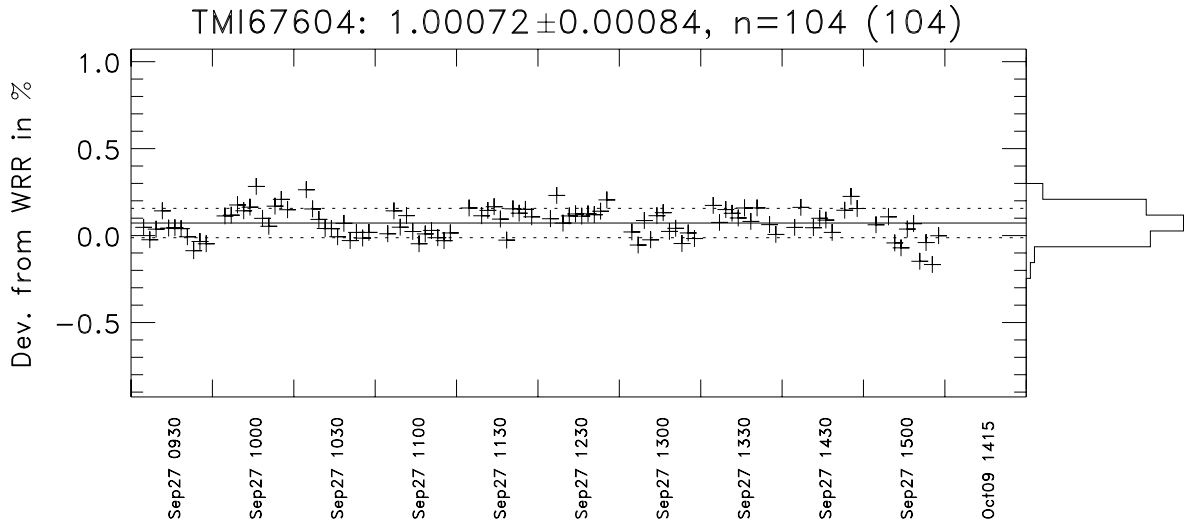

3.1.27 TMI68016, TMI68018, TMI68023

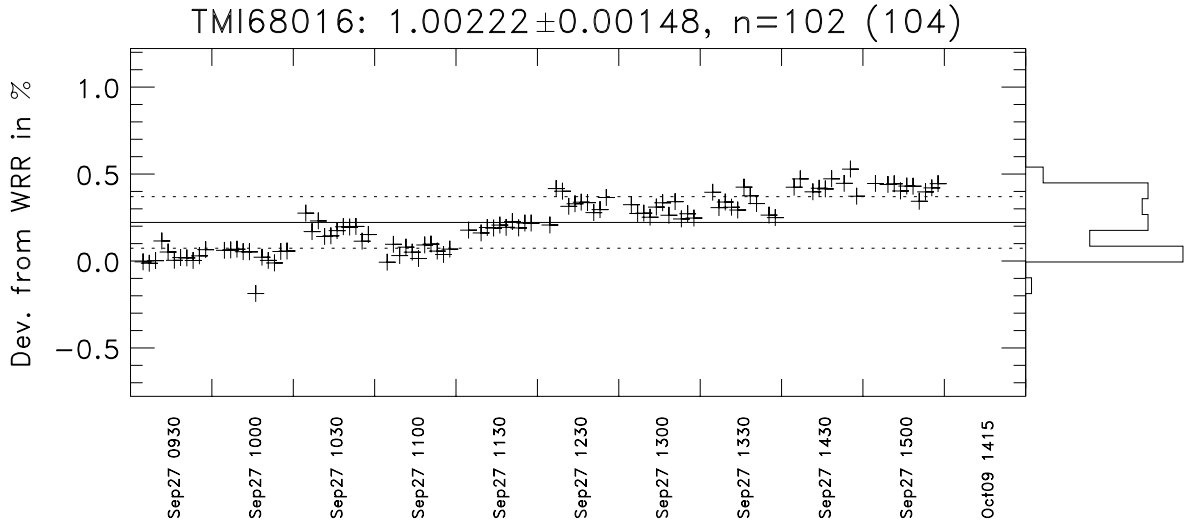

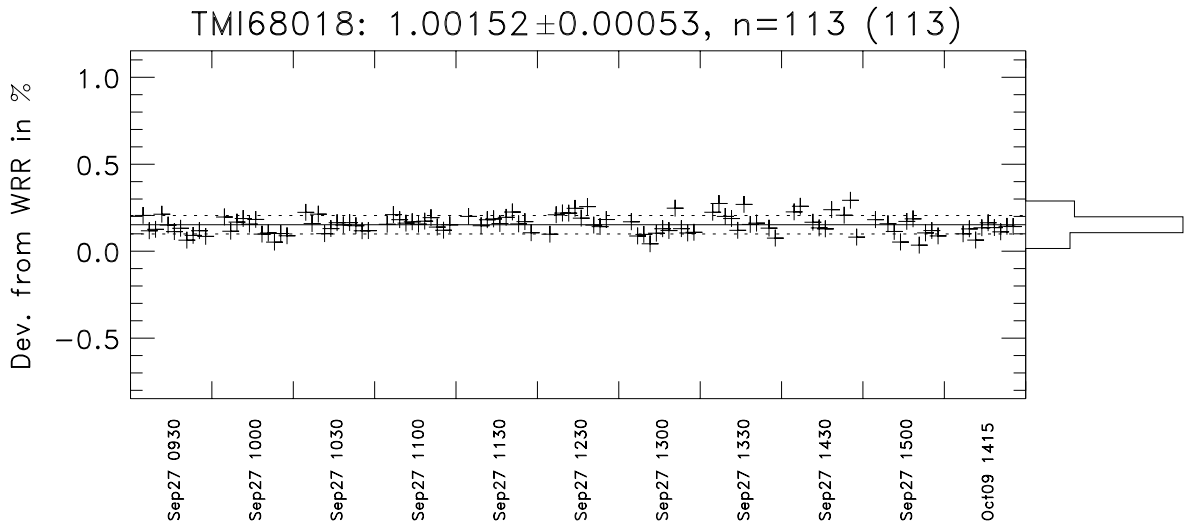

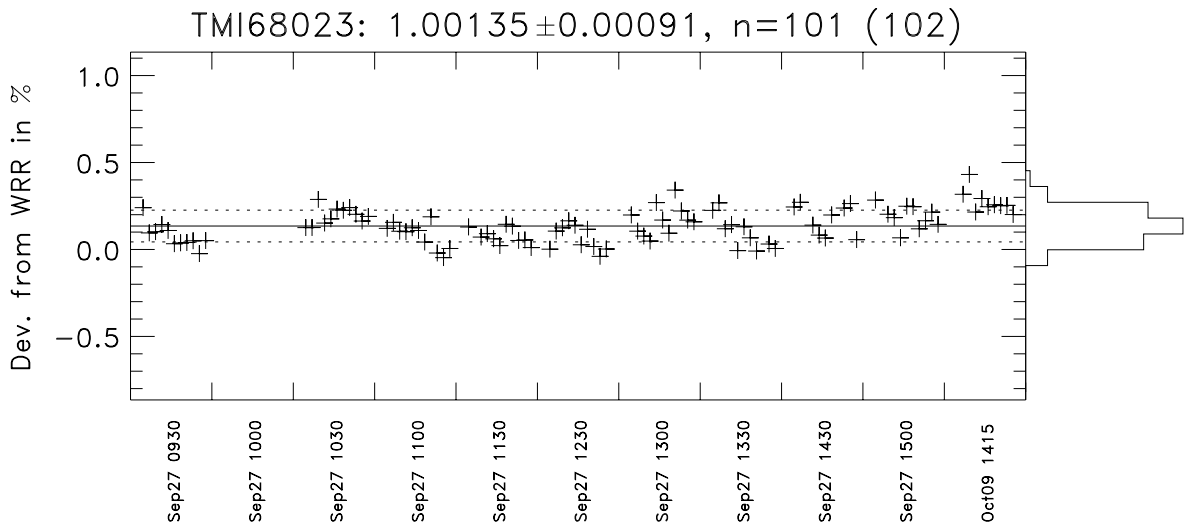

3.1.28 TMI68025, TMI69137, N-18653

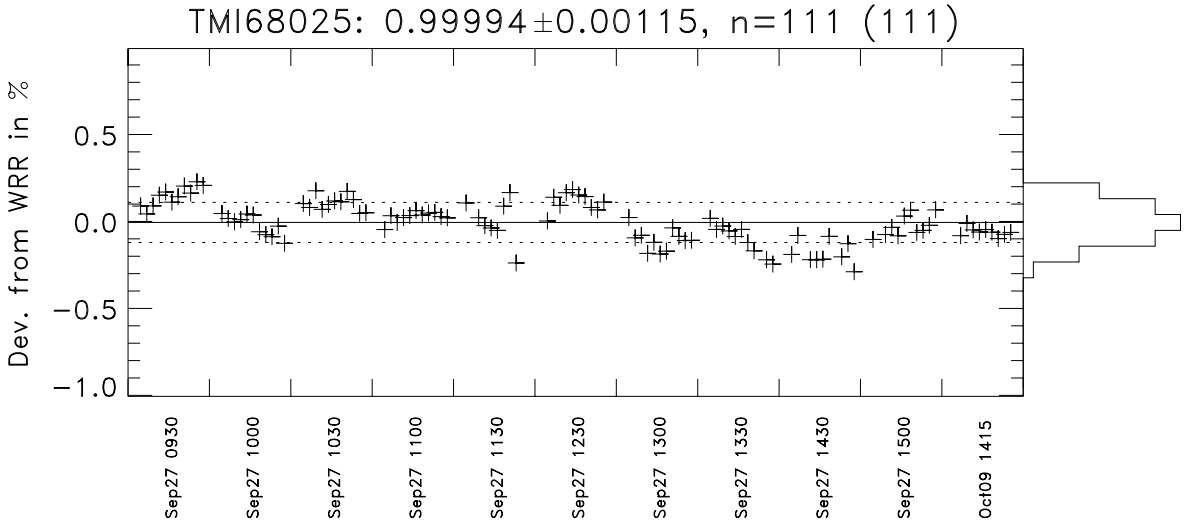

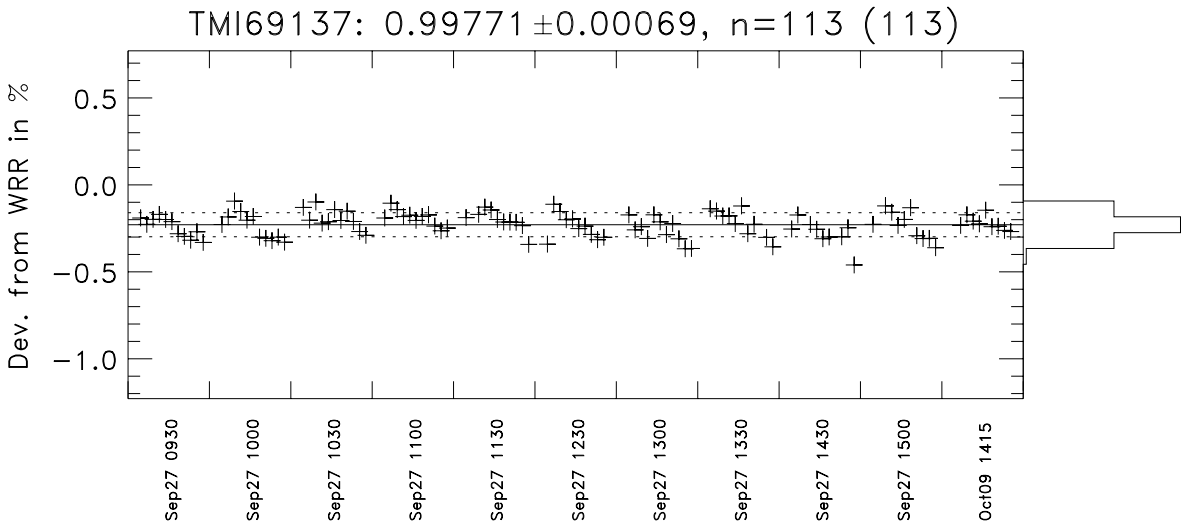

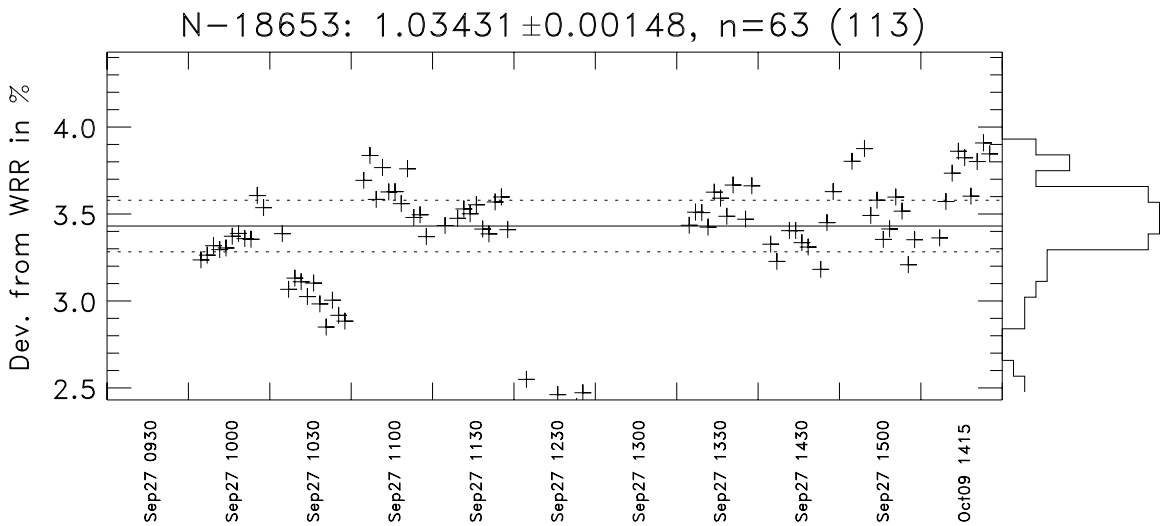

3.2 Auxiliary Data

3.2.1 Direct, Global and Diffuse Irradiance

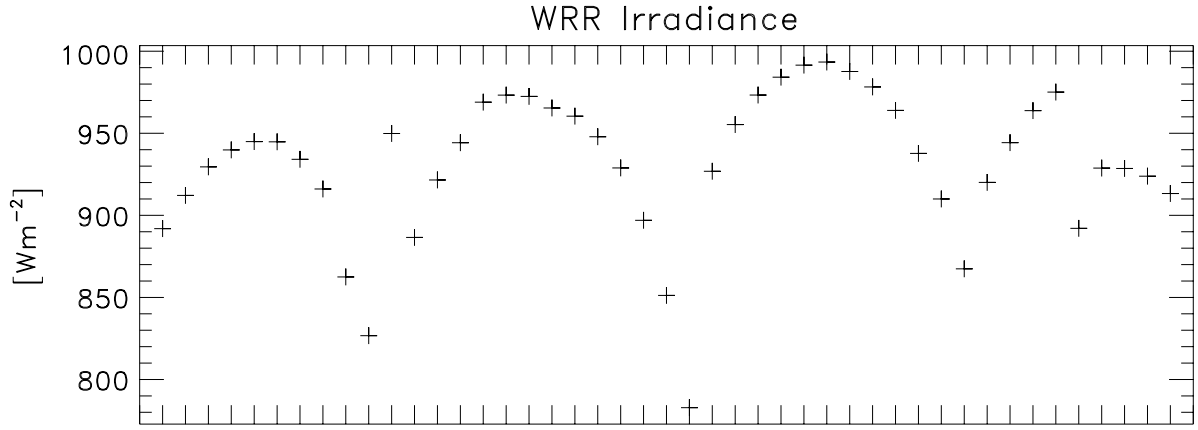

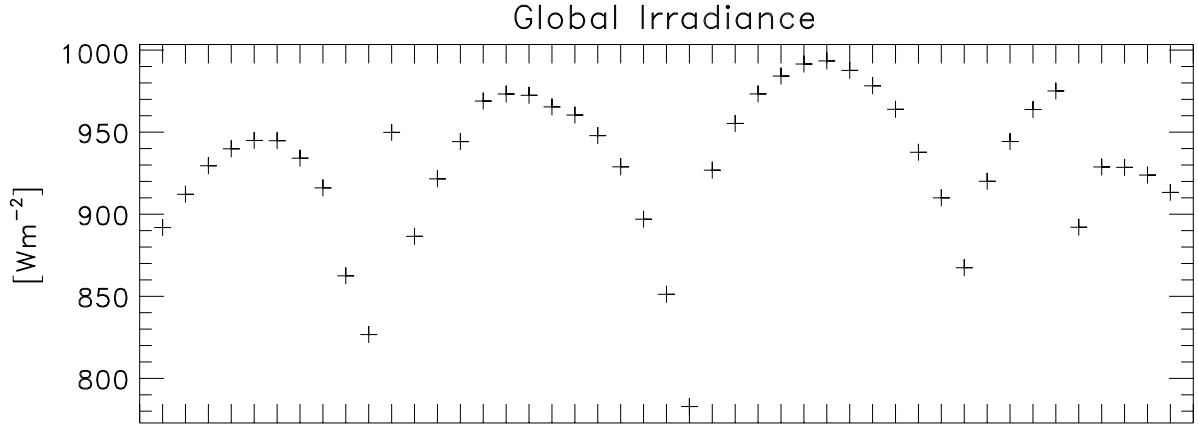

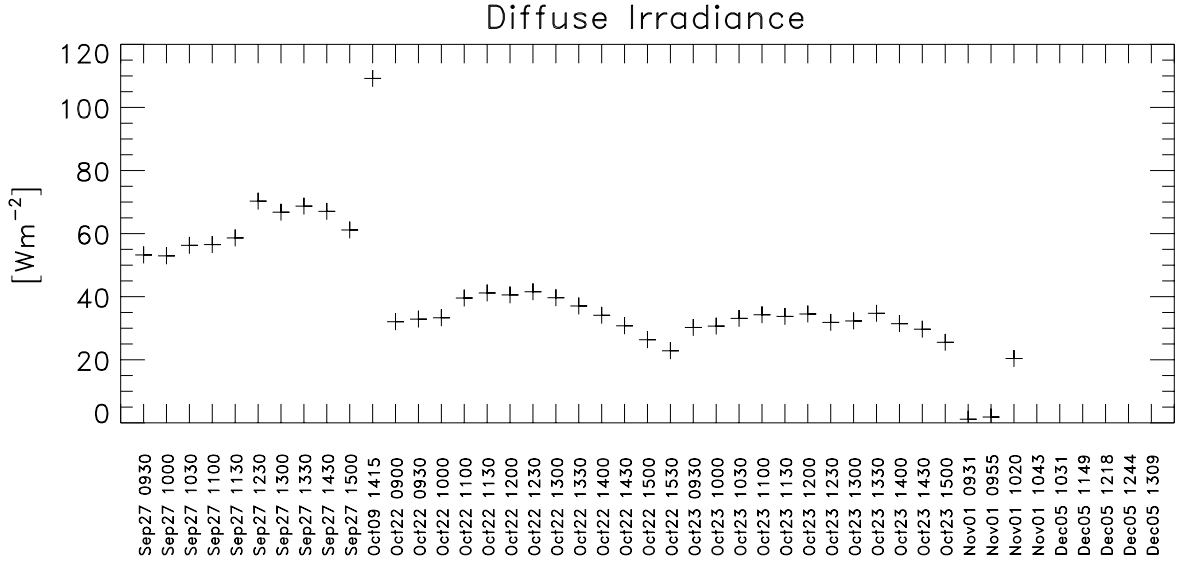

3.2.2 Meteorological Data

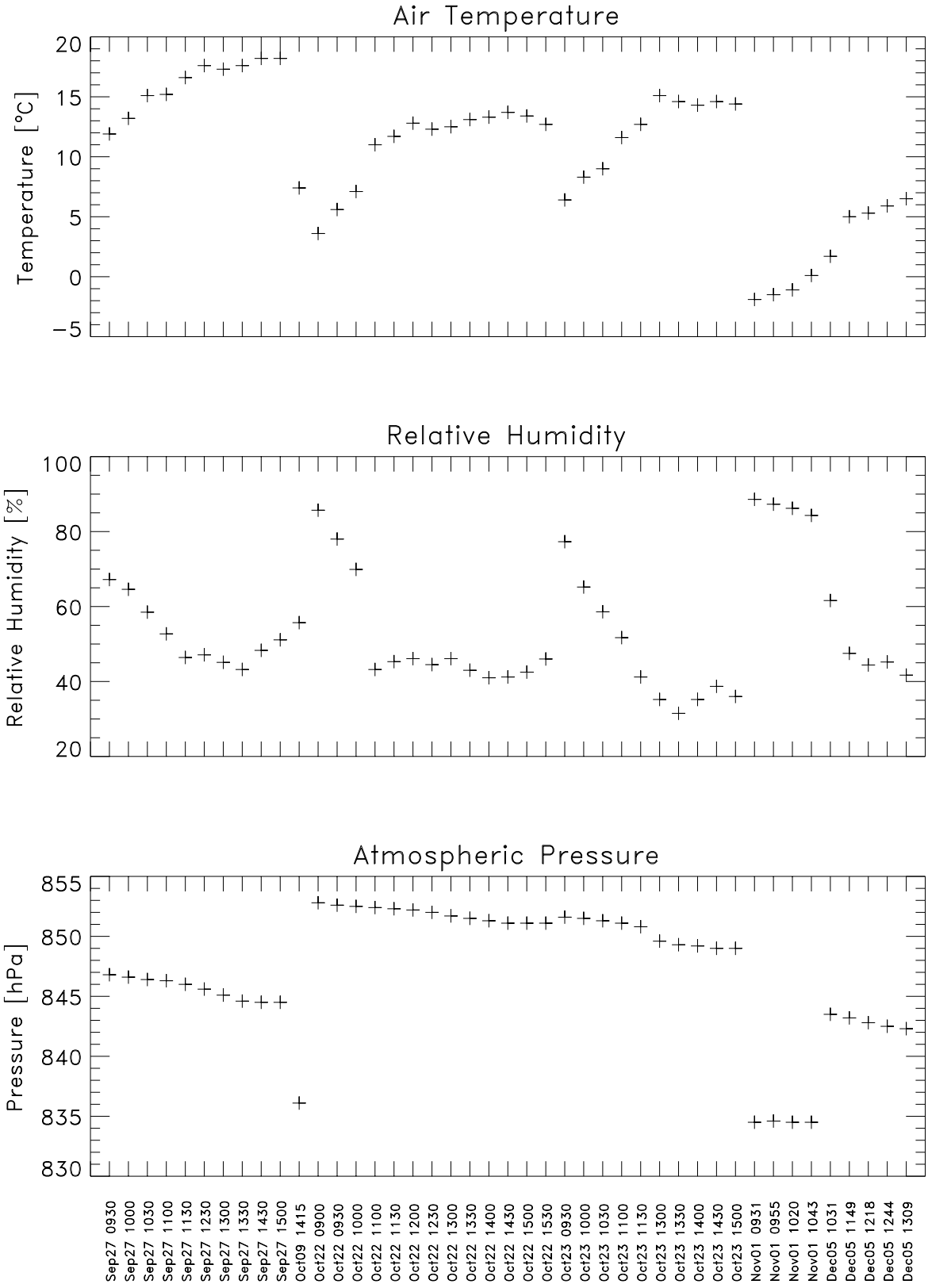

3.2.3 Airmass and Aerosol Optical Depth at 367, 500 and 776 nm

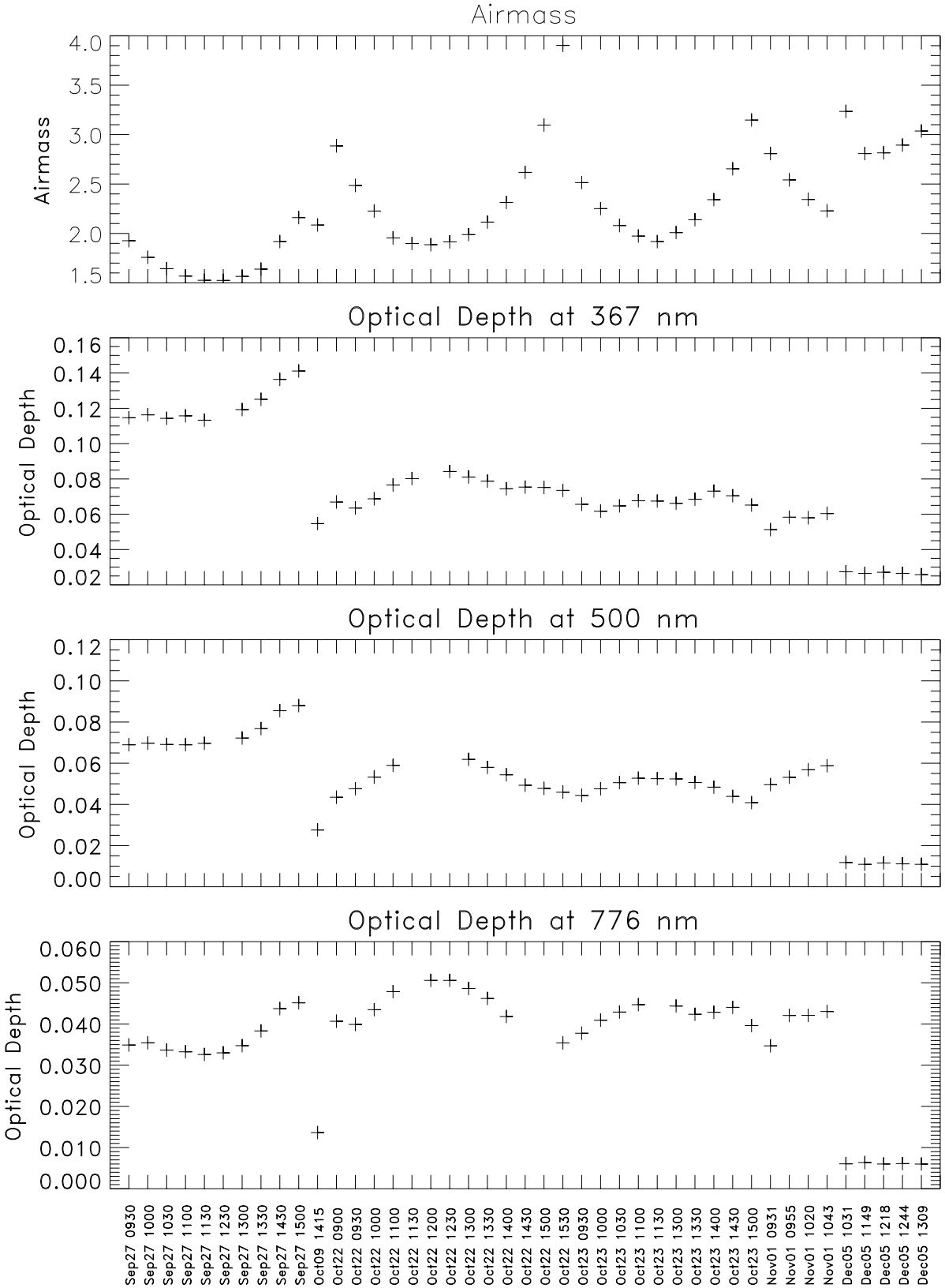

Chapter 4 Supplementary Information

4.1 View Limiting Geometry

Table 4.1: View limiting geometries of absolute radiometers (R: radius of front aperture, r: radius of receiver aperture, l: distance between apertures)

Radiometer Type	*R*	*r*	*l*
WSG			
PMO2	3.6	2.5	85.0
PMO5	3.7	2.5	95.4
CROM 2L	6.29	4.999	144.05
CROM 3R	6.25	5.0	144.0
PAC 3	8.18	5.64	190.5
HF 18748	5.81	3.99	134.7
TMI 67814	8.2	5.65	187.6
Other instruments			
CROM5R	5.225	4.0245	141.0
CROM6R	5.225	4.0172	141.0
CROM9L	7.5	4.994	141.0
EPAC generic	8.32	5.64	190.5
HF generic	5.81	3.99	134.7
MAR-1-1	6.0	3.0	137.4
P13219	8.37	5.64	191.7
PMO6 generic	4.1	2.5	94.0
PMO6-5	3.6	2.5	84.2
SIAR-1	8.365	3.9905	100.0
TMI generic	8.2	5.65	187.6
TMI-68016	8.18	5.64	190.5
NIP18653	10.3	4.0	111.0

Table 4.2: View limiting geometries of Ångström Pyrheliometers (v: vertical dimension of aperture, w: horizontal dimension of aperture, l: distance between aperture and detector, x: vertical dimension of detector, y: horizontal dimension of detector)

Ångström Type	*l*	*v*	*w*	*x*	*y*
Å-171	72.2	10.25	2.4	9.5	1.0
Å-212	50.0	11.8	2.5	9.5	1.0
Å-564	75.1	10.3	2.5	9.6	1.0
Å-578	70.5	10.3	2.5	9.6	0.8
Å-7636	111.0	10.3	4.2		
Å-13439	111.0	10.3	4.2		
Å-18020	111.0	10.3	4.2		
Å-Eppley	111.0	10.3	4.0		

4.2 Addresses of Participants

Eliphaz Bagarukayo
Ministry of Lands,
Water and Environment
Dept. of meteorology
P.O. Box 7025
Kampala
Uganda
phone: 00256 41 251798
fax: 00256 41 251797
e-mail: meteoug@infocom.co.ug

Alexander Baskis
Meteorological Service
P.O. Box 25
50250 Bet-Dagan
Israel
phone: 00972 3 9682144
Fax: 00972 3 9604065
e-mail: alexander@ims.gov.il

Klaus Behrens
Met. Observatorium Potsdam
Deutscher Wetterdienst
Postfach 600552
D-14405 Potsdam
Germany
phone: 0049 331 8889320
fax: 0049 331 8889336
e-mail: klaus.behrens@dwd.de

Barbara Bogdanska
Institute of Meteorology
and Water Management
Podlesna St. 61
PL-01-673 Warsaw
Poland
phone: 0048 22 8341651 ext.361
fax: 0048 22 835 2813
e-mail: barbara_bogdanska@imgw.pl

Fernanda Carvalho
Instituto de Meteorologia
Rua C. do Aeroporto
1749-077 Lisboa
Portugal
phone: 00351 21 8483961
fax: 00351 21 8464744
e-mail: mjoao.carvalho@mail.ineti.pt

André Chevalier
IRMB
Department of Aerology
3, Avenue Circulaire
B-1180 Bruxelles
Belgium
phone: 0032 2 373 0602
fax: 0032 2 374 6788

Christian Conscience
IRMB
Department of Aerology
3 Avenue Circulaire
B-1180 Bruxelles
Belgium
phone: 0032 2 3730 603
fax: 0032 2 374 6788
e-mail: christian.conscience@oma.be

Fred Denn
AS & M, NASA Langley
Suite 300
One Enterprise Parkway
23666 Hampton, Virginia
USA
phone: 001 757 827 4622
fax: 001 757 825 8659
e-mail: f.m.denn@larc.nasa.gov

Steven Dewitte
IRMB
Department of Aerology
Avenue Circulaire 3
B-1180 Bruxelles
Belgium
phone: 0032 2 3730624
fax: 0032 2 3746788
e-mail: steven.dewitte@oma.be

Meena Dhavraj
Norwegian University of
Science and Technology
Dept. Of Physics
Hogskoleringen 5,
N-7034 Trondheim
Norway
phone: 0047 73 551095
fax: 0047 73 597710
e-mail: dhavraj@phys.ntnu.no

Taha Nagy El-Hosary
Egyptian Meteorolog. Authority
Head of Physical Research Dep.
P.O. Box 11784
Koubry El-Quobba
Cairo
Egypt
phone: 0020 2 6820790
e-mail: radiat@nwp.gov.eg

Vivien S. Esquivel
Philippine Atmospheric, Geo-
phys. and Astron. Services
PAGASA
1424 Quezon Avenue
Quezon City
Philippines
phone: 0063 927 5509
fax: 0063 373 3420
e-mail: vsesquivel@hotmail.com

Brian Fabbri
AS & M, NASA Langley
Suite 300
One Enterprise Parkway
23666 Hampton, Virginia
USA
phone: 001 757 827 4638
fax: 001 757 825 8659
e-mail: fabbri@atmos.larc.nasa.gov

Wei Fang
Changchun Institute of Optics
Fine Mechanics and Physics
P.O. Box 1024
130022 Changchun
China
phone: 0086 431 5684692-2348
fax: 0086 431 568 23 46
e-mail: fangwei@mail.ciom.ac.cn

Patrick Fishwick
Meteorological Office
Beaufort Park
Easthampstead
Wokingham
UK-Berkshire RG40 3DN
United Kingdom
phone: 0044 1344 855834
fax: 0044 1344 855005
e-mail: pjfishwick@meto.gov.uk

Javier Fonseca
Universidad de Colima
Centro de Ciencias del Ambiente
Av. Bernal Diaz del Castillo 340
Col. Villas San Sebastian
28045 Colima, Col.
México
phone: 0052 33131165
fax: 0052 33130709
e-mail: fonseca@cuica.ucol.mx

Bruce Forgan
Bureau of Meteorology
GPO. Box 1289K
150 Lonsdale St.
Melbourne, VIC 3001
Australia
phone: 0061 3 96694599
fax: 0061 3 96694736
e-mail: b.forgan@bom.gov.au

Ignacio Galindo
Universidad de Colima
Centro de Ciencias del Ambiente
Av. Bernal Diaz del Castillo 340
Col. Villas San Sebastian
28045 Colima, Col.
México
phone: 0052 33131165
fax: 0052 33161137
e-mail: galindo@ucol.mx

Hailu Kiros Gedamu
National Meteor. Services Agency
P.O. Box 1090
Addis Ababa
Ethiopia
phone: 00251 1 615779
fax: 00251 1 517066
e-mail: nmsa@telecom.net.et

Federico F. Giménez
Servicio Meterológico Nacional
25 de Mayo 658
1002 Buenos Aires
Argentina
phone: 0054 11 45148067
fax: 0054 11 45148067
e-mail: ozono@meteofa.mil.ar

Serge Ginion
IRMB
3, Avenue Circulaire
B-1180 Bruxelles
Belgium
phone: 0032 2 373 0623
fax: 0032 2 374 6788
e-mail: serge.ginion@oma.be

Stuart Goldstraw
Meteorological Office
Beaufort Park
Easthampstead
Wokingham
UK-Berkshire RG40 3DN
United Kingdom
phone: 0044 1344 855834
fax: 0044 1344 855897
e-mail: sjgoldstraw@meto.gov.uk

John R. Hickey
The Eppley Laboratory Inc.
P.O. Box 419
Newport, RI 02840
USA
phone: 001 401 847 1020
Fax: 001 401 847 1031
e-mail: jhickeyeplab@ids.net

Kohei Honda
Japan Meteor. Agency
Regional Radiation Center RA-2
Tokyo
1-3-4 Otemachi, Chiyodaku
Tokyo 100-8122
Japan
phone: 0081 3 3287 3439
fax: 0081 3 3211 4640
e-mail: ko-honda@met.kishou.go.jp

Viera Horecká
Slovak Hydrometeorol. Institute
Jeséniova 17
P.O. Box 15
833 15 Bratislava
Slovakia
phone: 00421 7 59415170
fax: 00421 7 54772034
e-mail: viera.horecka@mail.shmu.sk

Ain Kallis
Estonian Meteor. &
Hydrological Institute
Toravere
EE-61602 Toravere
Estonia
phone: 00372 7 410136
fax: 00372 7 410205
e-mail: kallis@aai.ee

Gilberto Lara Azocar
Direccion Meteorologica de Chile
Aeropuerto Arturo Merino B
Casilla 63
Santiago
Chile
phone: 0056 2 676 34 39
fax: 0056 2 601 9613
e-mail: dimetchi@meteochile.cl

Kevin Larman
AS & M / NASA Langley
Suite 300
One Enterprise Parkway
Hampton, Virginia 23666
USA
phone: 001 757 827 4627
fax: 001 757 825 8659
e-mail: k.t.larman@larc.nasa.gov

Leif Liedquist
Swedish National Test-
ing and Research Institute
Box 857
S-50115 Boras
Sweden
phone: 0046 33 165 448
fax: 0046 33 165 620
e-mail: leif.liedquist@sp.se

Wenhua Lu
Chinese Academy of Me-
teorological Sciences
Baishiqiao Road
100081 Beijing
China
phone: 0086 10 68406866
fax: 0086 10 68406866
e-mail: lwh@cams.cma.gov.cn

Pierre Malcorps
IRMB
3 Avenue Circulaire
B-1180 Brussels
Belgium
phone: 0032 2 373 0601
fax: 0032 2 374 6788
e-mail: pierre.malcorps@oma.be

Bruce McArthur
Meteorological Service of Canada
National Atmosph. Radiation Centre
4905 Dufferin Street
Downsview, ON M3H 5T4
Canada
phone: 001 416 739 4464
fax: 001 416 739 4281
e-mail: bruce.mcarthur@ec.gc.ca

Joseph Michalsky
SUNY Albany / Battelle
3200 Q Ave,
ETB 2324
MS K9-24
99352 Richland, WA
USA
phone: 001 509 375 6494
fax: 001 509 372 4434
e-mail: joe@asrc.cestm.albany.edu

Darius Mikalajunas
Lithuanian Hydrometeor. Service
Rudnios Str. 6
LT-2600 Vilnius
Lithuania
phone: 00370 98 06354
fax: 00370 2 724160
e-mail: kaunoaes@takas.lt

Svetlana Morozova
All-Russian Research Institute
for Opto-physical Measurements
Ozernaya Str. 46
Moscow 119361
Russia
phone: 007 095 437 3700
fax: 007 095 437 3700
e-mail: morozova-m4@vniiofi.ru

Agustín Muhlia Velázquez
Universidad Nacional Autonoma
Instituto de Geofisica
Av. Universidad 3000
04510 México, D.F.
México
phone: 0052 5 6224141
fax: 0052 5 5502486
e-mail: muhlia@tonatiuh.igeofcu.unam.mx

Zoltan Nagy
Hungarian Meteorological Service
Div. f. Methodology/Quality Control
P.O. Box 39
H-1675 Budapest
Hungary
phone: 0036 1 346 4855
fax: 0036 1 346 4849
e-mail: z.nagy@met.hu

Donald W. Nelson
NOAA/CMDL
R/CMDL1
325 Broadway
Boulder, CO 80305-3328
USA
phone: 001 303 497 6662
fax: 001 303 497 5590
e-mail: dnelson@cmdl.noaa.gov

Ifeanyi D. Nnodu
Dep. of Meteor. Services
Radiation Department
Strachan Street
P.M.B. 12542
Lagos
Nigeria
phone: 00234 1 2633371
fax: 00234 1 2636097
e-mail: met@cyberspace.net.ng

Peter Novotny
Bureau of Meteorology
150 Lonsdale Street
G.P.O. Box 1289K
Melbourne, Victoria 3001
Australia
phone: 0061 3 9669 4050
fax: 0061 3 9669 4736
e-mail: p.novotny@bom.gov.au

Jean Oliviéri
Météo-France
Centre Radiométrique
785 Chemin de l'Hermitage
F-84200 Carpentras-Serres
France
phone: 0033 49063 6968
fax: 0033 490636969
e-mail: jean.olivieri@meteo.fr

Cristian Oprea
National Institute of Meteor.
Atmosph. Physic Laboratory
Sos. Bucuresti-Ploiesti 97
RO-71552 Bucaresti
Romania
fax: 0040 1 230 7762
e-mail: relatii@meteo.inmh.ro

Bouziane Ouchene
Office National Meteorologie
Chef Division Maintenance
P.O. Box 31
11000 El Hofra
Algeria
phone: 00213 29 34 46 73
fax: 00213 29 34 42 26
e-mail: b.ouchene@usa.net

Olga Pakhaljuk
Central Geophysical Observatory
Av. Nauky, 39 b.2
03028 Kyiv
Ukraine
phone: 00380 44 265 6921
fax: 00380 44 265 6969
e-mail: climate@gda.freenet.kiev.ua

Alexandre Pavlov
Main Geophysical Observatory
World Radiation Data Center
7, Karbyshev Str.
194021 St. Petersburg
Russia
phone: 007 812 247 4390
fax: 007 812 247 8661
e-mail: etalon@main.mgo.rssi.ru

Maria Pavlovitch
All-Russian Research Institute
for opto-physical Measurements
Ozernaya Str. 46
Moscow 119361
Russia
phone: 007 095 437 2992
fax: 007 095 437 3700
e-mail: morozova-m4@vniiofi.ru

Thomas Persson
Swedish Meteorological
and Hydrological Institut
Folkborgsvaegen 1
S-60176 Norrköping
Sweden
phone: 0046 11 495 8229
fax: 0046 11 495 8001
e-mail: thomas.persson@smhi.se

Jiri Pokorny
Czech Hydrometeor. Institute
Solar and Ozone Observatory
Hvezdarna 456
CZ-50008 Hradec Kralove
Czech Republic
phone: 00420 49 5260352
fax: 00420 49 5264127
e-mail: obshk@chmi.cz

Chintamani Rahalkar
Central Radiation Laboratory
Instruments Division
India Meteorological Dept.
Pune 411008
India
phone: 0091 20 5893415
fax: 0091 20 5535411

Ibrahim Reda
Nat. Renewable Energy Laborat.
1617 Cole Boulevard
Golden, CO 80401-3393
USA
phone: 001 303 3846385
fax: 001 303 3846391
e-mail: ibrahim_reda@nrel.gov

Georgina Rios
Universidad de Colima
Centro de Ciencias del Ambiente
Av. Bernal Diaz del Castillo 340
Col. Villas San Sebastian
28045 Colima, Col.
México
phone: 0052 33131165
fax: 0052 33130709

Tony Sample
European Commission
DG-JRC, Environment Institute
TP 450, Via Fermi 1
I-21020 Ispra (Va)
Italy
phone: 0039 0332 789062
fax: 0039 0332 789268
e-mail: tony.sample@jrc.it

David Shearn
Meteorological Office
Beaufort Park
Easthampstead
Wokingham
UK-Berkshire RG40 3DN
United Kingdom
phone: 0044 1344 855815
fax: 0044 1344 855005
e-mail: pdshearn@meto.gov.uk

Ovidio Simbaqueva
IDEAM
Diagonal 97 No 17 - 60
Piso 2
Bogota
Colombia
phone: 0057 418 11 70
fax: 0057 418 11 59
e-mail: ovidisim@ideam.gov.co

Tom Stoffel
Nat. Renewable Energy Laborat.
1617 Cole Boulevard
Golden, CO 80401-3393
USA
phone: 001 303 3846395
fax: 001 303 3846391
e-mail: tom_stoffel@nrel.gov

Nugool Suppjaroen
Meteorological Department
4353 Sukhumvit Rd.
10260 Bangkok
Thailand
phone: 0066 2 3960156
fax: 0066 2 3989861
e-mail: tmd@metnet.tmd.go.th

Irene Trebejo Varillas
National Meteorological &
Hydrological Service
SENAMHI
Jr. Cahuide 805
Lima 11
Peru
phone: 0051 1 2660216
fax: 0051 1 4717287

Fernando A. Vigón del Busto
Instituto de Meteorología
Investigador Agregado
Loma de Casablanca
11700 Habana
Cuba
phone: 0053 7 570723
fax: 0053 7 338010
e-mail: finubes@met.inf.com

Gang Wang
Changchun Institute of Optics
Fine Mechanics and Physics
P.O. Box 1024
130022 Changchun
China
phone: 0086 431 5684692-2747
fax: 0086 431 568 23 46
e-mail: wangg@mail.ciom.ac.cn

Ernst Wessely
Zentralanstalt für Meteo-
rologie und Geodynamik
Hohe Warte 38
A-1190 Wien
Austria
phone: 0043 1 36026 2703
fax: 0043 1 36026 2720
e-mail: ernst.wessely@zamg.ac.at

Yun Yang
Chinese Academy of Meteorological Sciences
46 Baishiqiao Road
100081 Beijing
China
phone: 0086 10 68406936
fax: 0086 10 68406866
e-mail: hao_p@sina.com

Haishun Yao
Changchun Institute of Optics
Fine Mechanics and Physics
P.O. Box 1024
130022 Changchun
China
phone: 0086 431 5684692-2747
fax: 0086 431 568 23 46

Arkawat Ying-Ariyakul
Meteorological Department
4353 Sukhumvit Rd.
10260 Bangkok
Thailand
phone: 0066 2 3960156
fax: 0066 2 3989861
e-mail: tmd@metnet.tmd.go.th

Bingxi Yu
Changchun Institute of Optics
Fine Mechanics and Physics
P.O. Box 1024
130022 Changchun
China
phone: 0086 431 5684814
fax: 0086 431 568 23 46
e-mail: ciomyu@public.cc.jl.cn

Willem J. Zaaiman
European Commission
DG-JRC, Environment Institute
TP 450, Via Fermi 1
I-21020 Ispra (Va)
Italy
phone: 0039 0332 785750
fax: 0039 0332 789268
e-mail: willem.zaaiman@jrc.it

4.3 Participants and Staff


Eliphaz Bagarukayo
(Uganda)


Alexander Baskis
(Israel)


Klaus Behrens
(Germany)


Barbara Bogdanska
(Poland)


Fernanda Carvalho
(Portugal)


André Chevalier
(Belgium)


Christian Conscience
(Belgium)


Fred Denn
(USA)


Steven Dewitte
(Belgium)


Meena Devi Dhavraj
(South Africa / Norway)


Taha Nagy El-Hosary
(Egypt)


Vivien S. Esquivel
(Philippines)


Brian Fabbri
(USA)


Wei Fang
(China)


Patrick Fishwick
(Great Britain)


Javier Fonseca
(Mexico)


Bruce Forgan
(Australia)


Ignacio Galindo
(Mexico)


Hailu Kiros Gedamu
(Ethiopia)


Federico F. Giménez
(Argentinia)


Serge Ginion
(Belgium)


Stuart Goldstraw
(Great Britain)


John R. Hickey
(USA)


Kohei Honda
(Japan)


Viera Horecká
(Slovakia)


Ain Kallis
(Estonia)


Gilberto Lara Azocar
(Chile)


Kevin Larman
(USA)


Leif Liedquist
(Sweden)


Wenhua Lu
(China)


Bruce McArthur
(Canada)


Joseph Michalsky
(USA)


Darius Mikalajunas
(Lithuania)


Svetlana Morozova
(Russia)


Agustín Muhlia Velázquez
(Mexico)


Zoltan Nagy
(Hungary)


Donald W. Nelson
(USA)


Victoria Nelson
(USA)


Ifeanyi Daniel Nnodu
(Nigeria)


Peter Novotny
(Australia)

Jean Oliviéri
(France)

Cristian Oprea
(Romania)


Bouziane Ouchene (Algeria)


Olga Pakhaljuk (Ukraine)


Alexandre Pavlov (Russia)


Maria Pavlovitch (Russia)


Thomas Persson (Sweden)


Jiri Pokorny (Czech Republic)


Chintamani Rahalkar (India)


Ibrahim Reda (USA)


Georgina Rios (Mexico)


Tony Sample (Italy)


David Shearn (United Kingdom)


Ovidio Simbaqueva (Colombia)


Tom Stoffel (USA)


Nugool Suppjaroen (Thailand)


Irene Trebejo Varillas (Peru)


Kiyotaka Uchida (Japan)


Fernando A. Vigón del Busto (Cuba)


Gang Wang (China)


Ernst Wessely (Austria)


Yun Yang (China)


Haishun Yao (China)


Arkawat Ying-Ariyakul (Thailand)


Bingxi Yu (China)


Willem J. Zaaiman (Italy)

4.4 IPC-Staff


Werner Schmutz


Isabelle Rüedi


Christoph Wehrli


Rolf Philipona


Hansjörg Roth


Claus Fröhlich


Sonja Degli Esposti


Jules Wyss


Klaus Kruse

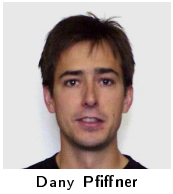
Dany Pfiffner


Remo Venturi


Mario Roveretto


Wolfgang Finsterle

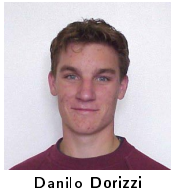
Danilo Dorizzi

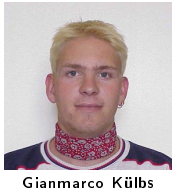
Gianmarco Külbs


Urs Zimmerli

Pascal Güntensperger

Klara & Guy Maynard

Part II

SYMPOSIUM

Chapter 5 Investigations of night-time zero offsets at short-wave broadband radiometers

Klaus Behrens and Dr. Klaus Dehne
Deutscher Wetterdienst
GB Forschung und Entwicklung
Meteorologisches Observatorium
Potsdam Postfach 60 05 52
D-14405 Potsdam, Germany
Tel.: +49 331 88893 20
Fax: +49 331 88893 36
E-Mail: klaus.behrens@dwd.de

Abstract

The improvement of the radiation measurements concerning the zero offsets is one of the main goals of pyranometrical research.

In a first part the results are discussed of special investigations of the zero offsets in dependence on different ventilation of the domes of CM21 pyranometers as well as of comparisons of CM21, CM22 and a STAR-pyranometer.

It is shown, that the night-time zero offsets are mainly influenced by the combination of atmospheric long-wave radiation and fan ventilation power.

Furthermore, the results are presented of a long-term investigation (about five years) of night-time zero offsets from routine measurements of pyranometers at the BSRN station at Lindenberg (Germany).

5.1 Introduction

The zero offset is defined as the output of the short-wave radiometer device if no short-wave radiation is received.

Principally, both the radiometer and the connected data acquisition device contribute to the zero offset, but the latter - measured simply by a short circuit - should be at modern systems of lower orders of magnitude.

All effects which influence the temperature difference ΔT_0 between the receiver surface and the body of the heat sink belong to the physical sources of zero offsets at thermal receivers - as used in broadband radiometers like pyranometers and pyrheliometers. In the case of a thermopile receiver having n junctions with an EMF of $k\mu V/K$ and of a radiometer responsivity of $R\mu V/Wm^{-2}$ the offset irradiance ΔE_0 corresponding to an offset effect of ΔT_0 is given by $\Delta E_0 = nk\Delta T_0$ / R. If $n = 100$ and $k = 30\mu V/K$ and $R = 10\mu V/Wm^{-2}$ ("low temperature thermopile") a ΔT_0 of $\pm 0,01K$ generates already an offset error ΔE_0 of $\pm 3Wm^{-2}$. Such ΔT_0 values could be produced first of all by:

1. Long-wave radiation, received through the domes

2. Different heat transfer to the receiver surface and the heat sink body caused by

- front passage or gusts etc.
- daily course of air temperature.

To reduce the zero offset in the case of pyranometers different measures have been applied:

1. Exposure of the active receiver body and the heat sink body in an equivalent position below the dome, realized in the STAR-pyranometer (receiver surface with black & white segments) for instance.

2. Use of two glass domes (realized in nearby all pyranometers having black receiver surfaces). Recent improvement: Use of two 4 mm thick quartz domes (more mass and heat conductivity) as realized in the CM22.

3. Ventilation of the outer dome, or more consequently: ventilation of the pyranometer casing (containing the heat sink) and the outer dome successively with the same air stream. The number of such ventilated pyranometers has been increased in the last decade.

The aim of this paper is to demonstrate the reduction of zero offsets by the above mentioned measures for the relatively simply detectable zero offset at night-time. The results of examples measured in the field may be supplemented at the end by long-term values of the German BSRN-Station in Lindenberg.

5.2 Performance of night-time offset measurements

The measurements of night time offsets of pyranometers were performed mainly during March 2000 and June 2000 at the National and Regional Radiation Centre in Potsdam $\phi = 52.37°$, $\lambda = 13.08°$, h = 89m).

The measurement in March should show first of all the reduction of night-time offset **by ventilation** of typical black surface pyranometers. Three Kipp & Zonen pyranometers of type CM21 ventilated by a 5 W-fan of Eigenbrodt (Königsmoor / Germany) were used. The pyranometers are encapsulated in a cylindrical table-casing at which the fan is flanged to blow the air around the pyranometer body.

The air leaves the casing between the radiation shield of the pyranometer and the foot of the outer dome and streams against the dome from all sides. For the standard operation the fan needs only (5 W, 24 V); the air is not pre-heated, the speed of the air is about 1,5 m/s.

To demonstrate the ventilation effect the three simultaneously operated pyranometers are ventilated with the standard power, with the half power and without any power, respectively.

The measurement in June 2000 were performed after the procurement of one of the new "thick quartz dome"-pyranometers of the Kipp & Zonen type CM22, announced as "low offset device". It has been compared with the classical **low offset pyranometer** type "STAR" (Ph. Schenk, Wien) and the "thin dome" pyranometer CM21. Both CM-pyranometers are ventilated (5 W power) while the STAR-pyranometer was unventilated. Later on the CM22 was also operated without any ventilation as the STAR-pyranometer.

The pyranometer output was recorded by data loggers “COMBILOG” of Friedrichs (Hamburg, Germany). During the experiment a short circuit together with the highest resolution of the logger was used to test the influence of the acquisition device. The registered voltage of the short circuit fluctuated within 0 and -0.7 μV. At a typical responsivity of 10 μV/Wm^{-2} the contribution of the logger is about -0.07Wm^{-2}.

5.3 Results

The investigations of the night-time zero offset were done by analyzing the pyranometer output if the sun was more than 5° below the horizon and no short-wave radiation disturbed the measurements.

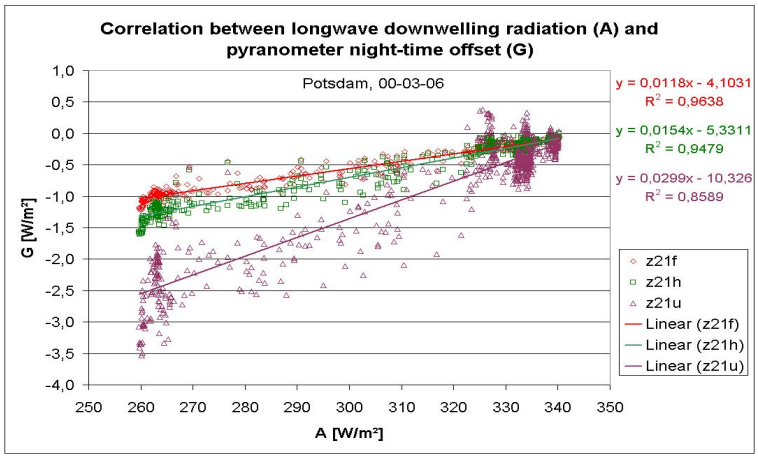

Figure 5.1: Night-time zero offset of three different ventilated CM21 (z21f: full power; z21h : half power; z21u: unventilated) and the corresponding long-wave downward radiation A Potsdam, 00-03-06/07

Figure 5.1 shows a typical picture of the course of the long-wave downward radiation A at changing cloudiness together with the courses of the night-time zero offset of the three (by different power ventilated) CM21 pyranometers. The three offset curves follow more or less the changes of the long-wave downward radiation. The curves of the full power (z21f) and of the half power (z21h) ventilated devices are relatively close together with offsets up to about -1.5 W/m^2. The unventilated pyranometer (z21u) shows a larger offset than the ventilated instruments. Especially during rapid changes of A the offset of the unventilated devices reaches values of about -3.5 W/m^2.

Figure 5.2 presents the corresponding scatter diagram displaying the correlation between the long-wave downward radiation and the night-time offsets. At first this picture gives an impression about the strength of the correlation between the zero offset at different ventilation power and at second it shows the bigger scattering as well as the bigger dependence of the unventilated pyranometer on long-wave downward radiation A.

Furthermore it is visible that there is a small difference but remarkable between the full and half power ventilated pyranometers.

Additionally to the zero offset of the CM21 and the long-wave downward radiation Figure 5.3 implies the natural wind speed measured by a ultrasonic anemometer at the level of the pyranometer domes. There is nearly no influence of the wind speed on the offset. A correlation coefficient of r = 0,18 between the wind speed and zero offset of the unventilated CM21 confirms this statement.

Typical courses of a CM21 (z21f), a CM22 (z22f) - both ventilated by full power - and an unventilated STAR-pyranometer (zSTu) together with the corresponding long-wave downward radiation A are shown in Figure 5.4. In comparison with Figure 5.1 it is evident that the zero offset of the STAR-pyranometer and of the CM22 are smaller than those of the CM21. Furthermore, the influence of rain on the zero offset is demonstrated. The rain droplets effect - at least by evaporation - a cooling of the domes with the consequence of a more or less rapid decline of the offset at all (!) pyranometers. After some minutes the offset follows again the changes of the long-wave downward radiation because of the adaptation of the system receiver/dome.

Table 5.1 gives an overview about the dependence of the night-time zero offset at the used

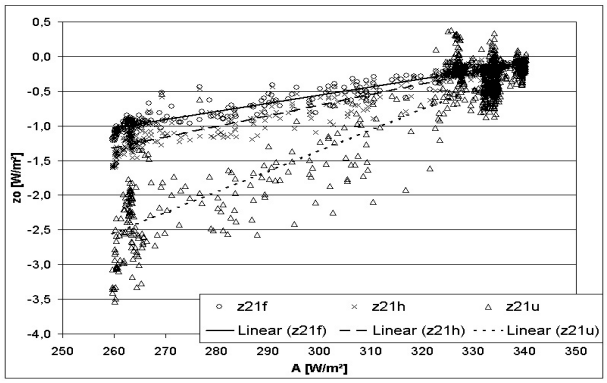

Figure 5.2: Scatter plot of the night-time zero offset of different ventilated CM21 (z21f: full power; z21h: half power; z21u: unventilated) and the corresponding linear regression lines in dependence on long-wave downward radiation A Potsdam, 00-03-06/07

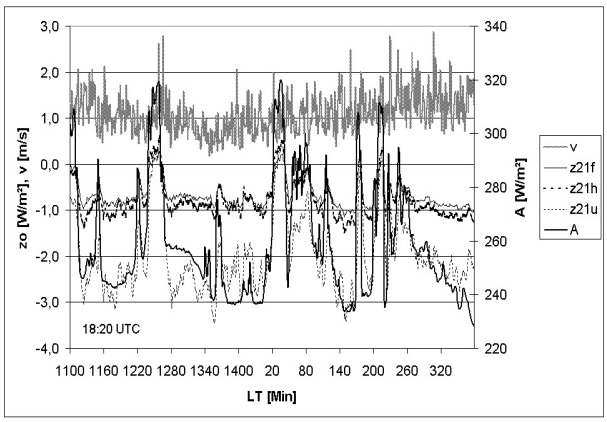

Figure 5.3: Night-time zero offset of three different ventilated CM21 (z21f: full power; z21h: half power; z21u: unventilated) and long-wave downward radiation A together with natural wind speed v Potsdam, 00-03-03/04

pyranometers with the respective ventilation power (Column a) on the long-wave downward radiation at selected days which was investigated by a regression analysis. Column b shows the change of the offset caused by a change of 100W/m^2 in long-wave radiation. The correlation cofficients are presented in Column c. All ventilated pyranometers are only very little ($\leq$1.5 W/m^2/100 W/m^2) influenced by changes in long-wave radiation. The ventilated CM22 and the unventilated STAR-pyranometer reach similar results at an offset level of < 0.3Wm^{-2}. The zero offset of a CM22 without any ventilation is nearly in the same level as a full power ventilated CM21.

The correlation coefficients of the unventilated CM21 and the STAR-pyranometer are remarkable lower than in the case of the unventilated CM22. This may be interpreted that the improvements at the CM22 reduce "thermal noise". The experiment showed that a stable and strong air stream in the case of the investigated pyranometers with a black receiver surface (CM21, CM22) enables much lower zero offsets than specified in the “CIMO Guide” [1].

The investigated data of a time series of about five years routine measurement concerning the zero offset of the with 5 W steadily ventilated CM21 installed at the German BSRN station Lindenberg are

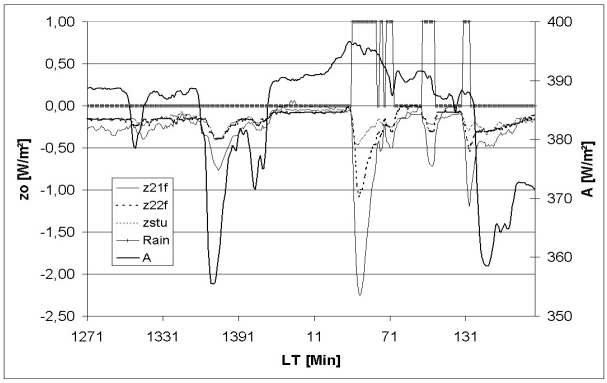

Figure 5.4: Night-time zero offset of a CM21 (z21f: full power ventilation), CM22 (z22f: full power ventilation), a STAR-pyranometer (zSTu: unventilated) and long-wave downward radiation A together with signed rain (Rain=1) Potsdam, 00-06-14/15

Date	a	b	c
00-03-06	z21f	1,2	0,982
	z21h	1,5	0,974
	z21u	3,0	0,927
00-06-24	z21f	1,2	0,937
	z22f	0,6	0,943
	zSTu	0,2	0,591
00-07-09	z21f	1,2	0,856
	z22u	1,5	0,860
	zSTu	0,5	0,760

Table 5.1: Legend: z21f: CM21 full power ventilation, z21h: CM21 half power ventilation, z21u: CM21 unventilated, z22f: CM22 full power ventilation, z22u: CM22 unventilated, zSTu: STAR-pyr. unventilated

in good agreement with the results found in this experiment; the nightly means are within $\pm 1,5 \mathrm{Wm}^{-2}$.

5.4 Conclusive remarks

1. It is recommendable that other radiation centres (main stations) at which other types of pyranometers and / or fans are in use should repeat the investigations of night-time zero offset because of its relatively low need of additional man-power.

2. To estimate the undesired zero offset component of the measured signal of solar irradiance the determined results of night-time zero offset can be evaluated qualitatively. At night-time the long-wave cooling effect dominates generally and causes the negative sign of the offset. During the sunny day the received solar fluxes should reduce or (over) compensate this long-wave effect by heating the domes first of all (absorption of IR-solar energy). The dome ventilation of the outer dome by fan or wind should reduce the resulting effect to an amount which is not higher

than during clear-nights.

3. In the last issue of the "CIMO Guide" Table 7.5, p. I.7-9 [1] the pyranometers are classified according to acceptable limiting values of errors in a list of characteristics. In the case of zero offsets the effect of 200Wm^{-2} net long-wave radiation or of a linear temperature change of 5Kh^{-1} has to be equivalent to less than 7Wm^{-2} and 2Wm^{-2}, respectively, for pyranometers of "high quality". At least the first value seems with regard to the presented results too high. This will be controlled by laboratory experiments at the Met. Obs. Potsdam soon.

4. Concerning the used pyranometers: At pyranometers with "low-temperature thermopile" 1000Wm^{-2} generates only a temperature difference of about 3 K. That means low tilt and linearity errors but higher zero offsets. At the Star-pyranometer the disadvantages arise with the ageing of the white paint and the relatively large receiver surface combined with the shallow dome.

5.5 References

[1] WMO: Guide to Meteorological Instruments and Methods of Observation, Sixth Edition, WMO-No. 8, Genf 1996

Chapter 6 Comparison of AOD estimates derived from spectral and broadband measurements

Thomas Persson
Swedish Meteorological and Hydrological Institute, SMHI
601 76 Norrköping
Sweden
thomas.persson@smhi.se

Abstract

An experimental comparison of spectral aerosol optical depth (AOD) derived from measurements by two spectral radiometers and an ordinary broadband field pyrheliometer has been made. The study was limited to the three wavelengths 368, 500 and 778 nm. At 500 and 778 nm the agreement between AOD derived from the two spectral radiometers, a Li-cor LI-1800 spectroradiometer and a CSEM SPM2000 sunphotometer, mostly was within 0.01 for optical airmasses ≥ 2. For wavelengths shorter than 500 nm and longer than 950 nm the performance of the LI-1800 does not permit accurate determinations of AOD. Estimates of spectral AOD from measurements with an Eppley NIP, using the parameterisation by Gueymard (1998) with a slight correction, and the Ångström relation with $\alpha = 1.3$, were on average 0.017, 0.016 and 0.011 higher at 368, 500 and 778 nm than the sunphotometer AODs. Using the original parameterisation by Gueymard, with the proposed circumsolar correction, would increase the positive difference to 0.061, 0.046 and 0.028 at the same wavelengths.

6.1 Background

As the design of instruments for spectral measurements of solar radiation evolves, and as the interest in and request for aerosol optical depth (*AOD*) data increase, more and more stations with more and more sophisticated spectral radiometers are established (almost) all over the world. But even today continuous spectral measurements are much sparser than broadband pyrheliometer measurements. Therefore, it is of greatest interest to utilise pyrheliometer measurements to derive the atmospheric turbidity and further to estimate spectral *AOD*. In Sweden, for example, continuous pyrheliometer measurements are made since 1983 at twelve sites. While continuous spectral measurements for *AOD* determination are only made at two sites since 1994/-95. (During some months in 1999 and 2000 an AERONET station was operating on the island of Gotland in the Baltic Sea. Hopefully, this station will become operational and permanent during 2001.) The question is how good *AOD* estimates from broadband measurements really are.

The original aim of this study was also to compare *AOD* at nine wavelengths in the range 368–1024 nm, derived with two different spectral instruments, a 3-channel sunphotometer and a simple spectroradiometer (300-1100 nm). However, it turned out that the performance and the calibration accuracy of the spectroradiometer were not good enough to be used as a reference. Therefore, the comparison is restricted to the three wavelengths of the sunphotometer only.

6.2 Measurements and methods

From March 1999 to March 2000 measurements with a spectroradiometer where taken when possible. Measuring site was the radiation measurement platform on the roof of the Swedish Meteorological and Hydrological Institute, SMHI, 58.58°N, 16.15°E. Altogether about 300 scans from 32 different days during all seasons were taken. At the research radiation station of SMHI 1-minute (mean values) radiation data are collected continuously. From this database data from the sunphotometer and the pyrheliometer at the times of the spectroradiometer scans were extracted.

6.2.1 Instruments

The spectroradiometer used was the manually operated Li-cor LI-1800 Portable Spectroradiometer No 178 (300-1100 nm, single monochromator, 6-7 nm FWHM, silicone photodetector, not temperature stabilised). To scan the full wavelength range at 1-nm intervals took about 45 seconds. The instrument was equipped with a screening tube (collimator) in order to allow measurements of the direct solar radiation with a field of view (FOV) of 2.5° (full angle). The instrument was either operated indoors, especially in cold weather, or mounted outdoors on a suntracker. The whole instrument had to be moved and pointed towards the sun. The instrument housing was always shaded from direct sun and the teflon diffusor (entrance optics) was shaded between the scans.

The sunphotometer was a 3-channel CSEM SPM2000, S/N 16, (CSEM2016 in the following), originally developed at PMOD/WRC. This instrument measure at approximately 368, 500 and 778 nm with 5 nm FWHM and 2.8° full angle FOV. Each channel has a Si photodiode detector with integrated interference filter in a sealed housing assembled into a temperature-stabilised enclosure.

The broadband direct solar irradiance was measured with an ordinary Eppley NIP (No 20919, 5.7° FOV).

6.2.2 Calibration

The LI-1800 was calibrated several times against standard lamps, Figure 6.1. The lines plotted represent the ratio of the spectral calibration factors derived at each calibration to the reference calibration factors, which simply were calculated as the mean of the four calibrations. The two standard lamps are 1000 W halogen lamps that were calibrated by the Swedish National Testing and Research Institute at a scale traceable to NIST. For wavelengths, λ, shorter than about 500 nm the calibration results indicate a strong degradation in responsivity with time. Between the calibrations on 1999.06.02 and 1999.10.22 the responsivity at 368 nm decreased by almost 3.6 %. For longer λ (λ still shorter than 500 nm) the change was smaller and for even shorter λ the change was larger. Therefore, for $\lambda < 550$ nm the responsivity change was modelled as a linear function of time and as a third degree polynomial function of λ. Comparison with the CSEM2016 sunphotometer 368-nm channel at optical airmass ≈ 2, also indicates significant responsivity degradation with time of the LI-1800. For the same period (142 days) the degradation was estimated to be 2.4 % using CSEM2016 as reference.

Also for wavelengths longer than 950 nm the calibration results vary a lot. However, there was not a continuous change in time. As already shown by Riordan et al. (1989) the LI-1800 has a very strong temperature dependence, especially in the IR region. Since neither the instrument nor the calibration room was temperature stabilised, the responsivity variations for $\lambda > 950$ nm are thought to be caused mainly by different detector temperatures. Unfortunately, since neither the LI-1800 was temperature stabilised nor the detector temperature was measured, the dependence on temperature could not be compensated for. For determination of AOD at $\lambda > 950$ nm this is a serious drawback. As final calibration for $\lambda > 550$ nm the average of the four lamp calibrations was applied on all LI-1800 measurements during the study.

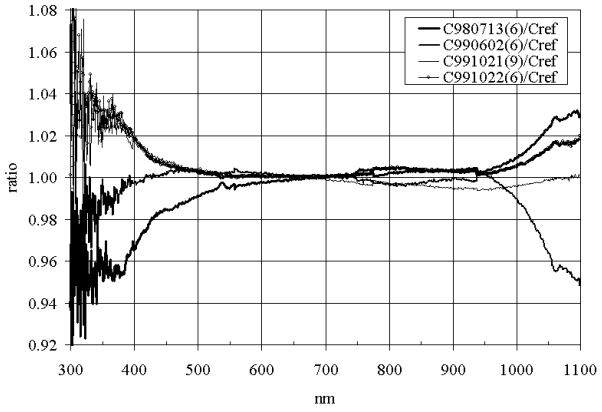

Figure 6.1: Lamp calibrations of LI-1800. Ratios of individual calibration results (spectral calibration factors) to the average of the results (Cref). Lamps: SP-6 and SP-9.

For a sunphotometer channel the expected output voltage, V_0, for a measurement outside the atmosphere at mean Sun-Earth distance is used as calibration constant. The CSEM2016 has been calibrated several times at PMOD/WRC, both against lamps and by comparison with the standard group of sunphotometers. Analysis of classical Langley-plots (about 50 suitable occasions 1995-2000) has also been made on data from the measuring site in Norrköping (43 m above sea level). The difference between lamp and sun calibration results at PMOD/WRC for CSEM2016 is 0–4 %. The sun calibration results are considered to be much more accurate (Schmid and Wehrli, 1995). The CSEM2016 was compared to the standard group both in February 1998 and in March 1999. For some unknown reason the resulting V_0:s were for all three channels 3-4 % lower in 1999 than in 1998. Linear regression of the (logarithm of) Langley-plot results from Norrköping agree within 0.8 % (778 nm) or better with the PMOD/WRC results of 1999, while they lie about 3 % lower than the PMOD/WRC calibration of 1998. For this reason the results of the 1999 PMOD/WRC calibration were applied on all sunphotometer data in the present study.

The NIP #20919 is regularly calibrated against the two reference pyrheliometers of SMHI, PMO-6 #811108 and Å-171. The NIP has been found to be very stable over time (Persson, 2000). A single calibration factor (111.0Wm^{-2}/mV) was adopted for the whole study.

6.2.3 Calculation of aerosol optical depth

For the calculations of *AOD* from the LI-1800 spectroradiometer measurements the wavelength range 360–1025 nm was used, excluding portions affected by gaseous absorption bands of water vapour and oxygen (viz 560-600, 616-666, 680-746, 754-774, 786-844 and 872-1014 nm, Adeyefa et al., 1997). Measurements in the range 300-360 nm, where irradiance is considerably low, have been excluded because of the low signal to noise ratio in that region. At the remaining wavelengths only the extinction due to Rayleigh scattering and ozone absorption where taken into account in the *AOD* calculations. The *AOD* at wavelength λ then becomes

$$\mathrm{AOD}_\lambda = \frac{\ln\left(\frac{E_{0,\lambda}}{R^2 E_\lambda}\right)}{m_a} - \frac{m_R}{m_a}\frac{p}{p_0}\delta_{R,\lambda} - \frac{m_0}{m_a}\delta_0, \tag{6.1}$$

where $E_{0,\lambda}$ = extraterrestrial solar irradiance at mean Sun-Earth distance, E_λ = measured direct solar irradiance, R = actual Sun-Earth distance expressed in AU, m_a = aerosol optical airmass, m_R

= Rayleigh optical airmass, m_o = ozone optical airmass, p = air pressure at station altitude, p_0 = standard pressure = 1013.25hPa, δ_R = Rayleigh optical depth (Fröhlich and Shaw, 1980), and δ_o = ozone optical depth = $l_o k_{o,\lambda}$, l_o = total column amount of ozone and $k_{o,\lambda}$ = extinction coefficient for absorption in ozone. Data on the extraterrestrial solar irradiance and $k_{o,\lambda}$ were taken from the SMARTS2 model (Gueymard, 1995) and data on total ozone was taken from co-located measurements with a Brewer MkIII spectroradiometer (Josefsson, 2000). Since the vertical distribution of the aerosol particles was not known, which mostly is the case, the approximation $m_a = m_R$ was made.

For the sunphotometer data *AOD* was calculated in the same way as for the LI-1800, except that $E_{0,\lambda}$ and E_λ in (1) were replaced by $V_{0,\lambda}$ and V_λ (= measured output voltage from $\lambda -$ nm channel). Only the 500-nm channel was corrected for ozone absorption.

A parameterisation by Gueymard (1998) was used for the estimation of spectral AOD from pyrheliometer measurements. With the aid of this parameterisation the Ångström turbidity coefficient, β, assuming a constant wavelength exponent $\alpha = 1.3$, can be derived. Possible inputs to the parameterisation are solar position, (total) direct irradiance (E_b), atmospheric water vapour content (w), air pressure, total ozone and atmospheric NO_2 content. However, since constant values of ozone and NO_2 are used in the operational turbidity analysis at SMHI, the same restrictions were applied here. The amount of ozone and stratospheric and tropospheric NO_2 were set to 0.35 atm cm, 0.1 matm cm and 0.1 matm cm, respectively.

A correction of the original parameterisation presented in the paper (Gueymard, 1998) has been applied. The reason for this is the result obtained by Tomas Landelius at SMHI from a comparison between β derived from a minimisation routine of the complete SMARTS2 model and β derived with the aid of the parameterisation. The result of this comparison is shown in Figure 6.2. The SMARTS2 minimisation gives lower β values. Apparently, the difference between the two methods is an almost perfect linear function of solar elevation. The reason for this discrepancy has not yet been found out in the discussions between Gueymard and Landelius. The original β values from the Gueymard parameterisation, β_{Gu}, were corrected to

$$\beta = \beta_{Gu} - 9.035E-05 \cdot h - 0.0027 \tag{6.2}$$

with h = (apparent) solar elevation (°).

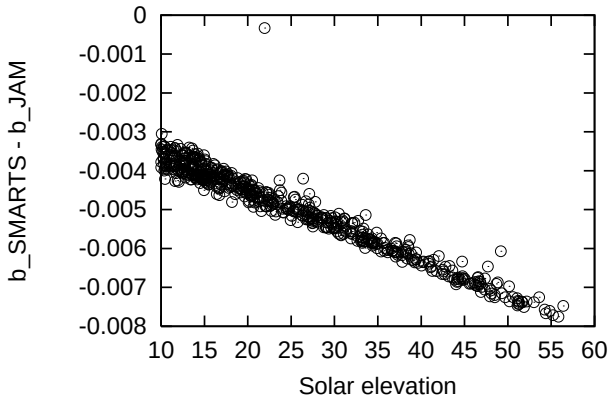

Figure 6.2: The difference between β derived from minimisation of SMARTS2 and β derived with parameterisation by Gueymard.

According to the paper by Gueymard it is also possible to compensate for the circumsolar radiation received by ordinary, relatively large FOV, pyrheliometers, such as the Eppley NIP. The circumsolar correction significantly increases the calculated β values. However, motivated by the results of this study below, the circumsolar correction was not applied.

The column amount of water vapour (w) is a critical input for a good estimate of β. In this study, w was calculated from the 6-12 hours forecast fields of the operational weather forecast model HIRLAM. In a comparison of w calculated from radiosounding data and HIRLAM fields from April and July 1997, it was found that on average w(HIRLAM) was higher than w(radiosoundings). But the difference was slightly less than 1mm ($=$ kg/m^2) only.

6.3 Results

Examples of instantaneous spectral AOD derived using the three different instruments are plotted versus wavelength in log-log diagrams in Figure 6.3. The AODs are from one very clear day (1999-04-19) and from a more turbid day (1999-09-14). For the more turbid case the Ångström relation (AOD$_\lambda = \beta\lambda^{-\alpha}$, λ expressed in microns) is a very good approximation of the spectral distribution of AOD ($\alpha = 1.7$, $\beta = 0.025$) both according to the spectroradiometer and the sunphotometer.

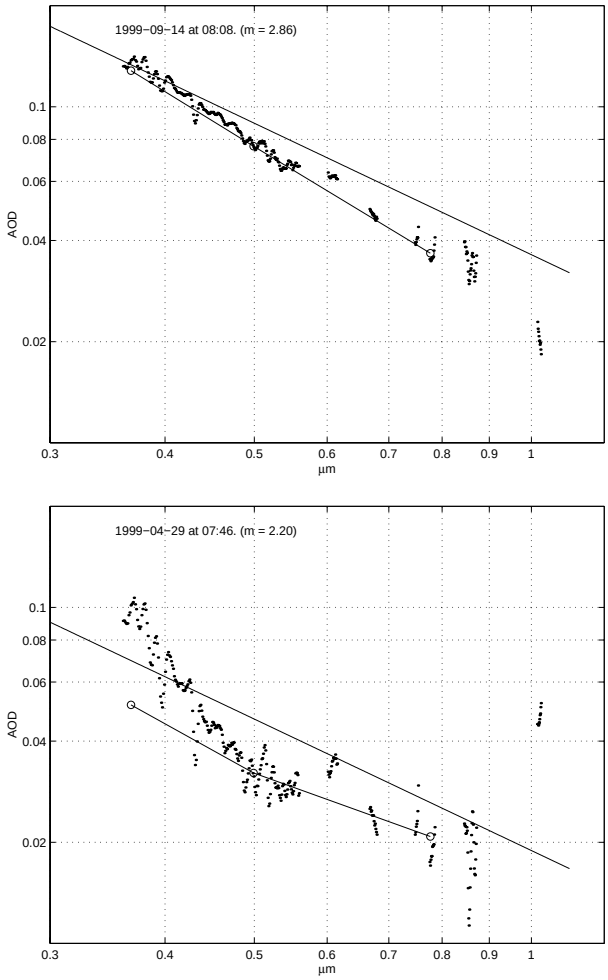

Figure 6.3: Examples of spectral AOD derived from measurements with LI-1800 (•), CSEM2016 (o—o),and NIP (—).

Using single α and β in the clear case does not work as well ($\alpha \approx 1.2$, $\beta \approx 0.015$). The log-log plot

could be a bit misleading, but nevertheless the disagreement between LI-1800 and CSEM2016 AODs for $\lambda < 450$nm and $\lambda > 950$nm is much higher in the clear case. In addition to the temperature dependence for $\lambda > 950$nm and the presumed responsivity degradation with time (or exposure?) for $\lambda < 500$nm in the LI-1800, also an airmass dependence at shorter wavelengths is indicated by comparison with the CSEM2016 at 368 nm.

Using the sunphotometer as reference, calibration factors for the LI-1800 at 368 nm, which would give the same AOD as the CSEM2016, were calculated. LI-1800 calibration factors for $\lambda = 368$nm appears to be very dependent on airmass, Figure 6.4. Possible explanations for this could be non-linearity, temperature dependence and tilting of the instrument. Of course, an erroneous $V_{0,368}$ applied on the CSEM2016 signals could also lead to such a result.

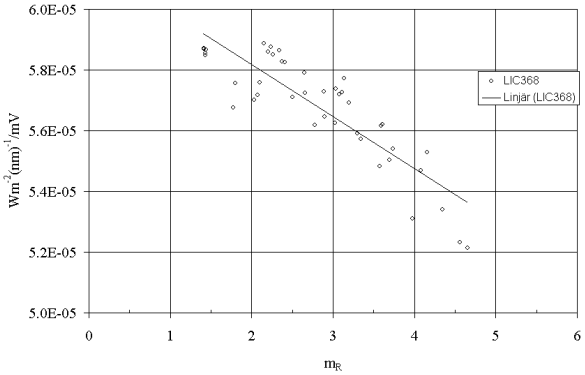

Figure 6.4: Calibration factors for LI-1800 at 500 nm using CSEM2016 as reference, 1999.04.27-29.

However, it is strongly believed that the error in $V_{0,368}$ (non-linearity included) is much less than the 10 % that at least is needed to give results similar to those in Figure 6.4. If such a large change had occurred after the calibration in 1999 at PMOD/WRC, this would have shown up even in the Langley-plots of sunphotometer data from Norrköping. After the calibration in Davos, 35 accepted Langley-plots have been made. The maximum deviation from the average $V_{0,368}$ is about $\pm 4\%$, but the deviation of the mean from the PMOD/WRC $V_{0,368}$ is only +0.3 %.
The differences between AOD derived from sunphotometer measurements and the other two methods for the three investigated wavelengths are plotted vs. optical airmass in Figure 6.5. The total number of cases is 279 originating from 32 days spread over a year. For m > 2 the agreement between the LI-1800 and the CSEM2016 AODs is very good, normally within 0.01, at 500 and 778 nm, Figure 6.5.

At 368 nm the difference is larger, especially for m < 3 and the dependence on optical airmass is also clear. Due to the problems at shorter λ the average difference between AOD(NIP) and AOD(CSEM2016) is actually less than the average difference between AOD(LI-1800) and AOD(CSEM 2016) at 368 nm (Figure 6.5 and Table 6.2).
Mostly, the broadband method overestimates AOD at all three wavelengths. The spectral AOD(NIP) estimates were on average 0.017, 0.016 and 0.011 higher than the sunphotometer AODs at 368, 500 and 778 nm, respectively. Using the original parameterisation by Gueymard, but still without the circumsolar correction, increased the average differences to 0.036, 0.029 and 0.018, respectively. Finally, adding also the proposed circumsolar correction increased the mean differences even further, to 0.061, 0.046 and 0.028 for the same wavelengths.

Naturally, there is a larger scatter in the difference between AOD derived from pyrheliometer and spectral (sunphotometer) measurements, Figure 6.5. This is mainly due to erroneous values of α and w used in broadband method. The scatter increases with decreasing airmass.

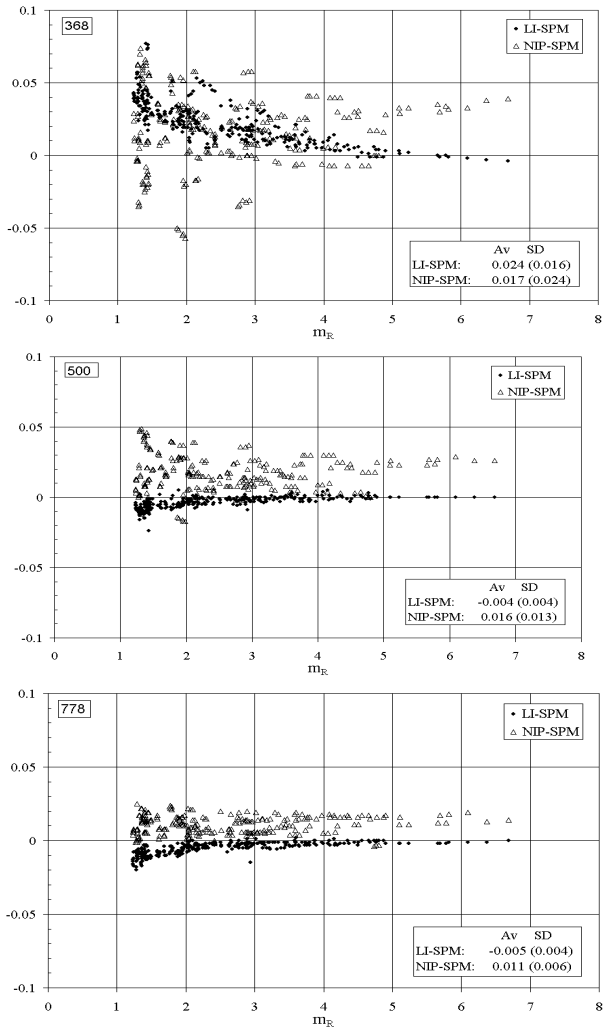

Figure 6.5: Differences in derived $AODs$ at 368, 500 and 778 nm. (LI=LI-1800, SPM=CSEM2016 sunphotometer.)

The aerosol conditions for the data used in this study (March 1999 to March 2000) as determined from CSEM2016 data are listed in Table 6.1. Statistics of the AOD comparison are summarised in Table 6.2. As is clear from Table 6.1, the atmospheric turbidity and the AOD where mostly low during the study, with no occasions of really high turbidity ($\beta \geq 0.200$).

6.4 Conclusions and discussions

From this small study the following conclusions are drawn:

- Especially due to its low accuracy and instability at $\lambda < 500$nm and $\lambda > 950$nm, the LI-1800, in its present configuration, is not suitable for AOD determination. In particular not for long-term monitoring and/or at locations with normally low turbidity.

- According to the CSEM2016 sunphotometer an average $\alpha = 1.36$ (in the wavelength range 368 – 778 nm) was found during the period of the study at the inland site in southern Sweden.

Table 6.1: Average aerosol conditions during the study.

	AOD(368)	AOD(500)	AOD(778)	α(regr)	β(regr)
Mean	0.115	0.073	0.040	1.364	0.028
Median	0.084	0.054	0.032	1.370	0.023
Max	0.428	0.292	0.158	1.940	0.113
Min	0.026	0.017	0.011	0.604	0.008
Std dev	0.087	0.057	0.028	0.247	0.019

Hence, using $\alpha = 1.3$ in the AOD determinations from broadband measurements is fairly well supported.

- On average estimates of spectral AOD ($\lambda < 1000$nm) from pyrheliometer measurements of the direct irradiance using the parameterisation by Gueymard (1998) exceeds the *AODs* as determined from accurate spectral measurements.

At present, the author can not explain why AOD mostly is overestimated with the broadband method. As long as there is not a significant error in the PMOD/WRC calibration of the CSEM2016 or in the NIP calibration, it appears rather certain that $AOD_{\lambda<1000nm}$ is overestimated with the broadband method. Using the original parameterisation by Gueymard without the correction by Landelius, and especially if the circumsolar correction is applied, would strongly enhance the overestimation of $AOD_{\lambda<1000nm}$ (Table 6.2). It was indicated that *w* values used on average were a little too high. Giving lower *w* as input, even higher β (and $AOD_{\lambda<1000nm}$) would have been returned by the turbidity parameterisation. It is not known how much water vapour there were above the highest points reached by the radiosounding balloons.

Table 6.2: Comparison statistics based on 279 number of cases. Difference in AOD between LI-1800 and CSEM2016 (LI-SPM), and between NIP and CSEM2016 (NIP-SPM; SEC= Solar elevation corrected β in this study, Orig=Original parameterisation of β by Gueymard, and OrigCS=Original parameterisation of β by Gueymard with circumsolar irradiance correction).

	368				500				778			
	LI-SPM	NIP-SPM			LI-SPM	NIP-SPM			LI-SPM	NIP-SPM		
		SEC	Orig	OrigCS		SEC	Orig	OrigCS		SEC	Orig	OrigCS
Mean	0.024	0.017	0.036	0.061	-0.004	0.016	0.029	0.046	-0.005	0.011	0.018	0.028
Median	0.023	0.018	0.038	0.061	-0.003	0.015	0.029	0.004	-0.004	0.011	0.018	0.028
Max	0.077	0.074	0.100	0.132	0.005	0.049	0.066	0.089	0.002	0.025	0.036	0.049
Min	-0.004	-0.057	-0.037	-0.006	-0.024	-0.017	-0.004	0.016	-0.020	-0.004	0.002	0.008
Std dev	0.016	0.024	0.025	0.021	0.004	0.013	0.014	0.015	0.004	0.006	0.006	0.008

Finally, if a higher α had been used in the development of the parameterisation, this would also have lead to higher AODs at 368, 500 and 778 nm in the end.
The atmospheric conditions during the study were very clear. Most probable this has influenced the results of the AOD comparison.

Acknowledgement The work has been carried out with financial support from the Swedish National Space Board, which is gratefully acknowledged.

6.5 References

Adeyefa, Z. D., B. Holmgren, and J. A. Adedokun, 1997, Spectral solar radiation measurements and turbidity: Comparative studies within a tropical and a sub-arctic environment, Solar Energy, Vol. 60, No. 1, pp 17-24.

Fröhlich, C., and G. E. Shaw, 1980, New determination of Rayleigh scattering in the terrestrial atmosphere, Applied Optics, 19, 1773-1775.

Gueymard, C., 1995, SMARTS2, a Simple Model for the Atmospheric Radiative Transfer of Sunshine: Algorithms and performance assessment. Tech. Rep. FSEC-PF-270-95, 78m pp. [Available from Florida Solar Energy Center, 1679 Clearlake Rd., Cocoa, FL 32922-5703.]

Gueymard, C., 1998, Turbidity determination from broadband irradiance measurements: A detailed multicoefficient approach, Journal of Applied Meteorology, Vol. 37, pp 414-435.

Josefsson, W., 2000, Measurements of total ozone 1997-1999, Reports Meteorology and Climatology No. 91, SMHI.

Kasten, F., A.T. Young, 1989, Revised optical airmass tables and approximation formula, Applied Optics 28, 4735-4738.

Persson, T., 2000, Measurements of solar radiation in Sweden 1983-1998, Reports Meteorology and Climatology No. 89, SMHI.

Riordan, C., D. Myers, M. Rymes, R. Hulstrom,
W. Marion, C. Jennings, and C. Whitaker, 1989, Spectral solar radiation database at SERI, Solar Energy, Vol. 42, No 1, pp. 67-79.

Robinson, N. (Ed.), 1966, Solar radiation, Elsevier, Amsterdam.

Chapter 7 Aerosol forcing of climate

Ignacio Galindo
Centro Universitario de Investigaciones en Ciencias del Ambiente,
UNIVERSIDAD DE COLIMA,
Colima, Mexico

Abstract

After clouds, atmospheric aerosols are the most important modulators of the radiation field. The radiation balance is affected due to changes in the amount of composition of aerosol particles. This effect is known as aerosol radiative forcing and it can be of the same order of magnitude as radiative forcing due to greenhouse gas concentrations. However uncertainties in forcings by changes in the atmospheric aerosol and cloud are much larger even in the sign of forcing. Here , I shall present our own results on mineral aerosols, volcanic aerosols, smoke aerosols and anthropogenic aerosols.

7.1 Introduction

The climate of the earth depends on the balance between the energy absorbed from solar radiation and outgoing radiation emitted in the form of long-wave radiation. Changes in this balance due to anthropogenic or externally imposed changes in the chemical composition of the atmosphere are referred to as *radiative forcings* measured in Watts per square meter (Wm^{-2}). This balance can be affected by a number of factors such as a change in the output of solar radiation, changes in greenhouse gas concentrations, and an increase in aerosol loading either in the troposphere and/or the stratosphere. While the uncertainties in the global mean greenhouse-gas forcing are not negligible ($\sim$15%), uncertainties in forcings by changes in the atmospheric aerosol and in clouds are much larger, and in some cases even include uncertainty in the sign of forcing (Charlson and Heintzenberg, 1994). Therefore, aerosol effects on atmospheric radiation are a leading source of uncertainty in predicting climate change.

Of the variety of mechanisms through which the aerosols affect climate there are three principal mechanisms

1. Direct effect of aerosols on the radiation budget of the surface-atmosphere system through a re-distribution of short-wave solar radiation and infrared thermal emissions

2. The crucial role of aerosol particles in the phase transformations of water in the atmosphere, in particular, in cloud formation, which may be more important for the energetic of the atmosphere than in the former mechanism. In this connection of great concern is the role of gas-to-particle reactions of aerosol formation (condensation nuclei, first of all) connected with natural and anthropogenic emissions to the atmosphere of the compounds such as dimethylsulfide (DMS) and sulfur dioxide (SO_2) (Andrea and Crutzen, 1997)

3. Heterogeneous chemical processes, in particular, the processes of disintegration of ozone molecules on the surface of aerosol particles, which affect the change in the ozone molecules on the surface of aerosol particles, which affect the change in the atmospheric gas composition (Finlayson-Pitts and Pitts, 1997)

7.2 The nature of aerosols and their effects

The atmospheric aerosol consists of particles which size ranks between super-micrometer (μm) and submicrometer scales of liquid and solid materials suspended in the air. Both natural and anthropogenic materials occur in the aerosol particles: most particles larger than *ca.* 1 μm are produced mechanically (e.g. windblown soil dust and sea salt from sea-spray and bursting bubbles) and particles smaller than ca. 1 μm are dominantly formed by condensation (e.g. low-temperature condensates such as sulfate from atmospheric oxidation of SO_2, and high-temperature condensates like soot and smoke from partial combustion). The super- and submicrometer materials are partially mixed by processes in the atmosphere (e.g., coagulation and cloud coalescence). Climatically relevant particles occur throughout the stratosphere and troposphere in number concentrations that range from tens to tens of thousands of particles per cubic centimeter. While in the atmosphere, the aerosol particles physically affect the heat balance of the Earth, both directly by reflecting and absorbing solar radiation and by absorbing and emitting some terrestrial infrared radiation and indirectly by influencing the properties and processes of clouds and, possibly by changing the heterogeneous chemistry of reactive greenhouse gases (e.g., O_3). Substantial perturbation of the sulfate aerosol has occurred due to anthropogenic SO_2. Other aerosol sources also are climatically important, including biomass combustion, volcanoes and dust storms. Besides anthropogenic aerosol, it is of particular significance to emphasize two key aerosol types that cause climate forcing (as defined above), namely biomass burning and volcanic aerosols.

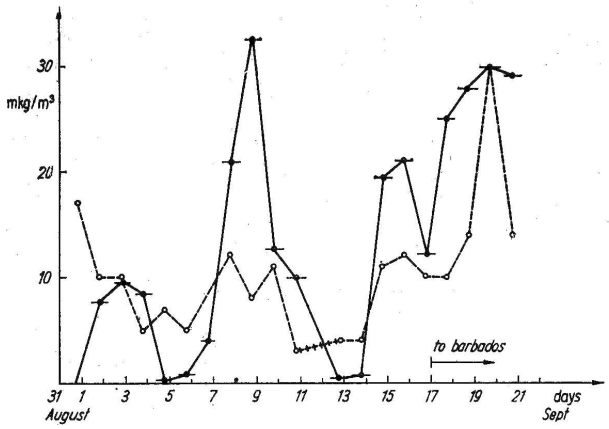

Figure 7.1: Aerosol concentration measured on board the A-scale Mexican R/V "'M. Matamoros"' during the third phase of GATE (8.5 N, 45.5 W). Continuous line is insoluble (mineral of aerosol concentration). Dotted line is soluble aerosol concentration (Galindo, 1978).

The functional relationships of the aerosol forcing to the source strengths of aerosol particles or their precursor gases are somewhat different for the clean versus the polluted case. The direct effect increases approximately linearly with aerosol number or mass concentration for the typical small optical depths observed in either clean or polluted locations, but (as pointed out by Toon (1994) the indirect effect goes as the logarithm of the number concentration of particles acting as cloud condensation nuclei (CCN). This is why, although a doubling of SO_2 emissions may produce direct and indirect effects of comparable magnitude in polluted regions of the Northern Hemisphere (NH), by contrast in remote marine regions the indirect effect of doubling dimethylsulfide emissions far exceeds the direct effect.

7.2.1 Aerosol measurements

The concentration of aerosol particles varies significantly due to their short lifetime (about a week) and transport of aerosols from one region to another. Therefore a complete assessment of aerosol characteristics, from remote or *in situ* measurements requires frequent measurements and high spatial coverage.

There is a number of instruments devoted either to direct or indirect aerosol measurements (see Jennings, 1993) here we shall concentrate mainly in radiometric measurements either at the surface or satellite measurements. The main limiting factor of radiometric measurements is that most of these sensors have spectral broadbands, whereas it has been proved that the best aerosol depth determinations are obtained by using narrow band filters. As the ones used in UVB narrowband radiometers or the precision filter radiometer for surface measurements, whereas for remote sensing measurements the SeaWiffs sensors from NASA satellites offer a unique opportunity for AOD dedterminations. In any case, here we shall present our own results after many years of experience.

Table 7.1: Chemical analysis data for the aerosol particles sampled on 4 September,1974, by the USSR IL-18 aircraft in the dust cloud*

Height	Elements, mkg/m^3					
Meters	Fe	Cu	Cr	Pb	Mg	Al
450	14.0	3.0	0.15	0.2	7.0	9.0
450	20.0	-	0.04	0.2	-	4.0
1500	14.0	3.0	0.15	0.2	7.0	9.0
4500	14.0	1.0	-	0.3	6.9	12.0
5200	14.0	-	0.04	3.4	-	-
6000	14.0	-	0.02	3.0	-	5.0

* *Taken and modified from Table 4 p. 51 from Kondratyev et al., 1976: Aerosol in the GATE area and its radiative properties. Trans. MGO, Leningrad, Issue No. 381, Atmos. Science Paper No. 247, Dept. Atmos Sci., Colorado State University*

7.2.2 Mineral aerosols

The primary sources are the arid and semiarid regions of the world. The global annual input of mineral aerosols to the atmosphere is probably $\varphi 1000 - 2000 \mathrm{Tgyr}^{-1}$ (Duce, 1994). Both the generation of this mineral dust and its atmospheric distribution are characterized by significant temporal as well as horizontal and vertical spatial variability. Concentrations can often change by several orders of magnitude within a day, Mineral particles are often found in a horizontal-layered structure that can be maintained for thousands of kilometers. Far from source regions the mass median radius of mineral particles is $\sim 0.5 - 1.5 \mu$m with larger sizes closer to the source. Climate forcing by atmospheric mineral matter is clearly important. Direct forcing by dust results from the scattering and absorption of solar radiation and from absorption of terrestrial (infrared) radiation by silicaceous material. In what follows we shall concentrate particularly on the Saharian Aerosol Layer (SAL). Most of the studies dealing with SAL were performed during the GATE experiment either by aircraft: Spectral SW (Kondratyev and Berlyand, 1974; Kondratyev and Ter-Markaryants, 1976) and filter Eppley pyranometer measurements (Drummond and Robinson, 1974; Carlson and Caverly, 1977; Cox, 1975 within others), or by ships (Galindo et al., 1977, Binenko and Harshvardhan, 1993, within others). The refractive index $\mathrm{m} = 1.54 - -0.008\mathrm{i}(\lambda = 0.55 \mu\mathrm{m})$ of SAL was determined by Carlson and Caverly, (1977). The imaginary part of m is responsible for the SW absorption. The chemical analysis revealed the presence of elements typical of continental aerosol (Fe $\sim 10 - 15 \mu\mathrm{gm}^{-3}$ as hematite; Al 5-10 μg m^{-3} (see Table 7.1). According with Galindo et al. (1977), during the dust

outbreaks (Figure 7.1), the diffuse radiation increased by 40-90% and the turbidity factor by 60%; the Angström extinction power drops from 1 to almost 0 (neutral extinction) (Table 7.2). The highest SW radiative heating rates were registered in the 1-2 km layer (up to 0.43°Chr^{-1}), while in the absence of SAL, these rates are at a maximum in the 0-1 km layer (about 0.12°Chr^{-1}) (Galindo, 1978). The above heating rates are in good agreement with those later reported by Ellingson and Serafino (1984)

Table 7.2: Atmospheric Transparency in the presence of dust

Site and Meteorological Conditions	Vertical Transparency of the Atmosphere		$\sigma = \beta\lambda^{-\alpha}$		Horizontal Transparency of the Atmosphere	
	P_2	σ_2	α	β	S_m, km^{-1}	α, km^{-1}
R/V "Akad. Kurchatov"10 August, 1972(Zone of dust outbreak)(18° 8´N, 16° 5´W)	0.58 (0.69)	0.545 (0.372)	0.2	0.34	12	0.250
R/V "Mariano Matamoros"8 September, 1974(Heavy haze)(06° 30´N, 48° 30´W)	0.58	0.581	0.5	0.42	10	
5 September, 1974(Haze-free)(06° 30´N, 48° 30´W)	0.74	0.300	1.1	0.14	20	
Average for the period of Tropex'72	0.66 (0.78)	0.416 (0.249)	0.6	0.12	30	0.200

Galindo, I.: On the presence of Saharian aerosol at the Western part of the Atlantic Ocean. Zeitschrift für Meteorologie, Heft 6, B 28, 352-360, 1978

7.2.3 Sulfate Aerosols

Cloud researchers are prone to the idea that a large part of the cloud condensation nuclei (CCN) in remote environments consists predominantly of sulfate compounds. Yet, does this sulfate in the Earth's atmosphere play a role of a causal factor in the formation of CCN and actually influence the properties of numbers of cloud droplets? (Möller, 1994) this question is still under discussion, especially regarding which sources of atmospheric sulfate dominate this role. Marine dimethylsulfide (DMS) is now believed the most natural sulfate precursor, and SO_2 from fossil-fuel combustion is the dominant anthropogenic one.

The direct climatic effect of sulfate aerosol is due simply to reflection of sunlight back to space, while indirect climatic effects of sulfate result from aerosol influence on cloud albedo and/or extent. Sulfate aerosols contribute to cooling, either directly or indirectly through their role in cloud formation. Droplet sizes and liquid water content are both important in controlling the cloud albedo, and droplet size is partly determined by the population of particles. Also, changes in the chemical composition of aerosols may either increase or decrease the number of CCN. Changes in cloud droplet number concentration can affect not only the albedo but also the cloud lifetimes and precipitation patterns. Precipitation is both an important aspect of climate and the ultimate sink for submicrometer particles.

The total mass of sulfur that is cycled through the global atmosphere has been drastically increased by industrial activity. Anthropogenic SO_2 emissions currently account for ca 84% of the total global flux of SO_2 and more than 90% is injected into the Northern Hemisphere (Langner and Rodhe 1991). Still, only 10% of the global anthropogenic sulfur emissions account for 50% of the sulfur budget of the Southern Hemisphere (Möller, 1994). Thus, even in remote areas we must assume that the sulfur budget is markedly disturbed by human activity.

Sources of sulfur to the atmosphere

Volcanic emissions It is necessary to distinguish between eruptive and non eruptive emissions, most of which is probably SO_2, within an estimated inventory of 13Tgyr^{-1} based upon an early 1970's to 1997 time frame (Andres and Kasgnoc, 1997). Volcanic emissions consists of solid particles (ash) and gases (mainly water vapor (H_2O), sulfur dioxide (SO_2) and carbon dioxide (CO_2) in very variable concentrations. SO_2 is a precursor to aerosol formation by gas to particle conversion. The ash particles are mainly in the coarse particle range and are formed by silicates (S_iO_2). Most of the known active volcanoes are in the Northern Hemisphere, and only 18% are between 10° S and the South Pole (Simkin et al., 1981). In regions with frequent volcanic activity, the emission of sulfur and other components may be important (Hobbs et. al., 1981) For example, Allard et al., (1991) estimate the sulfur emission of Etna/Sicily to be 0.7Tgyr^{-1} S averaged over the years 1975 to 1987. Actual measurements of subaerial SO_2 volcanic emissions indicate a time-averaged flux of 13Tgyr^{-1} S based upon an early 1970's to 1997 time frame. When considering the other sulfur species also present in volcanic emissions, a time-averaged inventory of subaerial volcanic sulfur emissions is 10Tgyr^{-1} S (Andres and Kasgnoc, 1997). On average, less than 10% of this amount reaches the stratosphere. This numbers may vary by an order of magnitude in individual years, for example following explosive eruptions like Mt. Pinatubo (9 TgS in 1991) and El Chichón (3.5 TgS in 1982) (Climate Change, 1994).

In what follows we shall present some results on volcanic aerosols mainly obtained from radiometric measurements.

The El Chichón Volcano Eruption On March 28, 1982, at 23:30 local time an eruption of the El Chichón volcano in Chiapas (a southeastern state in Mexico) started. El Chichón underwent three major eruptions in late March an early April 1982. As has been pointed out by Hofmann (1987, 1988) and Hofmann and Rosen (1987) more was learned about the effects of volcanic aerosols on the stratosphere following the El Chichón eruption than from all previous eruptions combined. Which was due mainly to the wealth of research techniques that could be brought to bear with little delay (Kondratyev and Galindo, 1997). Volcanic SO_2 was observed from space for the first time, and its conversion into H_2SO_4 vapor, condensation nuclei and finally sulfuric acid aerosol were monitored by both in situ and remote sensing techniques. The final eruption, on April 4, penetrated to altitudes in excess of 25 km and probably injected more sulfurous gases than any eruption in the previous 100 years. Optical, chemical and mineralogical properties of the Chichón ash: Patterson, et al. (1983) measured visible wavelength optical properties of ash from samples collected at three surface sites between 12 and 80 km from the volcano. Results show a complex refractive index $m = 1.53 - 001i$. The chemical composition of the samples is shown in Table 7.3. The optical microscopic analysis of our three ash samples reveals a particle size bimodal distribution with the coarse particle volume represented $\sim$ 20% due mainly to silicate particles which in turns means that 80% is due to small particles, probably sulfur particles (Patterson, et al., 1983).

Table 7.3: Mineralogical Composition of El Chichon Samples

CONSTITUENT Refractive Index (n_{RE})	FELDSPAR MINERALS $\sim$1.56	VOLCANIC GLASS 1.52-1.53	COLORED MINERALS* $\approx$1.7	OPAQUE** PARTICLES
AM 125	50%	20%	25%	5%
AM 106B	45%	30%	20%	5%
AM 101	30%	65%	5%	

Patterson, E.M., Pollard, C.O., and Galindo, I.: Optical properties of the ash from "El Chichón" volcano. Geophys. Res. Lett., 10, 317-320. 1983.

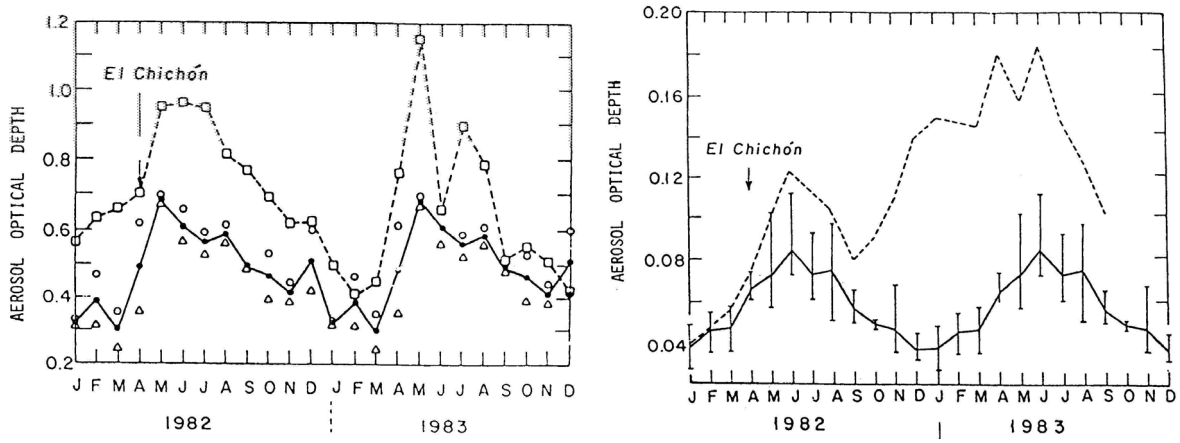

Figure 7.2: Left: Aerosol optical depths at Mexico City for 1982 and 1983 and the monthly mean aerosol optical depths (and absolute maximum (○) and minimum (△) values) for the five years prior to the eruption of El Chichon (Galindo et al., 1996). Right: The same at Vancouver (Hay and Darby, 1984)

The overall energy increase or decrease in the earth-atmosphere system due to the addition of the aerosol layer, the net heating of cooling depends on the relative amounts of scattering and absorption. In case of El Chichón, results indicate a very low value for the imaginary index, that is, radiation absorption is quite low, on the other hand, scattering increases the planetary albedo, in consequence and taking into account the powerful aerosol injection into the stratosphere, one may expect that the El Chichón eruption have a net effect of global cooling.

The assessment of the total amount of erupted SO_2 Total Ozone Mapping spectrometer (TOMS) data was 3.3 Mt. Purple colored twilights were observed for the next two years. Due to the stratospheric volcanic aerosol layer of El Chichón, the air pollution problem of Mexico City was severely impacted through a significant turbidity enhancement (Galindo et al., 1996), particularly during 1983 (Figure 7.2 left) similar results were observed in Vancouver (Figure 7.2 right) by Hay and Darby (1984). Using satellite-derived irradiance measurements I have determined solar radiation extinction anomalies with respect ot the mean values of 1984 for Mexico for the time period 1982-1983 (Galindo, 1992).

During May 1982 high extinction values covered most of the country. From June to August 1982 solar irradiance returned almost to normal values as stratospheric easterlies were well organized shifting the aerosol cloud westwards. After September 1982 solar radiation extinction increased reaching the highest values in December 1982 (27.5%). during January to May 1983 extinction remained high but variable, btween 10 to 22%. From June to August 1983 solar radiation returned again to normal conditions in most of the country although some areas persisted with important extinction anomalies (13%). During September to December 1983 solar radiation extinction remained between 16 to 14% showing that the stratosphere still contained a large amount of residual aerosol (Figure 7.3). The decay of the of the aerosol perturbation behave as a dampened oscillator with seasonal oscillation, maximum and minimum ocurring in local winter and local summer, respectively (Galindo, 1992). The above results are representative of the latitudinal variation of the stratospheric volcanic aerosol.

The Fuego Volcano Eruption On November 1974Volcán Fuego de Guatemala underwent a basaltic andesite minor eruption.

High quality radiometric measurements are capable to detect weak stratospheric volcanic aerosol layers. This was the case of actinometric measurements in Mexico City for the period of 1974-1975.

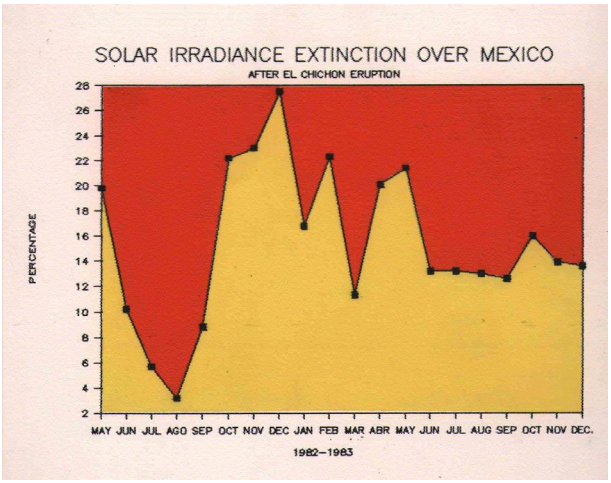

Figure 7.3: Monthly maximum solar radiance extinction over Mexico under cloudless conditions due to El Chichon stratospheric aerosol layer. From May 1982 to December 1983 (Galindo, 1992).

The Schüepp turbidity coefficient for that time period was substracted from the long period monthly averages. Figure 7.4 shows the small increases in turbidity observed from November 1974 to February 1975 (Galindo and Bravo, 1975).

The Popocatépetl volcano eruption On December 21, 1994, after 70 years of quiescence, Popocatépetl volcano, located approximately 55 km SE from Mexico City, quietly erupted and sent an ash cloud to a peak altitude of over 7 km. During the first week of the eruption we have performed airborne and ground-based (correlation spectrometer, cascade impactor and photoelectric counter together with intake filter probes) measurements. Electron microscopy of the samples shows typical aerosol sulfate and sulfuric acid aerosol and, ash fragments of probable basaltic origin (Figures 7.5a,b).

Volcanic aerosol elemental composition together with ash elemental composition were obtained with X-ray fluorescence. Figures 7.6a,b show that these samples were very reached in Fe, however ash elemental composition is also reach in Ca and Tl. Particle size distribution is bimodal (Figure 7.7), the fine particles (sulfates) are higher by almost two orders of magnitude with respect to concentration of ash coarse particles (silicates) (Galindo, et al., 1998).

Remote Sensing Silicate particles in the atmosphere can be detected by NOAA polar orbitters using temperature difference between the infrared channels 4 and 5. This temperature difference is negative while for meteorological clouds is positive (Prata, 1989) therefore we monitor on real time all active volcanoes of Mexico and Central America using our satellite ground receiving station. Using the satellite derived wind field and temperature profile we are able to identify the height and trajectory of the ash cloud (Galindo, 1996) (see Figure 7.8).

The Volcán de Fuego de Colima Eruption This volcano is considered the most active volcano of Mexico. The latest big eruption occurred in January 1913 producing a new crater of about 500 m depth. Ash emissions were transported by the wind very long distances. Mexico City is about 700 km eastward, an analysis of the time series of direct solar radiation measurements shows that the ash cloud came into the city the first days of February 1913 (Figure 7.9)

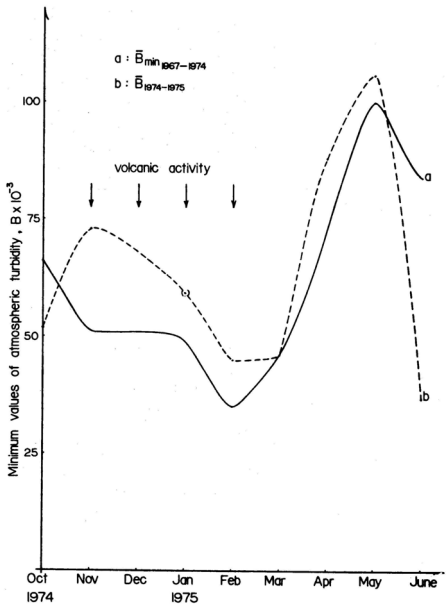

Figure 7.4: Atmospheric turbidity enhancement over Mexico city due to the volcanic cloud from the 1974 Fuego eruption (Guatemala), (Galindo and Bravo, 1975).

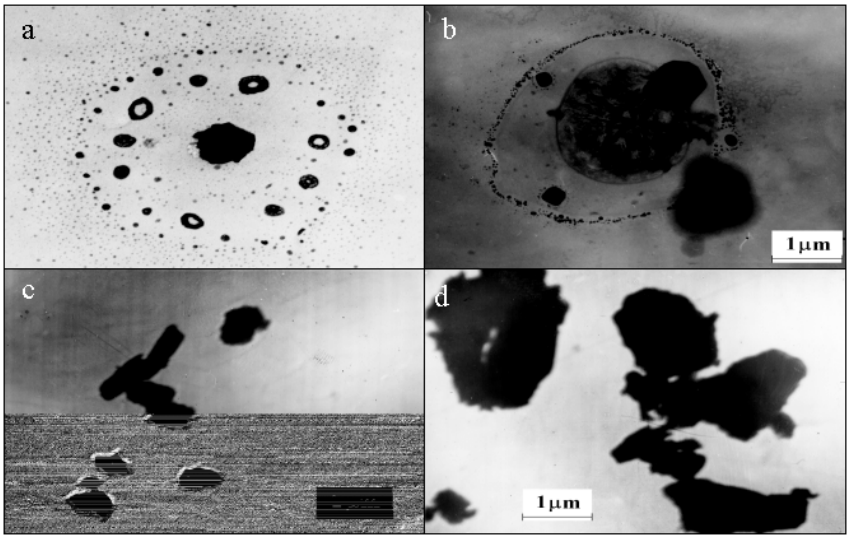

Figure 7.5: Electron microscopy showing typical aerosol sulfate (a) and sulfuric acid aerosol (b) with some traces of evaporated water. Ash fragments of probable basaltic origin are shown in (c) and (d) (Galindo et al., 1998).

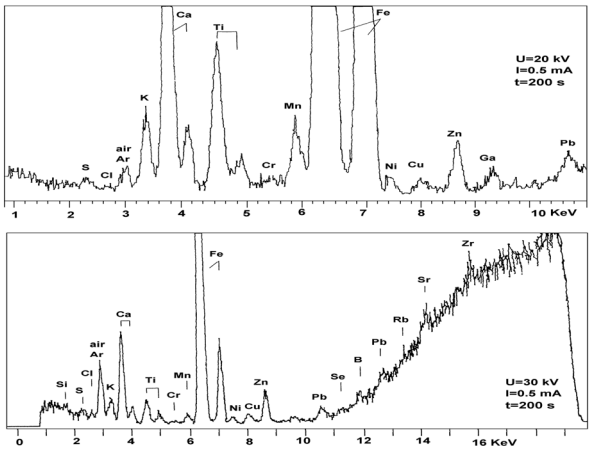

Figure 7.6: a) Volcanic aerosol elemental composition obtained with X-ray fluorescence. b) Volcanic ash elemental composition obtained with X-ray fluorescence (Galindo et al., 1998).

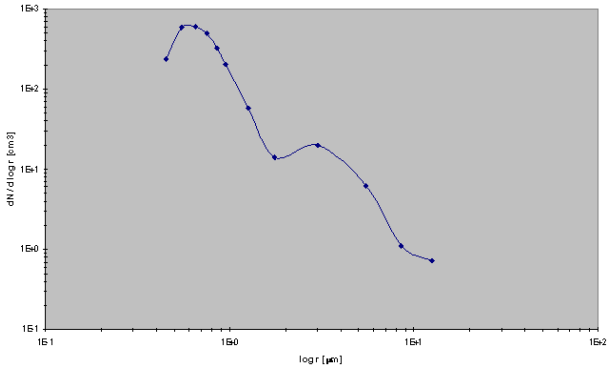

Figure 7.7: Particle size distribution from 24-h cycle of ground measurements taken at Puebla´s airport (Galindo et al., 1998).

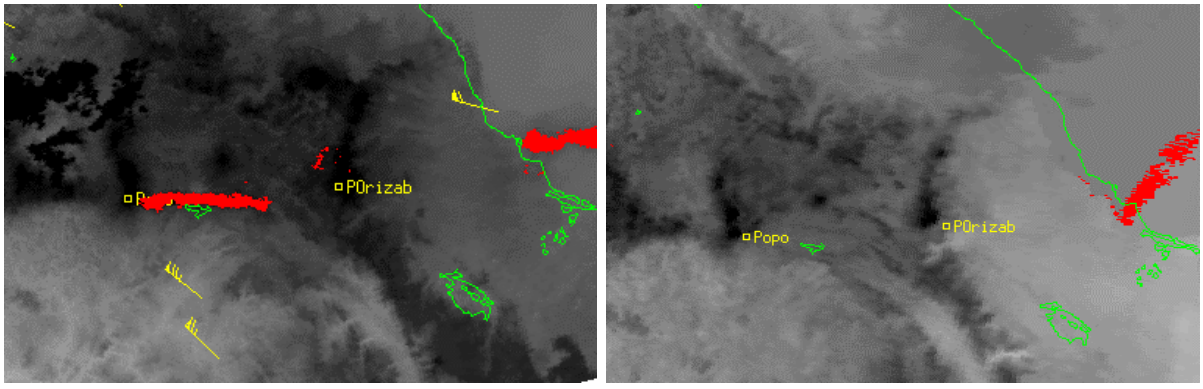

Figure 7.8: Band 4 thermal infrared image and the TDM overlay Popocatepetl Volcano 13/03/96 01:31 GMT (left) and 17/03/96 14:12 GMT (right)

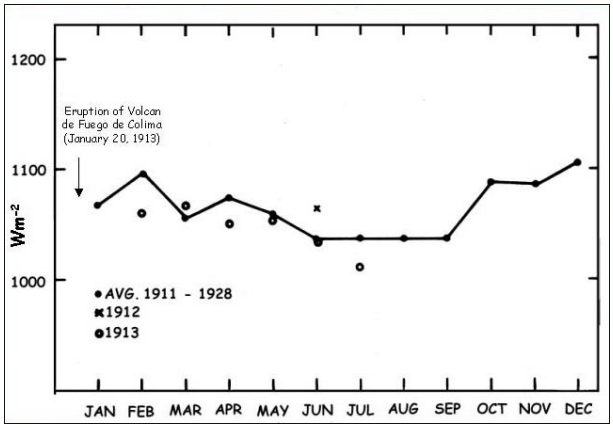

Figure 7.9: Maximum values of direct solar radiation under clear sky conditions measured between 12:00-14:00 local time at Mexico City.

The latest reactivation of the Colima's volcano took place on November 20, 1998. Two days before the lava effusion, the emitted SO_2 reached 1,600 t.day^{-1} (Gavilanes, 1998). In fact, we have detected small ash emissions since 1997 (Figure 7.10).

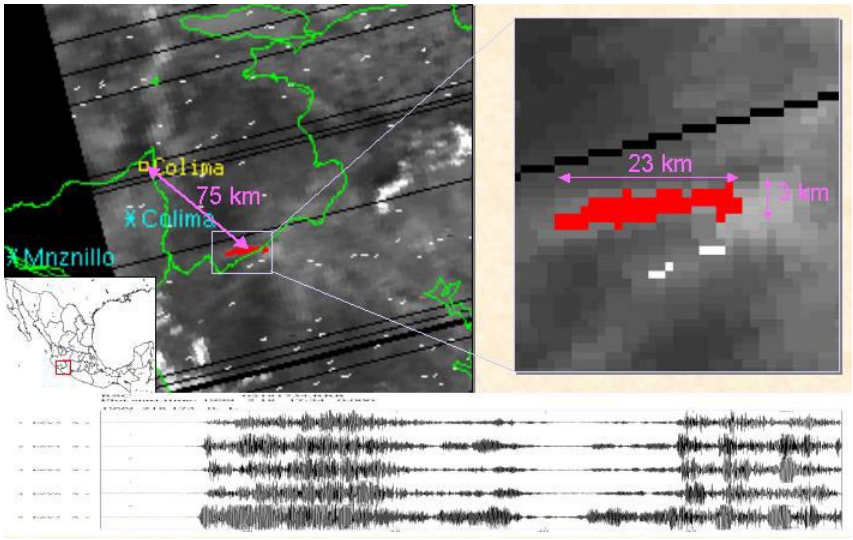

Figure 7.10: Volcanic ash cloud detected from AVHRR imagery after Colima´s volcanic explosion of February 18, 1999. Below are depicted seismic records showing the explosion.

Seasonal biomass burning associated with deforestation and agricultural practices.

Biomass burning is also a major source of atmospheric aerosols. It emits submicron particles composed mainly of partially oxidized organic materials. These particles are both efficient scatterers and absorbers of sunlight (direct forcing effect). They are also efficient cloud condensation nuclei (CCN) and therefore interact with clouds (Warner and Twomey, 1967),

To monitor aerosols from *biomass burning*, the source of the aerosols, fires can be observed from

present polar orbitters and geostationary satellites. Since the pioneer work of Croft (1977,1978) several methods have been developed for forest fire detection using remote sensors. In particular methods that use the Advanced Very High Resolution Radiometer (AVHRR) on board the NOAA satellites are described in Cracknell, 1997, Galindo and Solano (1999) have developed a real-time multispectral method that operates on real time basis. Kaufman, et al., (1990a) and Kaufman, et al., (1990b) detected smoke aerosols using appropriate AVHRR images and estimated the mass of aerosols emitted per fire. Some calculations of the upwelling radiance (at the top of the atmosphere), for particular aerosol distributions, as a function of optical thickness are described by Rao et al. (1989). The analyzed aerosol field was tested using a GOES image showing the smoke cloud from slash burning in Central America in April 1987. Aerosol optical depth retrievals from satellite data are complicated since the albedo is highly variable, most of these attempts have being made on sea surfaces assuming a constant sea albedo and additional sunphotometer data to correlate both determinations (Veefkind, et al., 1999). Actually, we are working in a similar algorithm to retrieve AOD from AVHRR data with smoke layers from biomass burning (see Figure 7.11).

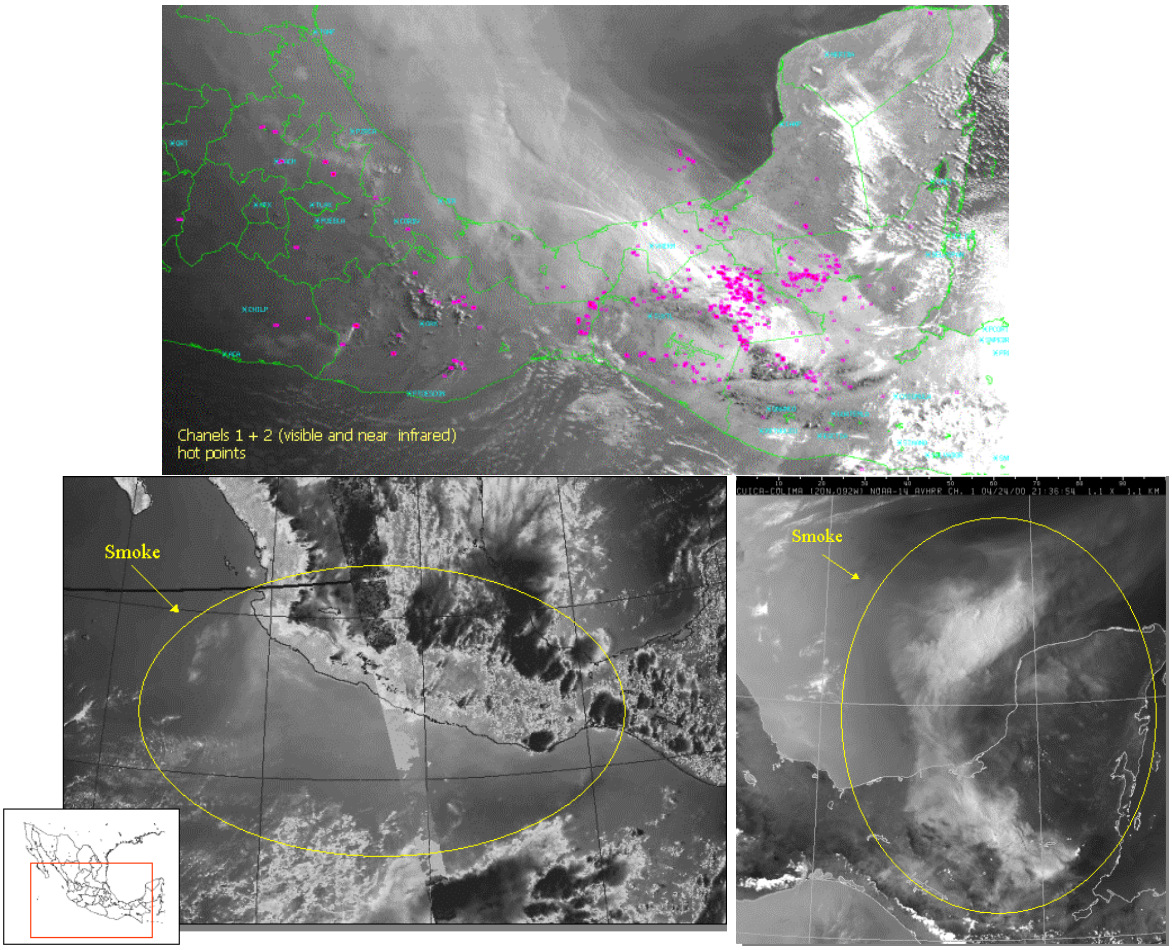

Figure 7.11: Composite AVHRR imagery showing smoke aerosol from forest fires in Mexico and Central America. Above: May 8, 1998, 7:07 local time; Left: May 27, 1999. 17:41 local time; Right: Apr 24, 2000. 16:36 local time.

Antropogenic SO_2 aerosols

Of great concern are the assessments of climate cooling foreseen as a result of increasing anthropogenic sulfate aerosols in the atmosphere, due to emissions of sulfur dioxide and subsequent gas-to-particle reactions of aerosol formation (Kondratyev and Galindo, 1994). Industrialization is associated with population increases which in turns are the main polluters to the atmosphere.

Figure 7.12 (left) shows a comparison of atmospheric turbidity in Mexico City in the period 1911-1928 with that of 1957-1962 over the annual cycle. The turbidity peaked in March and April at the end of the dry season and was mainly from natural sources in 1911-1928. However in recent times there are secondary maxima of turbidity caused by anthropogenic effects. The turbidity has increased considerably since 1967, as it is shown in Figure 7.12 (right) the actual average value is now 300% more than that in 1911-1928 (Galindo, 1984).

The increased turbidity has resulted in a decrease in the incoming direct solar radiation. The formation of an inversion layer in the early morning hours produces an enhanced polluted layer. The weakened beam of solar radiation is not strong enough to reach the threshold for the burning of the paper strip chart of the sunshine recorder. This results in a reduction in the apparent sunshine duration. Figure 7.13 shows the annual variation of sunshine in Mexico City and in a nearby rural station outside the valley. The results are summarized in Table 7.4. Over the last fifty years, atmospheric transmission has dropped by 10% (Galindo, 1984).

Table 7.4: Comparison of chemical elements relative concentrations normalized with respect to Al.

	Colima	Cd. de México	Popocatépetl
Al	1	1	1
Si	9.887999546	2.744599034	13.73251748
P	0.108937775	0.322006763	0.084353147
S	6.944011825	1.645681159	2.176573427
Cl	0.123620199	0.099536232	0.105375874
K	0.05891757	0.127609662	0.057298951
Ca	0.259739247	0.469642512	0.247770979
Ti	0.015632422	0.032637681	0.023942308
Cr	0.001701488	0.010937198	0.002556818
Mn	0.002906709	0.00975942	0.002683566
Fe	0.133694427	0.314707246	0.179195804
Ni	0.000921639	0.002445411	0.000939685
Cu	0.001417907	0.006083092	0.004558566
Zn	0.001843279	0.048182609	0.002263986
Ga	0.000212686	0	0.000161713
Se	0.000283581	0.002	0.000236014
Br	0.000510446	0.0056	0.000397727
Rb	0.000850744	0	0.001123252
Sr	0.001772383	0.000483092	0.001691434
Y	0.000921639	0	0.000659965
Zr	0.001488802	0	0.001311189
Hg	0.000382835	0	0.000227273
Pb	0.000233955	0.034815459	0.001984266

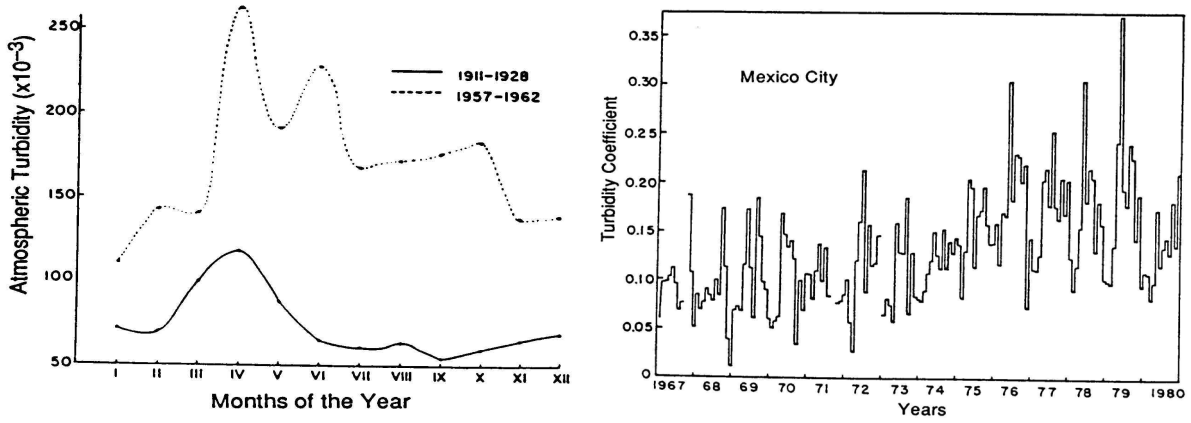

Figure 7.12: Left: Time evolution of atmospheric turbidity in Mexico City, 1911-1928. 1957-1962 (Galindo, 1984). Right: Positive trend of atmospheric turbidity (1967-1980) in Mexico City (Galindo, 1984).

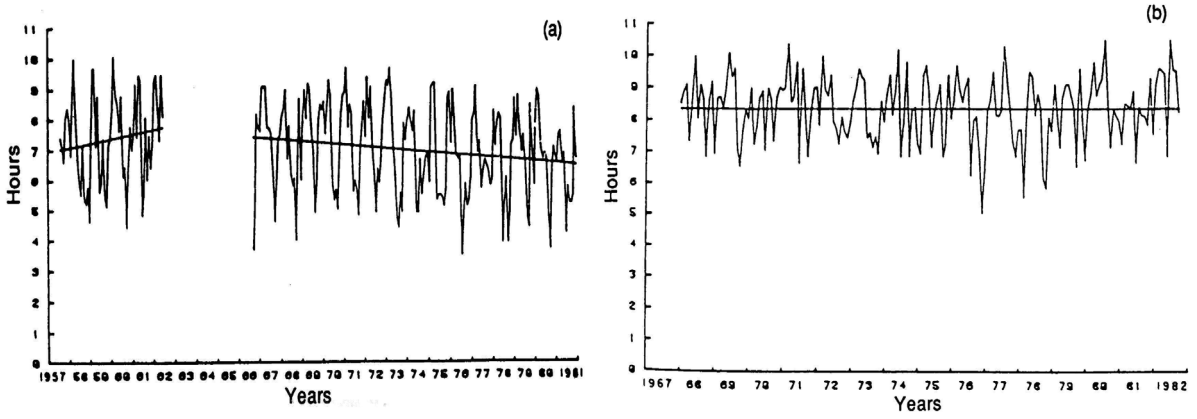

Figure 7.13: Annual variation of sunshine (a) in Mexico city (1957-1981) and (b) in Orizabita, Mexico 1967-1982 (Galindo, 1984).

7.3 Concluding remarks

The direct radiative forcing of the tropospheric aerosols is estimated to have a negative sign and differs significantly in character from the positive forcing due to greenhouse gases. The direct forcing due to the anthropogenic component of the sulfate aerosol is estimated to have a magnitude that is a significant fraction of the greenhouse-gas forcing on a global scale. On continental scales, the aerosol forcing magnitude can become comparable to or even exceed the greenhouse-gas forcing. The indirect aerosol-forcing problem is not as well-posed as that for direct forcing (Ramaswamy et al., 1994)

7.4 References

Allard, P. Carbonelle, J., D. Dajlevic, J. Le Bronec, P. Morel, M.C. Robe, J.M. Maurenas, R. Faivre-Pierret, D. Martin, J.C. Sabroux and, P. Zettwoog, 1991: Eruptive and diffuse emissions of CO_2 from Mount Etna, *Nature* **351**, 387- 391.

Andrea, M. O. and P. J. Crutzen, 1997: Atmospheric Aerosols: Biogeochemical Sources and Role in Atmospheric Chemistry. *Science* **276**, 1052-1057.

Andres, R.J. and A.D., Kasgnoc, 1997: A Time-averaged inventory of subaerial volcanic sulfur emissions. Global Emissions Inventory Activity, 23 pp.

Binenko, V. I. and H. Harshvardhan, 1993: Aerosol effects in Radiation Transfer in S. G. Jennings (Ed) *Aerosol Effects on Climate*. Chapter 5, 190-232.

Carlson, T.N. and R.S. Caverly, 1977: Radiative Characteristics of Saharan dust at solar wavelengths. *J. Geophys. Res.*, **82**, 3141-3152.

Charlson, R.J., and J. Heintzenberg, 1994: Introduction to R. J. Charlson and J. Heintzenberg (Eds.) *Aerosol Forcing of Climate*. John Wiley & Sons, Chichester. 1-10.

Cox, S.K., 1975: Relating broadband short-wave irradiance measurements to radiative properties of the atmosphere. Collection of Abstracts, AMS Second Conf. On Atmos. Rad., October 29-31, Arlington, VA, 237-240, 1975.

Cracknell, A.P., 1997: *The Advanced Very High Resolution Radiometer (AVHRR)*. Taylor and Francis, 534 pp.

Drummond, A.J., and G.D. Robinson, 1974: Some measurements on the attenuation of solar radiation during BOMEX. *Appl. Opt.,* **13**, 487-492.

Duce, R.A., 1994: Sources, Distributions, and Fluxes of Mineral Aerosols and Their Relationship to Climate. In R. J. Charlson and J. Heintzenberg (Eds.) *Aerosol Forcing of Climate*. John Wiley & Sons, Chichester. 43-72.

Ellingson , R.G., and G.N. Serafino, 1984: Observations and calculations of aerosol heating over the Arabian Sea during MONEX, *J.Atmos.Sci.*, **41**, 575-589.

Finlayson-Pitts, B. J. and J.N. Pitts Jr. (1997): Tropospheric Air Pollution: Ozone, Airborne Toxics, Polycyclic Aromatic Hydrocarbons, and Particles. *Science* **276**, 1045-1052.

Galindo, I., 1978; On the Presence of Saharian Aerosol at the Western Part of the Atlantic Ocean. *Z. Meteor*, **28** (6), 353-360

Galindo, I., 1984: Anthropogenic aerosols and their regional scale climatic effects. In H.E. Gerber and A. Deepak eds. *Aerosols and Their Climatic Effects*. A. Deepak Publishing, Hampton, VA., pp. 245-260.

Galindo, I., 1992: Extinction of short wave solar radiation due to El Chichón stratospheric aerosol. *Atmósfera* **5**, 259-268.

Galindo, I., 1996: Volcanic clouds detection from the low energy eruption of Popocatépetl volcano, Mexico, using AVHRR bands 4 and 5. Volcanic Ash Hazards and Aviation Worshop. Anchorage, Alaska, May 28-31

Galindo, I. and J.L. Bravo, 1975: On the presence of a volcanic stratospheric dust stratum over a polluted atmosphere. *Geofis. Int.*, **15**, 157-167.

Galindo, I. and R. Solano, 1999: Real Time AVHRR Detection of forest fires and smoke in Mexico Between January and June 1998. Norh American Science Symposium, Guadalajara, Jalisco, Mexico, November 1-6, 1998, USDA Forest Service Proceed. RMRS P-12, 68-75.

Galindo, I., A. Muhlia, and J.L. Bravo, 1977: Radiation experimental data on the energetics of the Saharian aerosol layer in the GATE synoptic scale. Proc. Int. Conf. On the Energetics of the Tropical Atmosphere, Tashkent, 14-21 September, 1977.

Galindo, I., K., Ya. Kondratyev and G. Zenteno, 1996: Determination of the atmospheric optical depth due to the El Chichón stratospheric aerosol cloud in the polluted atmosphere of Mexico City. *Atmósfera* **9**, 23-32.

Galindo, I., L.S. Ivlev, A. González and R. Ayala, 1998: Airborne measurements of particle and gas emissions from the December 1994-January 1995 eruption of Popocatépetl volcano (Mexico). *J. Volcanol and Geotherm. Res.* **83**, 197-217.

Gavilanes, J.C., 1998: personal communication.

Hay, J.E. and Darby, R., 1984: El Chichón – Influence on aerosol optical depth and direct, diffuse and total solar irradiances at Vancouver, B.C., *Atmosphere-Ocean* **22** (3), 354-368.

Hobbs, P.V., L.F. Radke, M.W. Eltgroth and, D.A. Hegg, 1981: Airborne studies of the emissions from the volcanic eruptions of Mount St. Helens. *Science* **211**, 816-818.

Hofmann, D.J., 1987: Perturbations to the global atmosphere associated with the El Chichón volcanic eruption of 1982. *Revs. of Geophys.* **25** (4), 743-759.

Hofmann, D.J., 1988: Aerosols from past and present volcanic eruptions. In P.V. Hobbs and M.P. McCormick (Eds.) *Aerosols and Climate*, Hampton, VA. A. Deepak Publ., pp. 195-214.

Hofmann, D.J. and, J.M. Rosen 1987: On the prolonged life time of the El Chichón sulfuric acid aerosol cloud. *J. Geophys. Res.* **92**, 9825-9830.

Intergovernmental Panel on Climate Change, 1994: *Climate Change 1994.* Cambridge University Press, 162 pp.

Jennings, S.G. (Ed.), 1993: *Aerosol Effects on Climate*. The University of Arizona Press. 305 pp.

Kaufman, Y.J., R.S. Fraser, and R.A. Ferrare, 1990a: Satellite remote sensing of large-scale air pollution: Method. *J. Geophys. Res.* **95**, 9895-9909.

Kaufman, Y.J., C.J., Tucker, and I. Fung, 1990b: Remote sensing of biomass burning in the tropics. *J. Geophys. Res.* **95**, 9927-9939.

Kondratyev, K. Ya. and M.E. Berlyand, eds., 1974: Joint-energy experiment (CAENEX,72), Trudy GGO (Proceedings of the Main Geophysical Observatory), issue 332, 116 pp.

Kondratyev, K. Ya. and N. E. Ter-Markaryants, eds, 1976: Total Radiation Experiment, Gidrometeoizdat (State Scientific and Technical Hydrometeorological Publishing House), Leningrad, 240 pp.

Kondratyev, K. Ya., and I. Galindo, 1994: Global climate change in the context of global ecodynamics. *Geofís. Int., 33* (3), 487-496.

Kondratyev, K. Ya., and I. Galindo, 1997: *Volcanic Activity and Climate.* A. Deepak Publ., Hampton, VA, 382 pp.

Möller, D, 1994: Sulfate Aerosols and Their Atmospheric Precursors In R. J. Charlson and J. Heintzenberg (Eds.) *Aerosol Forcing of Climate.* John Wiley & Sons, Chichester. 73-90.

Patterson, E.M., C.O. Pollard, and I. Galindo, 1983: Optical Properties of the Ash from El Chichón volcano. *Geophys. Res. Lett.*, **10** (4), 317-320.

Prata, A.J., 1989: Observations of volcanic ash clouds in the 10-12 μm window using AVHRR/2 data. *Int. J. Remote Sensing* **10**, 751-761.

Ramaswamy, V. (Rapporteur), 1994: Group Report: What Are the Observed and Anticipated Meteorological and Climate Responses to Aerosol Forcing? In R. J. Charlson and J. Heintzenberg (Eds.) *Aerosol Forcing of Climate*. John Wiley & Sons, Chichester.385-399.

Rao, Nagaraja, C.R., L.L. Stowe, E.P., McClain and J. Supper, 1988: Development and Application of Aerosol Remote Sensing with AVHRR data from the NOAA satellites. In P. V. Hobbs and M.P. McCormick (Eds.) *Aerosols and Climate.* A Deepak Publishing, Hampton, VA., 69-80.

Simkin, T., L. Siebert, L. McClelland, D. Bridge, C. Newhall, and J. H. Latter, 1981: Volcanoes of the World, Washington, D.C., Smithsonian Institution.

Toon, O.B., 1994: Modeling the Relationships between Aerosol Properties and the Direct and Indirect Effects of Aerosols on Climate. In R. J. Charlson and J. Heintzenberg (Eds.) *Aerosol Forcing of Climate*. John Wiley & Sons, Chichester. 197-214.

Veefkind, J.P., G. de Leeuw, Ph.A. Durkee, Ph. B. Russell, P. V. Hobbs, and John M. Livingston, 1999: Aerosol optical depth retrieval using ATSR-2 and AVHRR data during TARFOX. *J. Geophys. Res.*, **104** (D2), 2253-2260.

Warner, J., and S. Towmey, 1967: The production of cloud nuclei by cane fires and the effect on cloud droplet concentration. *J. Atmos. Sci.*, **24**, 704-706.

Appendix A Considerations on the Future of the International Pyrheliometer Comparisons

[1]The Ad-hoc Group of the Ninth International Pyrheliometer Comparison (IPC) has met several times to discuss means of ensuring the future stability and transfer of the World Radiation Reference (WRR) in coming years. Specific concerns that the committee has addressed below include:

- The transfer from the WRR to Regional Radiation Centre (RRC) absolute instruments. Several comparisons have resulted in limited data sets, even after the three weeks of time allotted for the comparison.
- The increase in the number of National Radiation Centres (NRC) being invited to the IPC because RRCs are unable to hold Regional Association (RA) pyrheliometer comparisons during the intervening time periods. This has led to an increased concern that the transfer from RRCs to NRCs has become less effective, and that the overall level of communication between the two types of centres has been reduced.
- The increase in the cost of the comparison at the same time the budget for comparisons within CIMO has decreased.

The effectiveness of maintaining the World Standard Group (WSG) of instruments at PMOD over the last 30-or-so years is indicated by the nearly insignificant change in the WRR during this time period. The expertise developed must remain in tact along with the on-going maintenance of the individual WSG instruments. However, the increasing age of the WSG is becoming a concern to both the staff of the WRC and the Ad-hoc Group. CIMO indicates that the WSG must consist of a minimum of 4 absolute cavity instruments of different types so that the WRR may be maintained. At present the WSG consists of seven instruments, however, over the last 5 years three of these instruments have shown signs of aging (note that many of these instruments are more than 30 years old), with the possibility that they may have to be removed from the WSG because of increased uncertainties. The PMOD has explored several possibilities to obtain different instruments to operate along with the WSG, but these investigations have led to the deployment of only one further instrument during the last 5 years. There is a further time delay from the deployment of an instrument and its acceptance into the WSG because of the need to ensure that the new instrument is stable over an inter-IPC period. This present state of instrumentation may well make the need for constant monitoring of the WRR more critical at this time than in previous years.

The number of National Radiation Centres at the last two comparisons is also a concern to both the staff of the WRC and the Ad-hoc Group. The combining of the Regional Radiation Comparisons (RPCs) with the IPC increases logistical support significantly. Furthermore, members of the Ad-hoc Group believe that the combining of RPCs with the IPC both reduce the maintaining of the WRR through comparisons throughout the 5-year period between comparisons and reduce the educational opportunities afforded to National Centres when an RPC is held within the Region.

Based upon the above general discussion, the Ad-hoc Group present the following recommendations:

1. **That an International Pyrheliometer Comparison be held once every five years at the World Radiation Centre.** The regular bringing together of experts with Regional Standard

[1]This document presents the results of the Ad-hoc Group discussions on the future of the International Pyrheliometer Comparisons. It should support the work of the CIMO-Rapporteur on Meteorological Radiation Measurements for presentation at the next CIMO session (CIMO-XIII). It is included in this report for the sake of completeness and as information to the participants.

instruments provides a necessary check on the stability of the WSG of instruments and increases the probability of detecting any bias in the WRR. Keeping the WSG at the WRC reduces the risk in altering the WRR by eliminating the need to move the entire WSG of instruments and the electronic equipment associated with these instruments.

2. **That the comparison be open-ended to ensure that the amount of data collected is sufficient to assure the quality of the World Radiation Reference and the transfer of this reference to the participating Regional Radiation Centres.** Comparisons during 1980, 1990 and 2000 had limited numbers of observations due to inclement weather conditions during the 3-week period of the IPC. During the 1995 comparison, more data than necessary was collected to statistically ensure the stability of the WRR. If the amount of data collected is insufficient, ending the comparison prematurely on a fixed date tends to increase the uncertainty in the calculation of the WRR. This in turn may have significant effects on the clients utilizing the services of the Regional and National Centres. By fixing the location of the comparison in Recommendation One, the working group encourages the WRC to carefully determine the best portion of the year to host such a comparison so that the time required to obtain the necessary quantity of measurements is minimized. From climatological mean data there are several times of the year when the minimum required number of clear days for a successful comparison can be expected within a 14 day period. At the same time it is recognized the clear weather conditions cannot be guaranteed.

3. **That the Regional Associations within CIMO ensure that a minimum of one RRC from within the region be represented at the IPC and that the regional centre(s) representing the region be fully compliant with the regulations of an RRC as outlined in Annex C of the CIMO Guide (WMO No. 8, 1996).** The Ad-hoc Group recognizes that for many regions the cost associated with sending a delegation from a RRC is significant, but it is crucial that a well-equipped and trained individual(s) be sent from each region. During past IPCs a number of RRCs have not had the appropriate equipment and therefore have not been able to participate to the fullest extent. The sending of such centres is counter-productive. The Regional Associations are encouraged to examine each RRC within the region to determine whether they meet the standards set down in the CIMO Guide.

4. **That RPCs are held separately and not be in conjunction with the IPC.** The primary task of an IPC is the transfer of the WRR to instruments maintained by RRCs. The combining of RPCs with the IPC increases the complexity and logistics of the task considerably. Furthermore, the educational aspects of both the IPC and the RPCs are diluted. Specific courses that should be provided to individuals of RRCs cannot be given because of the divided interests of the participants. Of greater concern is the limited number of individuals from NRCs that are able to attend due to cost. Specific courses that could be normally tailored for NRCs within Regional Associations are not available at a combined RPC and IPC.

5. **That organizations that are not RRCs be charged a participants fee for attending the IPC and that all funds obtained from such fees be used to offset the cost of shipping equipment from the WRC to the RPC.** During the last two IPCs several participants have represented either private sector or government laboratories not associated with the WMO. In some cases government and private-sector laboratories are now mandated under law to maintain standards directly traceable to the WRR through participation in an IPC every five years. These participants illustrate the demand for such a comparison of absolute radiometers for users other than those associated directly with meteorological organizations. Furthermore, these organizations use the calibrations obtained while attending the IPC for commercial advantage. The Ad-hoc Group suggests that such institutions be charged a fixed participants fee to partake in such a comparison. National laboratories desiring, or mandated to attend the IPC should

also be charged the same rate, although these institutions are strongly encouraged to attend only the appropriate regional comparison. As recognition of past practices those laboratories or manufacturers providing instruments to the WSG would be exempted from all charges as a courtesy for donating instruments. It is hoped that this latter exemption may encourage the donation of instruments of different designs to the WSG. All fees collected will be used to offset the cost of transporting WRR equipment to the RPCs. The distribution of the funds will be a weighted against the distance from the WRC to the six regions.

6. **The maximum number of attendees at an IPC be determined by the WRC.** While the above recommendations are meant to reduce the number of active participants to any IPC, the final number of participants to an IPC must be controlled by the WRC because of the logistics associated with such an important task. The success of an IPC cannot be jeopardized because of too many participants. Under reasonable circumstances the attendance priority should be RRC, NRC and finally commercial interests.

7. **That the dissemination of the WRR through RPCs be revitalized to protect the integrity of the WRR through the five-year period through participation in regional comparisons in each of the 6 WMO regions.** Changes in the WRR through the comparison of instruments directly related to the WRR with those of regional centres would be more quickly noticed. Six RA comparisons during a 3.5-year period provide a crosscheck against the WRR at intervals of roughly 7 months. An RPC would require that a minimum of one instrument from the WSG, and two absolute cavities that have been compared with the WSG within a six-month period before the RPC and that a statistically significant data set be obtained to show the stability of these instruments to the WRR (these instruments should be of different manufacture).

8. **That it is the responsibility of each Regional Association to provide a host for an RPC, which will be held in the period 6 months to 4 years following the completion of an IPC. The date and duration of the RPC will be established in conjunction with the WRC.** The reduction in the number of RPCs during the last ten years is a disturbing trend. Recommendations Three and Four are meant to encourage the re-establishment of the RPC. It is recommended strongly that RAs become more involved in the measurement of radiation and the transfer of the WRR through RPCs. For example, budget freed by sending only one RRC to the IPC could be used to build the necessary infrastructure and provide travel grants to increase the number of participants from NRCs. This decentralization will provide NRCs the opportunity to discuss problems found within the region, but may not be significant to the larger global community, while at the same time reducing travel costs, and probably the time required to fulfill the measurement requirements of an RPC. The combining of RPCs is encouraged if RAs believe that the benefit to the participating NRCs is increased over organizing separate regional comparisons. Furthermore, it would be ideal if one RRC from outside the RA also attend the RPC. This would increase expertise with respect to teaching NRC personnel and provide further crosschecks on the stability of the WRR during the period between IPCs. The Ad-hoc Group further suggests that to increase the capability of individual RRCs that any funding provided by the RA be linked to that RRC hosting the RPC during the following inter-IPC period. The WRC is committed to providing the necessary salary and travel expenses to ensure that qualified staff is available to operate the WSG instrument(s).

9. **That the Regional Radiation Centres be provided with education courses directly related to hosting an RPC during their attendance at the IPC.** As part of the reduction in numbers at the IPC and the focus of the IPC on RRCs, the education program can be better tailored to meet the needs of the attendees. To encourage the successful operation of an RPC,

courses will be developed by the WRC to provide a means of aiding RRCs to successfully host such comparisons.

10. **That during an RPC education courses be provided to NRCs that will increase the capability of National Centres in the calibration of radiometers and the development and maintenance of national radiation networks.** It is believed that the decentralization of regional comparisons away from the IPC will provide opportunities for educating individuals from National Centres not available elsewhere. As part of the program associated with hosting an RPC, the RRC would have opportunity to develop special courses suitable for the participants of the region. These courses could either be taught by individuals within the region or in cooperation with WRC staff that would be attending the RPC. By keeping comparisons on a regional base, many members of the Ad-hoc Group believe that issues of culture and language would be reduced, thus encouraging increased participation by NRCs.